Republic of Iraq

Ministry of Higher Education and Scientific Research

University of Babylon

College of science for women

Chemistry Department

Preparation of (SA-g-P(ITAC-co-VBS)/RC) Hydrogel Nanocomposite Surface Highly Efficient Removal of Dyes and Role of its as a Wound Adhesive

A Thesis Submitted
to the Council of the College of Science for Women, University of Babylon as a Partial Fulfillment of the Requirements for the Degree of Master in Chemistry

By

Ishraq Talib Hasan Musafer

B.Sc. Chemistry, College of Science for Women, Babylon University, 2019 - 2020

Supervised by

Asst. Prof. Dr. Aseel Mushtaq Aljeboree

2023 A.D **1444 A.H**

Supervisor Certification

I certify that this thesis entitled

Preparation of (SA-g-P(ITAC-co-VBS)/RC) Hydrogel Nanocomposite Surface Highly Efficient Removal of Dyes and Role of its as a Wound Adhesive

Was prepared under my supervision at the University of Babylon / College of Science for Women as a partial Requirement for the degree of Master in Chemistry Science.

Signature
Dr. Aseel Mushtaq Kadum
Scientific Order: Asst. Prof.
Address:
University of Babylon / College of
Science for Women
Date: / /2023

Recommendation of Head of Chemistry Department

According to the available recommendation, I forward this thesis for Discussion.

Signature of Chemistry Department
Dr/ Sadiq A. Karim
Scientific order: Prof.
Address: Head of Chemistry Department
University of Babylon / College of
Science for Women
Date: / /2023

DEDICATIONS

To the one who gives me great pleasure and pride to dedicate my modest thesis to the supervisor and wonderful teacher and the butterfly of my heart, **Dr. Aseel Mushtaq** , who assumed the great responsibility of guiding and teaching and walked with me to the ladder of dreams.

For those who helped me start this life, who harvested thorns from my path to pave the way for knowledge , my mother and father, who are present in my heart and my reality, so they were my support from the softness of the roots to what I am now To my loved ones, my extended family and friends , and to everyone who supported me of all kinds.

Ishraq

ACKNOWLEDGMENTS

Thanks Allah and thank to him so much, for everything that comes from him is beautiful, makes us rejoice and forget what has gone. Thank you, Allah, for your door is not closed, your presence is uninterrupted, and your mercy is a sustenance to every thirst.

After Allah, a special thanks to the virtuous professor, ***Dr. Aseel Mushtaq*** , the owner of professional and scientific supervision, and Thanks to ***Dr. Ayad Alkaim*** and ***Dr. Hazim Aljebore*** who were the best role model and teachers during every minute of the research period.

The honorable Dean and Head of the Department of Chemistry have our sincere gratitude. All gratitude and thanks to my sisters and friends for their efforts to help me complete my scientific career.

All the gratitude and love to my beautiful family , especially my mother and father, for their constant love and prayers.

Thank you to the makers of our days with their kindness.

Summary

Synthesis superabsorbent polymer, Sodium Alginate-g-Poly (Itaconicacid-co-Sodium4-vinylbenzenesulfonate)/Ricinus communis , (SA-g-P(ITA-co-VBS)/ RC) hydrogel nanocomposite, was prepared by free-radical graft co-polymerization for sequestration of toxic two dyes malachite green (MG) dye and brilliant green (BG) dye as a cationic dyes model. In this work, an eco-friendly, simple, stable new adsorbent included the preparation of two surfaces the first (SA-g-P(ITA-co-VBS) hydrogel and the second surface hydrogel after loading RC onto (SA-g-P(ITA-co-VBS) and these new surfaces were prepared from different monomers. The physical characterizations of these prepared materials have been studied. The obtained powders are characterized by using different techniques like Ultraviolet-Visible Spectroscopy (UV–Vis), Fourier Transform Infrared (FT-IR), Thermal gravimetric analysis (TGA), Surface Area Analyzer (BET), Field Emission Scanning Electron Microscopy (FE-SEM), Transmission Electron Microscopy (TEM), Energy Dispersive X-Ray (EDX) and X-ray Diffraction Spectroscopy (XRD).

The practical experiments included calculation of the maximum wavelength and study optimizing the synthesis conditions produced a hydrogel nanocomposite with the highest swelling ratio like: Effect of amount RC, effect of VBS, effect of Itaconic acid, effect of sodium alginate, effect of cross-linker, effect of initiator, effect of pH, effect of solvent, effect of temperature, and effect of time. Also, study optimum condition of the effect of adsorption parameters are :effect of contact time, effect of adsorbent dose, effect of initial concentration of dyes , effect of pH solution, Zero point charge, effect of temperature solution, adsorbent regeneration experiments (Desorption), comparative adsorption

between different surfaces to removal two dyes , removal of laboratory sample aqueous Pollutants , biological activity bacterial , fungus test and treating Mice Wounds Using a three Surface Prepared from RC, (SA-g-P(ITA-co-VBS) hydrogel and ,(SA-g-P(ITA-co-VBS)/ RC) hydrogel nanocomposite**.**

The results of the adsorption study show that percentage removal increases with the increase of the weight of the surfaces; and contact time. The optimized value of agitation time is 1 hr. after which the adsorption becomes constant. The increase of adsorbent amount about rang (0.01- 0.1)g, the percentage removal of MG dye, and BG dye increase from (90.11 - 99.8%) , (75.88% - 95.99%) and adsorption capacity decrease from (6695 – 995 mg/g) , (5020– 695 mg/g) onto ,(SA-g-P(ITA-co-VBS)/ RC) hydrogel nanocomposite at the same order about 1h of adsorption time . The enthalpy (ΔH) values is positive indicating that the adsorption process is an endothermic reaction. All processes of adsorption where considered spontaneous from the negative value of Gibbs free energy ΔG. While, entropy (ΔS) have positive value that refer the interaction of molecules caused random of the total system. The Freundlich and Langmuir models are also introduced. It has been found that all results follow the Freundlich model in the presence of two dyes; this nonlinearity is higher when using the Freundlich model. Kinetics adsorption models of two dyes onto (SA-g-P(ITA-co-VBS)/ RC) was studied by using three kinetic models .

Comparative between (Natural Ricinus Communis (RC), Activated untreated - acid Ricinus Communis Pericarp(ACRC) and acid-treated Ricinus Communis Pericarp (AACRC)). The best results of the percentage of removal (E%) of two dyes arrange in order increasing (RC , ACRC , AACRC). Also, Comparative between ((SA-g-P(ITA-co-VBS)/

RC), ,(SA-g-P(ITA-co-VBS) and RC) surfaces as adsorbents .The good results of the percentage of removal (E%) of ,(SA-g-P(ITA-co-VBS)/ RC) 92,451%, and 82.56 for MG, and BG at the same order .

Recyclability and Desorption studies indicated the best recycling performance of the prepared composite. Based on the results, the prepared nano-composites can be useful as a promising, eco-friendly , cost-effective, and efficient material for dyes decontamination . The (SA-g-P(ITA-co-VBS)/ RC), was regeneration with 100% can be desorbed in diluted HCl .

The biological activity of one type of fungus (Aspergillus flavus) and two types of bacteria were Gram-positive bacteria (staphylococcus) and Gram-negative bacteria (Pseudo monas). The results of the inhibition regions three compounds where it was given that the compound (SA-g-P(ITA-co-VBS)/ RC) had high antibacterial activity. In two to seven days, according to the results, there is complete healing of the mice and the return of the skin to its natural color. This is due to the fact that (SA-g-P(ITA-co-VBS)/ RC) hydrogel nanocomposite have high effective efficiency in treating and healing mice.

List of Contents

List of Tables

List of Figures

List of Abbreviations

Shorten	Full name
SA	Soudium alginate
RC	Ricinus communis
MG	Malachite green
BG	Brilliant green
MBA	N´,N-methylene-bis-acrylamide
ITA	Itaconic acid
KPS	Potassium persulfate
VBS	Sodium4-vinylbenzenesulfonate
AC	Active carbon
AM	Acrylamide
BC	Bentonite
GO	Graphen oxide
PEO	Poly ethylene oxide
VFA	Vinyl form amide
NaAla	Soudium alginate
Gel	Gelatin
GK	Gum karaya
BC	Bentonite clay
T	Absolute temperature
Abs	Absorbance
pH	Acidic function
q_e	Amount of adsorbate per unit weight of adsorbent at equilibrium
BET	Brunauer-Emmett-Teller
ΔH	Change of enthalpy

Shorten	Full name
ΔS	Change of entropy
Conc.	Concentration
R^2	Correlation coefficient
K_e	Distribution coefficients
EDX	Energy Dispersive X-Ray
K_{eq}	Equilibrium constant
C_e	Equilibrium dye concentration
FE-SEM	Field emission scanning electron microscopy
FT-IR	Fourier Transform Infrared
K_f	Freundlich constant
ΔG	Gibbs free energy
Q	Heat of adsorption
C_o	Initial Concentration
k_L	Langmuir constant
M	Mass of adsorbent
Q_m	Maximum adsorbed
X_m	Maximum adsorption
q_m	Maximum Adsorption Capacity
λ_{max}	Maximum wavelength
E%	Removal percent
q_t	The amount of adsorbent at a given time
k_1	The pseudo-first-order rate constant
K_2	The pseudo-second-order rate constant
TGA	Thermal gravimetric analysis
T	Time
TEM	Transmission electron microscopy
UV–Vis	Ultraviolet-Visible Spectroscopy

Shorten	Full name
R	Universal gas constant
XRD	X-ray diffraction spectroscopy

Chapter One

Introduction

1- Introduction

1-1 General Introduction

Wastewaters from industries like textile, dyeing, printing, cosmetics, food coloring, and paper making, etc. are the major contributors of colored effluents. However, textile industries consume large amount of water and different type of dyes imparting color to the effluents. The dyes and colors are toxic, their adverse effects on fauna, flora, and human beings are well documented[1].

Color is probably the most important contaminant that could be recognized in water even at minute levels. Color has to be removed from wastewater before discharging it into water bodies as it impedes light penetration and retards photosynthesis. Color increases chemical oxygen demand (COD) and biological oxygen demand (BOD) levels of aquatic sources. It has a tendency to chelate metal ions, which results in micro-toxicity to aquatic lives. Therefore, discharge of these dyes into effluents affects the people who may use these effluents for living purposes such as washing, bathing and drinking [2]. Therefore, it is very important to verify the water quality, especially when even just 1.0 mg/L of dye concentration in drinking water could impart a significant color, making it unfit for human consumption . Furthermore dyes can affect aquatic plants because they reduce sunlight transmission through water. Also dyes may imparted of toxicity to aquatic life and may be mutagenic, carcinogenic and may cause severe damage to human beings, such as dyes function of the kidneys, reproductive system, liver, brain and central nervous system. The removal of color from waste effluents becomes environmentally important because even a small quantity of dye in water can be toxic and highly visible [3].

1-2 Dyes

Dyes are an organic chemical which on binding with materials, it will give a color to the materials. The color of a dye is provided by the presence of a chromophore group. A chromophore is a configuration consisting of conjugated double bonds containing delocalized electrons.

Other common chromophore configurations include azo (-N=N-), carbonyl (-C=O); carbon (-C=C-); carbon-nitrogen (>C=NH or -CH=N-); nitroso (-NO or N-OH); nitro(-NO_2 or =NO-OH); and sulphur (C=S). The chromogen, which is the aromatic structure normally containing benzene, naphthalene or anthracene rings, is part of a chromogen-chromophore structure along within an auxo-chrome [4, 5].

Generally, the dyes used in the textile industry are basic dyes, acid dyes, reactive dyes, direct dyes, azo dyes, mordant dyes, vat dyes, disperse dyes and sulfur dyes, where azo derivatives dyes are the major class of dyes that are used in the industry today[6]. Table (1-1) shows the typical dyes used in textile dyeing operations.

Table (1-1): Typical dyes used in dyeing operations[5].

Dye class	Description
Acid	Water-soluble anionic compounds
Basic	Water-soluble, applied in weakly acidic dye baths; very bright dyes
Direct	Water-soluble, anionic compounds; can be applied directly to cellulosic without mordents (or metals like chromium and copper)
Disperse	Not water-soluble
Reactive	Water-soluble, anionic compounds; largest dye class
Sulfur	Organic compounds containing sulfur or sodium sulfide
Vat	Water-insoluble; oldest dyes ; more chemically complex

Dye class	Description
Azo	highly water-soluble, cause bladder and liver cancers.

1-2-1 Brilliant Green (BG)

Brilliant Green (BG) dye is odorless yellow-green to green powder and is one of the commonly known cationic dye (structure is shown in Fig. 1-1) used for various purposes, e.g. biological stain, dermatological agent, veterinary medicine, and an additive to poultry feed to inhibit propagation of mold, intestinal parasites and fungus. It is also extensively used in textile dying and paper printing. About 0.8– 1.0 kg of BG is consumed per ton of paper produced [7]. However, in human's BG causes irritation to the gastrointestinal tract; symptoms include nausea, vomiting and diarrhea. It also causes irritation to the respiratory tract, leading to cough and shortness of breath. Skin contact causes irritation with redness and pain. Brilliant Green may form hazardous products like carbon oxides, nitrogen oxides, and sulfur oxides when heated to decomposition [8, 9] .

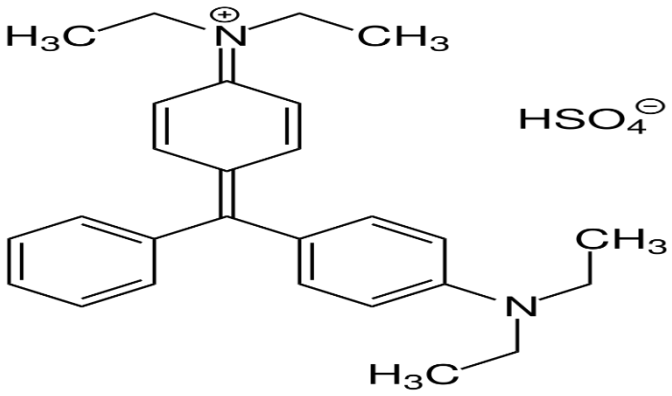

Figure (1-1): Chemical structure of Brilliant Green (BG) dye.

Table(1-2): Physicochemical properties of Brilliant Green (BG)dye

Physicochemical properties	Methyl violet
Molecular formula	$C_{27}H_{34}N_2.O_4S$
Type of dye	Cationic
Molecular Weight	482.64 $g.mol^{-1}$
Maximum wavelength (nm)	630
Color	Green
IUPAC	[4-[[4-(diethylamino)phenyl]-phenylmethylidene]cyclohexa-2,5-dien-1-ylidene]-diethylazanium

1-2-2 Malachite green(MG)

Malachite green is an organic compound that is used as a dyestuff and controversially as an antimicrobial in aquaculture. Malachite green is traditionally used as a dye for materials such as silk, leather, and paper. Despite its name the dye is not prepared from the mineral malachite; the name just comes from the similarity of color [10].

Its application extents in the aquaculture, commercial fish hatchery and animal husbandry as an antifungal therapeutic agent, while for human it is used as antiseptic and fungicidal. However, its oral consumption is carcinogenic. The available toxicological information reveals that in the tissues of fish and mice MG easily reduces to persistable leuco-Malachite Green, which acts as a tumor promoter. Thus, the detection of MG in fishes, animal milk and other food stuff designed for human consumption are of great alarm for the human health. Studies also confirm that the products formed after the degradation of Malachite Green are also not safe and have carcinogenic potential. Thus it becomes necessary to

remove such a toxic dye from wastewater before it released into aquatic environment. and shown the table (1-3) [11]

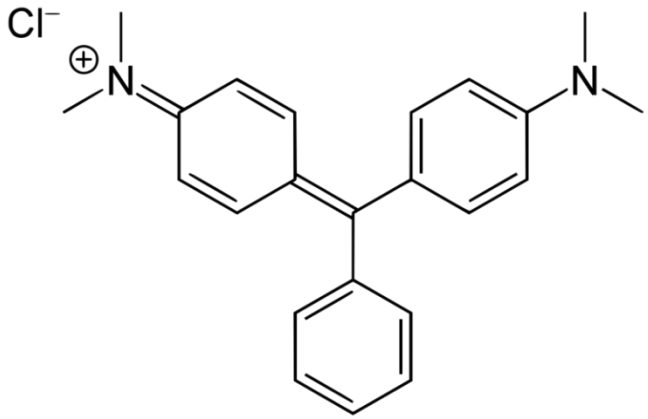

Figure (1- 2): Chemical structure of Malachite Green(MG)

Table(1-3): Physicochemical properties of Malachite Green(MG)dye

Physicochemical properties	**Methyl violet**
Molecular formula	$C_{23}H_{25}ClN_2$
Type of dye	Cationic
Molecular Weight	364.9g.mol^{-1}
Maximum wavelength (nm)	624
Color	Green crystals
IUPAC	[4-[[4-(dimethylamino)phenyl]-phenylmethylidene]cyclohexa-2,5-dien-1-ylidene]-dimethylazanium;chloride.

1-3 Hydrogels

Hydrogels are hydrophilic polymer chains that are crosslinked to form gel structures that swell in aqueous solution and trap fluids for a long period without dissolving. Hydrogels may contain carboxylic, amine, imide, hydroxyl and sulfonyl groups in their 3D structure that are responsible for the hydrophilicity and swelling capacity[12, 13]. The hydrogel must have the following properties, High absorption capacity ؛ low residue monomer and soluble content؛ cost-effective .reusable ؛high biodegradability and not produce harmful byproducts ؛must retain neutral pH after swelling in water and easy recoverability[14, 15].

Depending on the nature of the hydrogel, it can be classified based on various properties. Classification of hydrogels (Figure 1-3) can be based on whether they are synthetic (involves the use of synthetic monomers), natural (involves using biopolymers) or a combination of synthetic and natural monomers resulting in a hybrid hydrogel. The polymeric composite classification can be based on the method used to synthesize the hydrogel [16, 17]:

a. Homopolymeric hydrogels: they are hydrogels consisting of the same type of monomer.

b. Copolymeric hydrogels: these hydrogels comprise two or more different kinds of monomers such that the network would have at least one hydrophilic component on the polymer network chain.

c. Multipolymer interpenetrating polymeric hydrogel (IPN): the hydrogel network consists of two components (natural and/or a synthetic polymer) that are independently cross-linked.

It was also demonstrated that hydrogels can be categorized based on whether they are.

i. crystalline,
ii. amorphous
iii. semi-crystalline: showing properties of both crystalline and amorphous phases.

The other classification is based on whether the crosslinking of hydrogels occurs via chemical or physical means[18] :

One. physical crosslinking in hydrogels may be through

1-formation of a hydrogen bond

2-hydrophobic interactions between chains.

3- crystallization.

Two. Chemical crosslinking can be achieved by

1- using aldehydes such as acetaldehyde, glutaraldehyde (GA) and formaldehyde

2- formation free radical

3- free-radical polymerization .

In addition, the hydrogels may be classified based on the charge on their cross-linked polymer network. The charge may be a. ionic (cationic/anionic), b. non-ionic (neutral), c. amphoteric (comprising both basic and acidic groups) and d. zwitterionic (contains anionic and cationic components on each repeating structural unit). The net charge of the gel is zero[19].

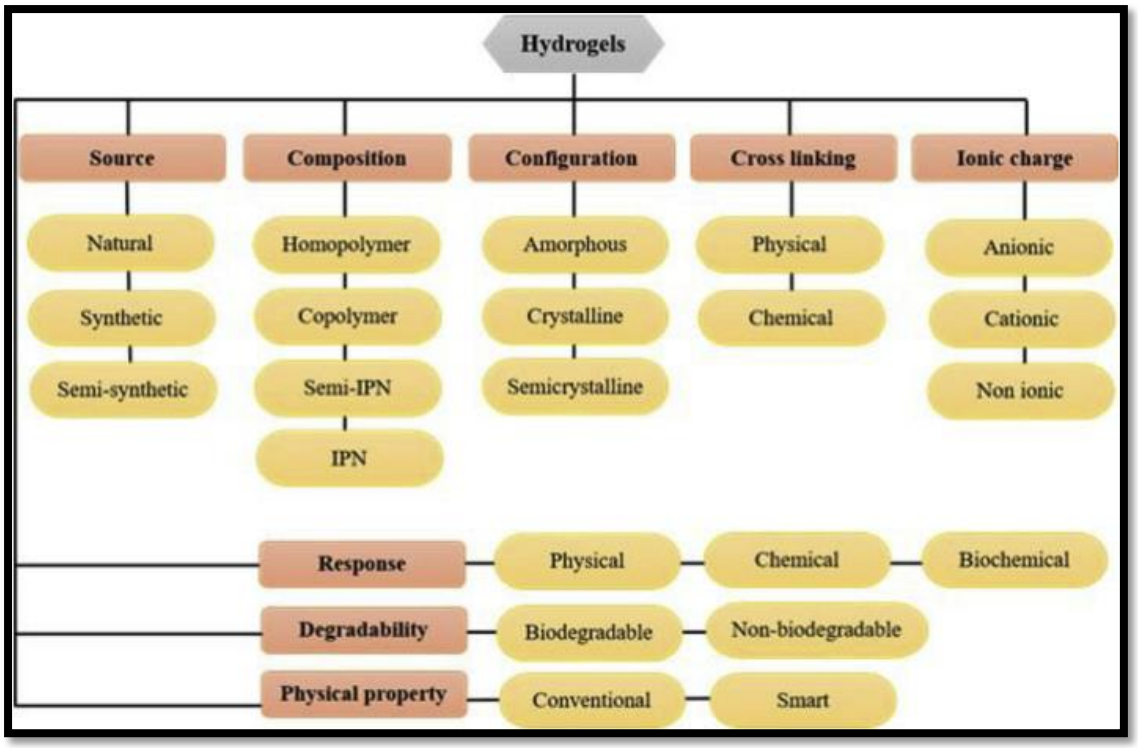

Figure (1- 3). Classification of hydrogels [12].

1-3-1 Sodium Alginate

Sodium alginate (SA, Figure 1-4) is made up of poly-β-1, 4-D-mannuronic acid and α-1, 4-L-guluronic acid. The structure consists of carboxylic groups and hydroxyl groups, which can react with metal ions or crosslinking agents to form hydrogels. Alginate can be extracted from its salt forms by ion-exchange methods. Because of the presence of divalent ions, monovalent, water-soluble salts of alginates can transform into water-insoluble salts [20]. The COO and -OH functional groups on the alginate backbone will allow adsorption of cationic dye pollutants. However, sodium alginate just like other polysaccharides suffers from a lack of stability[21]. To enhance the stability of SA and its adsorption capacity, the biopolymer may be cross-linked with synthetic polymers into forming a hydrogel. This will allow their use as adsorbents without in dissolving them in the adsorbate solution. The major disadvantage of

polysaccharides as adsorbents is that they dissolve in water and have low mechanical stability. To resolve this problem, polysaccharides are cross-linked to form hydrogels, which do not dissolve in water [22].

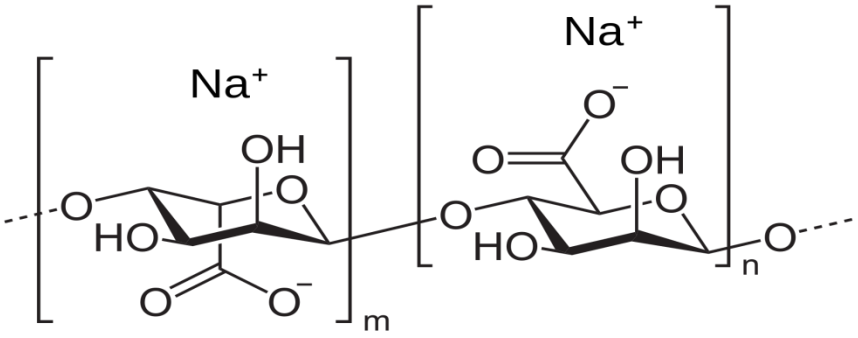

Figure (1-4): The chemical Structure of sodium alginate [23]

1-3-2 Itaconic acid

Itaconic acid (2-methylidenebutanedioic acid) is an unsaturated di-carbonic acid, a white solid that is soluble in water, ethanol, and acetone as shown in figure (1-5). Some selected physicochemical properties of Itaconic acid, like Chemical formula ($C_5H_6O_4$), Molar mass(130 g/mol), Density: 1.63 $g.cm^{-3}$, and Solubility in water: 1 g/12 mL . also have high potential as a biochemical building block, because they can be used as a monomer for the production of a plethora of products including resins, plastics, paints, and synthetic fibers [24, 25].

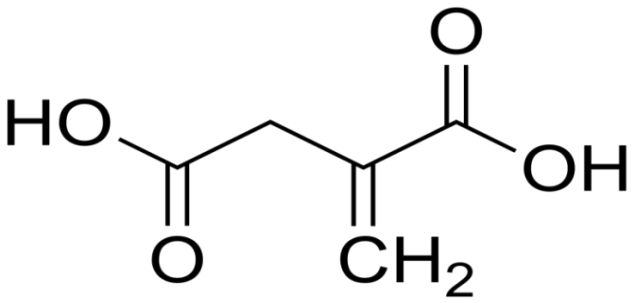

Figure (1-5): The chemical Structure of Itaconic acid.

1-4 Adsorption

Adsorption is a rapid phenomenon of passive sequestration separation of adsorbate from an aqueous/gaseous phase onto a solid phase. Adsorption occurs between two phases in transporting pollutants from one phase to another. It is considered to be a complex phenomenon and depends mostly on the surface chemistry or the nature of the adsorbent, adsorbate and the system conditions in between the two phases. Adsorption processes offer the most economical and effective treatment method for removal of dyes from wastewater., by adding adsorbent to a vessel containing contaminated water, stirring the mixture for a sufficient time, then letting the adsorbent settle, and drawing off the cleansed water. The adsorbate is the substance that is being removed from the liquid phase at the interface. The adsorbent is the solid, liquid or gas phase onto which the adsorbate accumulates[26, 27].

The term adsorption is used also to describe two kinds of forces of interaction between the adsorbate and the adsorbent. These interaction forces are broadly described as physisorption (physical adsorption) and chemisorption (chemical adsorption) . Physical adsorption (physisorption) is relatively non-specific and is due to the operation of weak forces between molecules. In this process, the adsorbed molecule is not affixed to a particular site on the solid surface; it is free to move over the surface [28]. The physical interactions among molecules, based on electrostatic forces, include dipole-dipole interactions, dispersion interactions, induced dipole and hydrogen bonding. When there is a net separation of positive and negative charges within a molecule, it is said to have a dipole moment. Molecules such as H_2O and N_2 have permanent dipoles because of the configuration of atoms and electrons within them. Hydrogen bonding is a special case of dipole-dipole interaction and the

hydrogen atom in a molecule has a partial positive charge, which attracts with partially negative atom on another molecule to result a hydrogen bonding. When two neutral molecules which have no permanent dipoles approach each other, a weak polarization is induced because of interactions between the molecules, known as the dispersion interaction[29].

Chemical adsorption, (chemisorption) occurs a chemical bonding is also based on electrostatic forces, but much stronger forces act a major role in this process. In chemisorption, the attraction between adsorbent and adsorbate is a covalent or electrostatic chemical bond between atoms, with the occurrence of shorter bond length and higher bond energy . The enthalpy of chemisorption is very much greater than that for physisorption، and typical values are in the region of 200 kJ/mol, whereas this value for physisorption is about 20 kJ/mol [30] basic characteristics of chemisorption and physisorption are given in (Table 1-4).

Table 1-4: Properties of physisorption and chemisorption .

Physisorption	Chemisorption
Multilayer adsorption	Monolayer adsorption
Low degree of specificity	Depends on the reactivity of adsorbent and adsorbate substance
Desorption is possible(reversible)	Desorption is impossible (irreversible)
Always exothermic (adsorb molecules keeps their identity) less than 40 kJ/mole	Exothermic, or endothermic chemical bonds forms (the energy involved can reach several hundreds of kJ/mole)
The system generally reaches thermodynamics equilibrium rapidly	Activation energy is involved and at low temperatures, the system may not reach equilibrium.

1-4-1 Factors Affecting on Adsorption Process

1-4-1-1 Effect of Initial Concentration

Adsorption capacity of dyes removal from aqueous solutions depends on the primary dye concentration. The effect of primary dye concentration depends on the direct relationship between dye concentration and active sites on the surface of the adsorbent material. In addition, we note the reduced efficiency of the dyes removal with increased primary dye concentration owing to the saturation of sites available on the surface of the adsorbent material [31].

1-4-1-2 Effect of Amount of Adsorbent

Adsorbent dosage is an important process parameter to determine the capacity of an adsorbent for a given amount of the adsorbent at the operating conditions. Generally, the percentage removal increases with increasing adsorbent dosage, where the quantity of sorption sites at the surface of adsorbent will increase by increasing the amount of the adsorbent. The effect of adsorbent dosage gives an idea for the ability of a dye adsorption to be adsorbed with the smallest amount of adsorbent, so as to recognize the capability of a dye from an economical point of view [32].

1-4-1-3 Effect of pH

pH Plays a major role in the phenomena of adsorption, because within the pH values the structure of dyes will change, and the adsorption process will be affected also by this change, therefore the ability of adsorption may increase, decrease, or remain unchanged as a result of changing pH . [33] The pH of the solution affects the surface charge of the adsorbents as well as the degree of ionization and speciation of different pollutants. Change in pH affects the adsorptive process through

dissociation of functional groups of the active sites on the surface of the adsorbent.[34]

1-4-1-4 Effect of Temperature

It is well known that temperature plays an important role by the adsorption process, when increases, the thickness of the effective layers for adsorption decreases. That means the adsorption process in general. This can be explained by the exothermic spontaneity of the adsorption process and by the weakening of bonds between dye molecules and active sites of adsorbents at high temperatures. [35].

1-4-1-5 Ionic Strength:

The ionic strength of the solution is one of the factors that control both electrostatic and non-electrostatic interactions between the adsorbate and the adsorbent surface. The solubility of ionic salts is affected in the adsorption process because when the ionic salts having solubility are better than the adsorbent substances caused an increase in adsorption, or decrease because the ionic salts caused interference on the surface adsorption [36].

1-4-1-6 Nature of The adsorbent

Adsorption is affected by the adsorbent surface nature and the presence of polarity groups on the surface, which helps to bind with the most polarity components in the solution. Adsorption is also affected by surface area, pore size, and increased surface activity [37] . As adsorption increases with the decrease in the particles size (increasing the surface area), the material of the adsorbent, which has narrow open porous, has greater susceptibility to adsorption [38].

1-5 Adsorption Isotherms:

Adsorption Isotherm model data is typically plotted in the form of an adsorption isotherm with the mass adsorbed on the y-axis and the mass in the fluid on the x-axis at a constant temperature. Adsorption isotherms are mathematical models that describe the distribution of the adsorbate specie among liquid and solid phases, based on a set of assumptions that are related to the heterogeneity/homogeneity of the solid surface, the type of coverage, and the possibility of interaction between the adsorbate species. There are two models applied for adsorption isotherms, Freundlich and Langmuir models are used as follows:[39]

1-5-1 Langmuir adsorption isotherm model

The Langmuir adsorption isotherm model assumed that adsorption takes place at specific homogeneous sites within the adsorbent, and it has been used successfully for many adsorption processes of monolayer adsorption. The Langmuir equation is expressed by the following relation in equation (1-1)[40]:

$$q_e = \frac{q_m K_a C_e}{1 + K_a C_e} \qquad \textbf{(1-1)}$$

Where C_e the residual concentration, q_m, q_e are the adsorption capacity at equilibrium and the maximum adsorption capacity respectively, K_a Langmuir constant. The linear form of the equation of Langmuir isotherm is according to the following equation (1-2) [41]:

$$\frac{C_e}{q_e} = \frac{C_e}{q_m} + \frac{1}{K_a q_m} \qquad \textbf{(1-2)}$$

1-5-2 Freundlich Isotherm:

The Freundlich equation is one of the most important used isotherms in the case of adsorption of solution. This model assumes that the surface of the adsorbate material is heterogeneous because of the different energy levels for adsorption sites, and adsorption does not reach saturation. The mathematical relationship of the Freundlich isotherm can be expressed as the follows in equation (1-3) [42]:

$$q_e = K_f C_e^{\frac{1}{n}} \qquad \textbf{(1-3)}$$

where; qe : Amount adsorbed per unit weight of adsorbent at equilibrium ($mg.g^{-1}$), ($mol.g^{-1}$)
Ce : Equilibrium concentration of adsorbate in solution after adsorption ($mol.L^{-1}$) ,K_f : Empirical Freundlich constant or capacity factor ($L.gm^{-1}$).
1/n : Freundlich exponent

The exponent 1/n is an index of the diversity of free energies associated with the adsorption of the solute by multiple components of a heterogeneous adsorbent. When $\frac{1}{n} = 1$ the isotherm is linear and system has a constant free energy at all adsorbate concentrations. When $\frac{1}{n} < 1$, the isotherm is concave and sorbates are bound with weaker and weaker free energies, when $\frac{1}{n} > 1$, the isotherm is convex and more adsorbate presented in the adsorbent enhances the free energies of further adsorption. The good fit of Freundlich isotherm to an adsorption system means there is almost no limit to the amount adsorbed and there is a multilayer adsorption. The applicability of the Freundlich equation to a particular case is tested by plotting log q_e against log C_e from the logarithmic form of equation (1-4): [43]

$$\log q_e = \log k_f + \frac{1}{n} \log C_e \qquad \textbf{(1-4)}$$

1-6 Microorganisms

Microorganisms, the category of microbes includes a large group of living organisms including bacteria, fungi and algae. In this study, two types of bacteria were used, like bacteria Gram-positive and bacteria Gram-negative, and two types of fungi, like Aspergillus flavus and Aspergillus terrenes.

1-6-1 Streptococcus pneumoniae

Streptococcus pneumonia is a Gram-positive bacteria was first isolated in 1881 and established as the causative agent of pneumonia. Streptococcus *pneumoniae* is a facultative anaerobe. The non-motile, nonspore-forming, alpha-haemolytic lancet-shaped diplococci or chains are resistant to bacitracin and sensitive to optochin and bile-mediated lysis. Genetic variation amongst serotypes varies considerably. Some serotypes have relatively high genetic diversity, whereas others have a relatively homogeneous genetic background. The pneumococci also have incomplete biosynthetic pathways for numerous amino acids, including cysteine, glycine, histidine, glutamine and glutamate. Streptococcus pneumoniae primarily relies on carbohydrate fermentation coupled to substrate-level phosphorylation for energy generation. [44]

1-6-2- Pseudomonas Aeruginosa

Pseudomonas aeruginosa is a ubiquitous Gram-negative bacterium belonging to the family *Pseudomonadaceae* that is able to survive in a wide range of environments . The genome of Pseudomonas aeruginosa (5.5–7 Mbp) is relatively large compared to other sequenced bacteria such as Bacillus subtilis (4.2 Mbp), *Escherichia coli* (4.6 Mbp) and Mycobacterium tuberculosis (4.4 Mbp), and encodes a large proportion of

regulatory enzymes important for metabolism, transportation and efflux of organic compounds. Pseudomonas aeruginosa has been recognized as an opportunistic pathogen that is the most common bacterium associated with nosocomial infections and ventilator-associated pneumonia. It rarely affects healthy individuals, but causes high morbidity and mortality in cystic fibrosis (CF) patients and immunocompromised individuals. [45]

1-6-3 Aspergillus Flavus

Aspergillus flavus has a broad host range as an opportunistic pathogen/saprobe. It is an extremely common soil fungus. The major concern with this fungus in agriculture is that it produces highly carcinogenic toxins called aflatoxins which are a health hazard to animals in the field, Aspergillus flavus is predominantly a problem in the oilseed crops maize, peanuts, cottonseed and tree nuts. Under improper storage conditions, Aspergillus flavus is capable of growing and forming aflatoxin in almost any crop seed. It also is a pathogen of animals, insects and in humans.it is predominantly an opportunistic pathogen of immunosuppressed patients. [46].

1-6-4 Aspergillus Terreus

Aspergillus terreus is one of the most harmful filamentous fungal pathogen of humans, animals and plants. Recently, researchers have discovered that Aspergillus terreus can cause foliar blight disease in potato (Solanum tuberosum L.). Aspergillus terreus belongs to the group of filamentous fungi which produces two types of asexual conidia ., 1) the ultra-small size phialidic conidia (PC), mainly produced at the tips of conidiophores, and 2) the globose-hyalinated accessory conidia (AC), which emerges laterally from hyphae. Disturbingly, there is prediction that 4% of all patients who die in hospitals die of invasive aspergillosis .

Aspergillus terreus causes severe loss to important crops worldwide, and destroying over 125 million tons of rice (Oryza sativa L.), wheat (Triticum aestivum), potato (Solanum tuberosum L.), maize (Zea mays) and soyabean (Glycine max L.) every year. Recently, Aspergillus terreus is shown to cause root rot diseases in wheat and Lolium species . In potato, foliar blight caused by a terreus amounts to 30-60% of the total leaf surface, but the infection process is not elucidated. [47]

1-7 Literature Survey of application for removal of dyes by using different surfaces:

The table below represents a comparison between the current work and previous research on the high ability of hydrogel to remove different types of dyes. This was reported in Table (1-5):

Table (1-5): Removal of pollutant Using Different Surfaces.

No.	Sorbent	Pollutant	T (°C)	pH	t /h	Dose (g)	Q_e (mg/g)	E%	C_o ($mg.L^{-1}$)	Ref.
1.	(SA-g-(PAAc-co -VBS) /ZnO	Crystal violet	30	6.6	2	0.03	956.56	>80	200	[48]
2.	SA-g-p(AAc-AAM)\BC hydrogel	Crystal violet	25	7	1	0.05	1.2422	-	100	[49]
3.	(SA-g-PAAc) Hydrogel	Rose Bengal	25	6	1	0.05	49.505	-	200	[50]
4.	Ag-g-PAAc / AC hydrogel	Crystal violet	25	6.2	1	0.05	180	90.56	100	[51]
5.	GO\ P(AAc - co-AM)	Congo red	20	6	2	0.05	52.55	-	200	[52]
6.	SA-g-(PAAc-co-AM)/CdS	Congo red	25	2	1	0.03	280	80.16	100	[53]
7.	NTADB-P-P(AAc-co-CA)	Methylene green	25	7	1	0.05	19.723	-	100	[54]
8.	SA-g-P(AAc-co -MA) /TiO_2	Brilliant green	25	6	1	0.05	1200	99.9	700	[55]
9.	(SA-PEO-MNIM)	Methylene blue	20	12	6	0.05	3021.0	93	500	[56]
10	(SA-g-p(AAc-co-VFA) hydrogel	Methylene green	25	5	23	0.1	1915	94	100	[57]
11	P (AAm - DADMAC) / CNS hydrogel	Methyl orange	25	7	2	0.1	409	-	100	[58]

12	(ItA-g-p(AAc-co-ANi)) hydrogel	Rhodamine B	25	7	1	0.03	925.9	85.2	50	[59]
13	(SA-g-p(VFA-co-AAc)\ BC) hydrogel	Methylene green	25	7	23	0.1	2108	-	200	[60]
14	(SA-g-pAAc) hydrogel	Crystal violet	25	7	1	0.05	333.33	-	250	[61]
15	GO/P (AAc-MA)	Crystal violet	25	7	2	0.05	163.934	-	200	[62]
16	(SA-poly(AAc)/ZnO)	Methylene blue	25	6	1	0.1	1129	90.2	100	[63]
17	SA-Gel-cl-pAAm	Crystal violet	30	5	16	0.03	0.03	86.9	10	[64]
18	SA-g-PAA/TiO2	Methyl violet	25	6	1	0.3	1156	98.2	100	[65]
19	poly (AAm-MA) hydrogel	Malachite green	25	7	1	0.05	19.4552	-	100	[66]
20	GK-cl-PAAc hydrogel	Malachite green	25	7	1	0.5	757.57	91	50	[67]
21	GK-cl-PAAc hydrogel	Rhodamine B	25	7	1	0.6	497.51	86	50	[67]

1-8 Objectives

This work aims to investigate the following:

1- Synthesizing a new adsorbent surface by the free-radical-induced graft copolymerization of Itaconic acid and VBS in the presence of alginate bio-polymer and RC, (SA-g-P(ITAc-co-VBS)/RC) hydrogel nanocomposite for the uptake of two dyes (Malachite green (MG) , and Brilliant Green (BG)).

2- The characterized SA-g-P(ITAc-co-VBS)/RC hydrogel nanocomposite is used as adhesives and dressings for the treatment of wounds and burns mousses, and also to inhibition the growth of two types of negative and positive bacteria and one type of fungus Aspergillus flavus.

3- Studying the Removal of laboratory sample aqueous pollutants by using SA-g-P(ITAc-co-VBS)/RC hydrogel nanocomposite

4- Determination two isotherms Freundlich, Langmuir and thermodynamic parameters as a models and determine the adsorption constants of two dyes on to hydrogel nanocomposite surfaces.

5- The prepared surface (super absorbent) was characterized by its ease of preparation and use as an environmentally friendly surface through recycling, revitalization, and its use more than once with diluted HCl and its use in removing pollutants to reduce the economic cost.

Chapter Two
Experimental Part

Experimental Part

2-1 Instruments

There are several techniques were used in the current study, most of them are listed in table (2-1) .

Table (2-1): Instruments used in this Research

No.	Instrument	Model	Company supplied	Location of current measurement
1	UV-Visible spectrophotometer, Double beam	PC 1650	Shimadzu, Japan	University of Babylon / College of science for women- Chemistry Department
2	UV-Visible spectrophotometer, Single beam	UV mini-1240	Shimadzu, Japan	University of Babylon / College of science for women- Chemistry Department
3	Field-Emission Scanning electron microscope (FE-SEM)	MIRA3	TESCAN ,Czechia Republic	University of Tehran
4	Transmission electron microscope (TEM)	912AB	Leo, Germany	University of Tehran
3	FTIR spectrophotometer	8400S	Shimadzu, Japan	University of Babylon / College of science for women- Chemistry Department
5	X-Ray diffraction (XRD)	D2 Phaser	Bruker AXS Gmbh, Germany	University of Tehran
6	Thermogravimetric analysis (TGA)	DTG-60	Shimadzu, Japan	University of Babylon / College of science for women- Chemistry Department
7	Energy Dispersion X-ray (EDX)	MIRA3	TESCAN ,Czechia Republic	University of Tehran

8	surface area analyzer (BET)	NanoSORD	Haskarsazan Iran	University of Tehran
9	Shaker water bath	CL002	K&K Scientific, Korea	University of Babylon / College of science for women- Chemistry Department
10	Centrifuge	CL008	JANETZI - T5, Belgium	University of Babylon / College of science for women- Chemistry Department
11	Ultrasound bath	405 power sonic	Hwashin, Korea	University of Babylon / College of science for women- Chemistry Department
12	Oven	LDO-060e	Labtech, Korea	University of Babylon / College of science for women- Chemistry Department
13	Hot plate stirrer	LMS-1003	Labtech, Korea	University of Babylon / College of science for women- Chemistry Department
14	pH meter	HI 83141	Hanna, Romania	University of Babylon / College of science for women- Chemistry Department

2-2 Chemical Materials

The chemical materials used in this study are shown in Table (2-2) :

Table (2-2): Materials used in the study, purity, and their manufacturers

No.	Material	Formula Compound	Molecular weight (g/mol)	Purity (%)	Supplier
1	Malachite green	$C_{23}H_{25}ClN_2$	364.9	99.8	Sigma-Aldrich
2	Brilliant green	$C_{27}H_{34}N_2.O_4S$	482.64	99.7	Sigma-Aldrich
3	Sodium hydroxide	NaOH	39.997	99.0	(B.D.H)
4	Sodium alginate (SA)	$C_6H_9NaO_7$	216.12	99.0	Sigma-Aldrich
5	Itaconic acid	$C_5H_6O_4$	130.099	99.9	Sigma–Aldrich
6	Potassium persulfate	$K_2S_2O_8$	270.3	99.5	Sigma-Aldrich
7	N´,N-methylene-bis-acrylamide	$C_7H_{10}N_2O_2$	154.17	> 99.5	Sigma – Aldrich
8	Sodium4-vinylbenzenesulfonate	$C_8H_7NaO_3S$	206.09	98.0	Sigma-Aldrich
9	Phosphoric acid	H_3PO_4	97.9	98.0	Sigma-Aldrich
10	Nitric acid	HNO_3	98.9	98	Sigma-Aldrich
11	Ethanol	C_2H_5OH	46.07	99.0	(B.D.H)

12	Methanol	CH_3OH	32.04	99.0	Sigma-Aldrich
13	Hydrochloric acid	HCl	37.46	37.0*	Sigma-Aldrich
14	Sulfuric acid	H_2SO_4	36.07	98*	Sigma-Aldrich

*(W/W)

2-3 Preparation of Activated Carbon (AC) :

The castor plant called Ricinus communis(RC) is a perennial shrub, obtained from farms in Iraq. Initially, Ricinus communis (RC) leaves is washed with distilled water to get rid of suspended dust, then dried in the sun and ground to obtain a powder sieved particle size of 25 - 50 µm. To preparation of acid activated carbon of Ricinus communis (ACRC). About 100g were impregnated with 4 % HCl with stirring about 2 hr. and washing in distilled water several time to remove the residual acid from pores of carbon until the pH to reached 7 ± 0.3. Then it was dried in oven at 60 ± 5ºC for 24h. Finally, the material is burned at a temperature (300^{o}C) for 2 hr. to obtain activated carbon (AACRC). Then ground, sieved to get the particle size of 25 - 50 µm, (AACRC) was stored in bottle an airtight to applied in experiments. [68] Note: used to prepare the activated carbon of Ricinus communis ACRC without the acid treatment. as shown in Schema (2-1).

Scheme (2-1): Preparation of activated carbon (AC)

2-4 Preparation of SA-g-P(ITA-co-VBS)/RC hydrogel nanocomposite

Synthesis of super-absorbent (SA-g-P(ITA-co-VBS)/ RC) hydrogel nanocomposite . A series of hydrogel utilizing several amounts of sodium alginate, initiator, cross-linked, monomers (ITA , VBS) and Ricinus communis (RC) were prepared by the following way to obtain the best optimum conditions: Sodium alginate SA (0.1–2) g was dissolved in deionized water 20 mL was taken in a 250 mL beaker and magnetic stirrer for 1 hr at 600 rpm. Suitable amounts of RC (0–2 g) were added with stirring to form a solution and after stirring 10 min, (0.5-2g) of Itaconic acid(ITA) was dissolved in 10 mL of deionized water, certain amount of VBS (0.1–2.5 g), N,N'-methylene-bis-acrylamide (MBA) (0.003–0.1 g) and potassium per-sulphate KPS (0.03–0.1 g), dissolved in 3 mL of water were added. Then, 2hr of free radical co-polymerization at 75 ◦C had been carried out. The transparent in-soluble colloidal gel has been attributed to the of (SA-g-P(ITA-co-VBS)/RC) hydrogel nanocomposite formation. The hydrogel was washed thoroughly with an ethanol/water mixture (4:1 v/v), and hydrogel was cut into little pieces and washed by distilled water for several time to get rid of unreacted chemicals, dried in an oven at 60 °C [48], finally stored in a desiccator as shown in Schema (2-2).

Based on these results, the formation mechanism of SA-g-P(ITA-co-VBS)/RC is proposed as shown in Schema (2-3a). Free radicals are generated from the decomposition of initiator and transferred onto SA to initiate the polymerization of ITA and VBS. Both monomers are then grafted onto the SA backbone. Polymer chains are then cross-linked to form a three-dimensional (3D) network as the cross-linker added. Also, Scheme (2-3b) shows the proposed adsorption process of dyes.

Study of several reaction parameters to performed optimize the (SA-g-P(ITA-co-VBS)/ RC) hydrogel nanocomposite for superior swelling in water. like (reaction contact period, temperature variation, solvent volume, pH, variation in quantity of monomer, initiator, and cross-linker) .

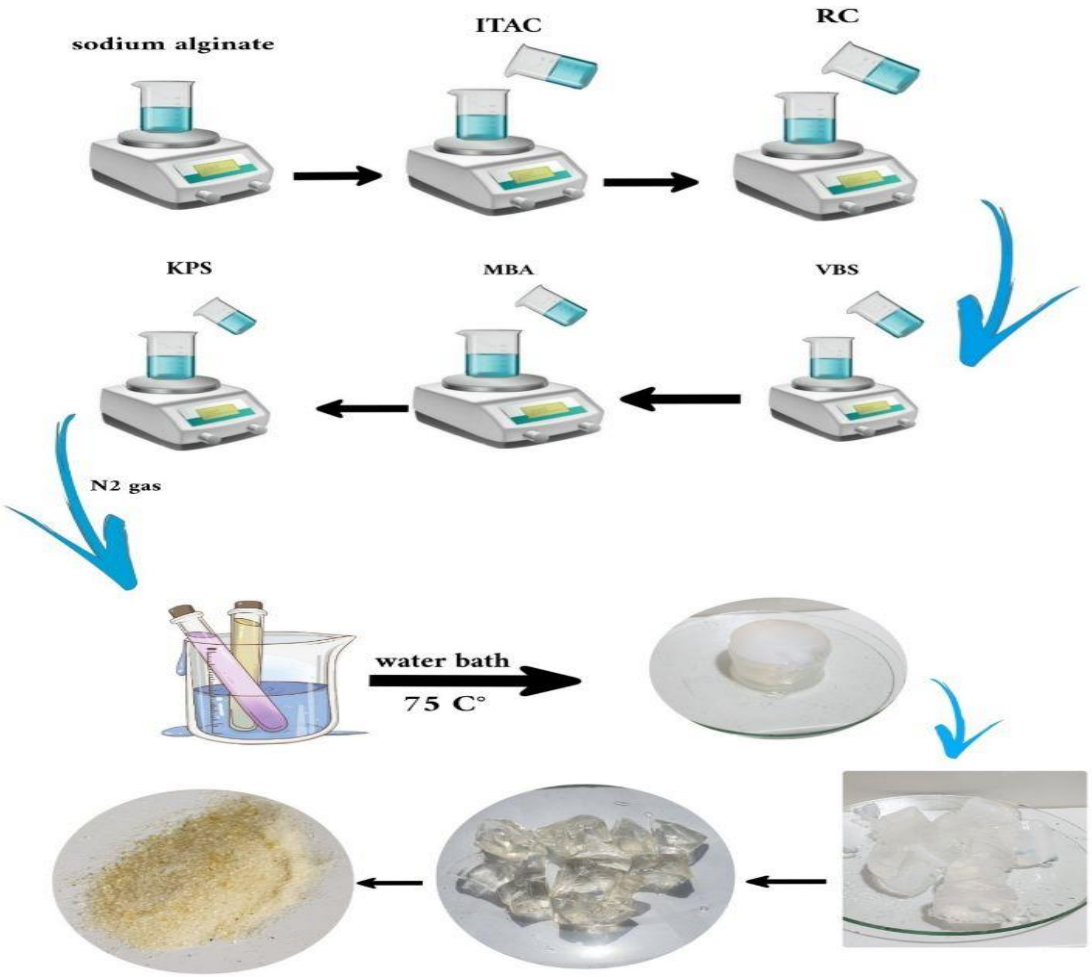

Schema (2-2): Preparation of (SA-g-P(ITA-co-VBS)/ RC) Hydrogel

(a)

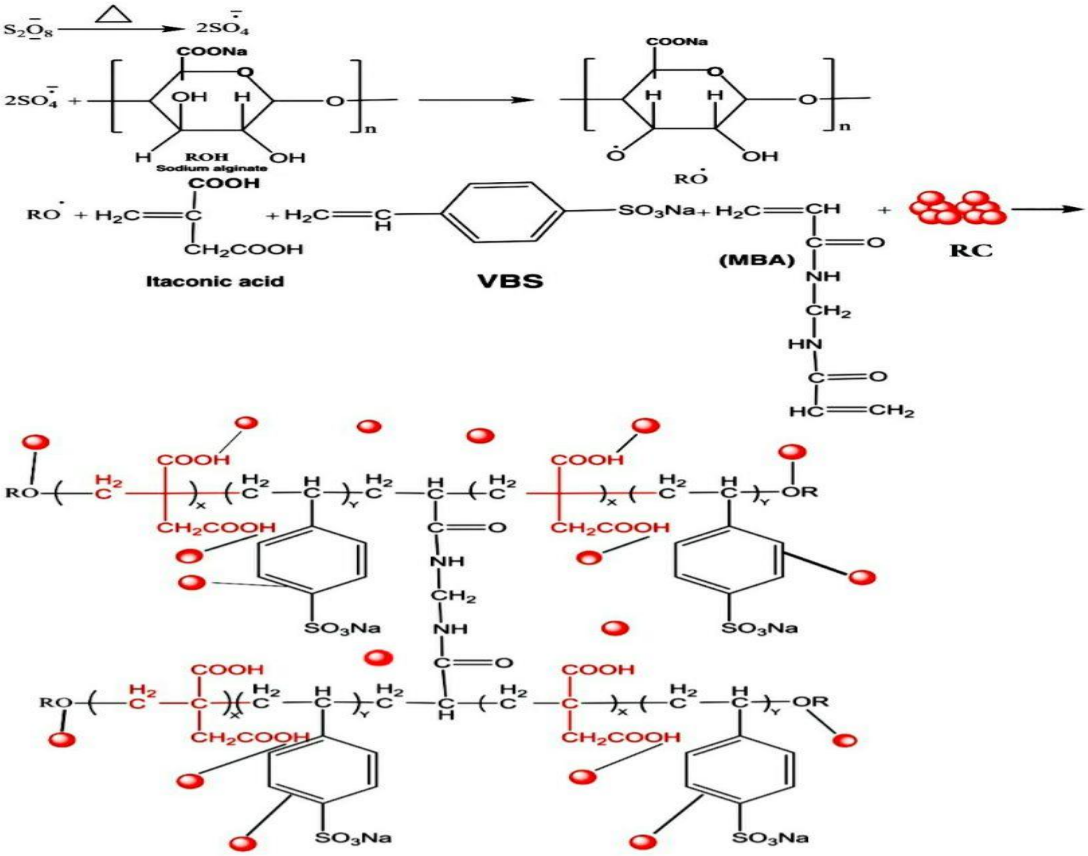

(b)

Scheme (2-3): (a) proposed the mechanism formation of SA-g-P(ITA-co-VBS)/RC, (b) Image shows the proposed adsorption process of MG and BG dyes.

2-5 Swelling Studies of (SA-g-P(ITA-co-VBS)/ RC) Hydrogel Nanocomposite

The pre-weighted (SA-g-P(ITA-co-VBS)/ RC) hydrogel nanocomposite was placed in deionized water and kept at room temperature (25 ^{o}C) for 24 h without any disturbance. The swollen (SA-g-P(ITA-co-VBS)/ RC) hydrogel nanocomposite blotted with filter paper to remove the extra water, and then weighed. An analytical weighing balance was used to weigh the swelled (SA-g-P(ITA-co-VBS)/ RC) hydrogel nanocomposite. The maximum swelling percentage was determined using the following equation: (2-1) as:

$$\% \textbf{ Swelling} = \frac{\mathbf{Ws - Wd}}{\mathbf{Wd}} \times \mathbf{100} \qquad \textbf{(2 -1)}$$

Ws denotes the weight of the swelled (SA-g-P(ITA-co-VBS)/ RC) hydrogel nanocomposite, while Wd denotes the weight of dried (SA-g-P(ITA-co-VBS)/ RC) hydrogel.

2-6 Characterization and Measurements of the prepared hydrogel Nanocomposites

The prepared samples were examined using ultraviolet-visible spectroscopy (UV–Vis) , transmission electron microscopy (TEM), Field emission scanning electron microscopy (FE-SEM), X-ray diffraction spectroscopy (XRD), Thermal gravimetric analysis (TGA), Fourier Transform Infrared (FT-IR) .

2-6-1 Ultraviolet-Visible Spectroscopy (UV–Vis)

An important technique used to measure absorption and transmission for dye solution. Where 0.1 g.L^{-1} of the composite was placed in the dye solution and then filled the quartz cells for measurements wavelength and concentration.

2-6-2 Fourier Transform Infrared (FT-IR) Analysis

FTIR spectra were recorded using the FTIR instrument (Shimadzu. 8400S) in the 4000-400 cm^{-1} frequency range. Dried absorbance (1 mg) was mixed with KBr powder (10 mg) in an agate mortar. The mixture was pressed into a pellet under 10 tons load for 2–4 min, and the spectrum was recorded immediately.

2-6-3 Field Emission Scanning Electron Microscopy (FE-SEM)

FE-SEM is a powerful device that is used in characterizing sample morphology such as grain size, particle size, particle distribution, crystal defects, and surface structure. FE-SEM has several features like a large depth of field, higher resolution, and more control in the degree of amplification because it also uses electrons as the probe Aboutb50μL of aqueous or ethanol suspension of sample was placed on a clean silicon wafer surface. Then dried at $80^{o}C$ to remove the solvent.

2-6-4 Transmission Electron Microscopy (TEM)

TEM is a microscopy technique that is used as a beam of electrons transmitted across an ultra-thin sample where the electrons are transformed into light and form an image. TEM provides information on phase composition, structure, and lattice defects.

2-6-5 Thermogravimetric analysis (TGA)

The thermodynamic analysis is performed to determine the thermal stability of prepared nanomaterials and to determine the purity of these particles. The sample was heated from 10 °C to 600 °C and at a heating speed of 10 $°C.min^{-1}$.

2-6-6 X-ray Diffraction Spectroscopy (XRD)

X-ray diffraction is a powerful nondestructive technique for characterizing crystalline materials. Provides information about the average spacing between layers or rows of atoms, the orientation of a single crystal or grain, the crystal structure of an unknown material, measures the size, shape, and internal stress of small crystalline regions. The crystalline properties of materials prepared using an X-ray deflection technique were studied using a single-wavelength light (1.5104nm) from the CuKα source using nickel as a filter. Where the range is taken from deviation angles (2Θ) in this measurement is between (5-80) degrees.

2-7 Removal of Dyes by Using (SA-g-P(ITAC-co-VBS)/RC) surfaces as Adsorbents

2-7-1 Determination of optimum wavelengths (λmax) and Calibration curves of (Malachite green (MG) , and Brilliant green (BG) dyes.

2-7-1-1 Malachite green (MG)

A Malachite green dye is a very well-known cationic dye that has a molecular formula ($C_{23}H_{25}ClN_2$), and molecular weight (364.9g/mol); the dye is odourless green crystals powder used for various purposes. A stock solution (1000 mg L^{-1}) was prepared by dissolving (1.0 g) of dye in (1000 mL) distilled water.

To determine the maximum wavelength of Malachite green dye the ultraviolet-visible absorption spectra of Malachite green dye solution was recorded within wavelengths of 200-800 nm. Where the maximum wavelength of the solution was determined from its highest absorption in the UV-Vis spectrum found at the wavelength λ_{max} MG= 624 nm in Figure (2-4).

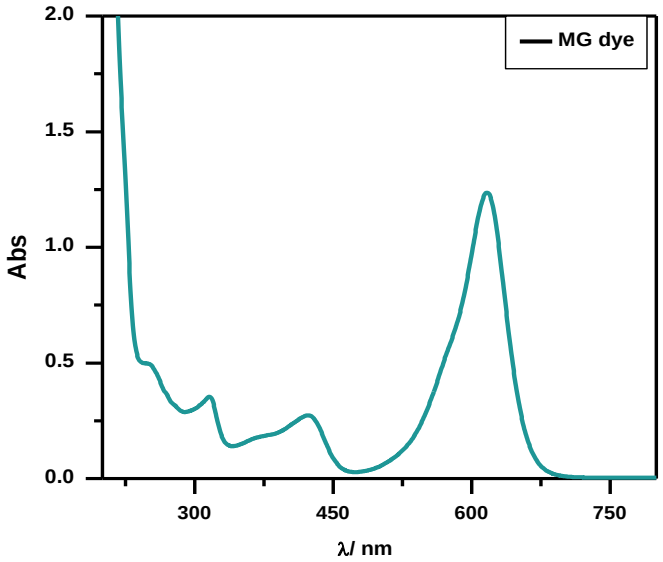

Figure(2-4): UV-Visible Absorption Spectra of Malachite Green (MG) dye

.

The calibration curve of different concentration of MG dye was prepared in serial dilutions (2-30 mg.L^{-1}). Absorbance was measured at the λ_{max} MG dye and plotted against the concentration values of MG dye in (Figure 2-5).

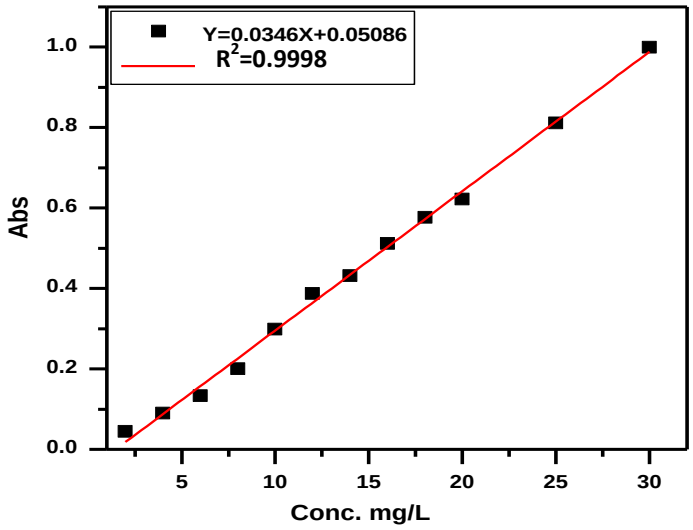

Figure (2-5): Calibration curve for Malachite Green(MG) dye .

2-7-1-2 Brilliant Green (BG)

A Brilliant Green (BG)dye is a very well-known cationic dye that has a molecular formula ($C_{27}H_{34}N_2.O_4S$), and molecular weight (482.64 $g.mol^{-1}$); the dye is BG powder used for various purposes. A stock solution (1000 $mg.L^{-1}$) was prepared by dissolving (1.0 g) of brilliant green in (1000 mL) distilled water.

To determine the maximum wavelength of Brilliant Green (BG) dye, the ultraviolet-visible absorption spectra of BG dye, solution recorded within wavelengths of 400-800 nm. While the maximum wavelength of the solution was chosen as the highest absorption in the UV-Vis spectrum found at the wavelength λ_{max} BG= 630nm, as shown in Figure (2-6).

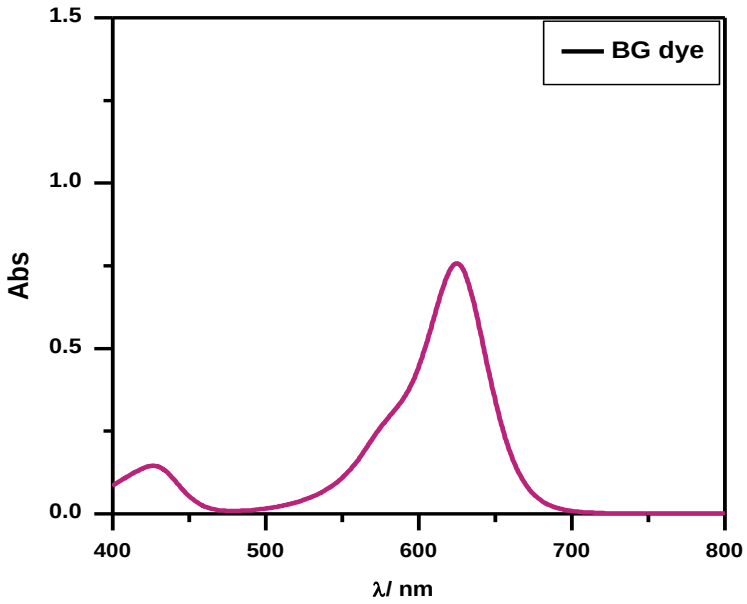

Figure(2-6): UV-Visible absorption spectra of Brilliant Green (BG)dye

The calibration curve of different concentration of Brilliant Green (BG)dye was prepared in serial dilutions of (2-20 $mg.L^{-1}$). Absorbance was measured at the λ_{max} for BG dye and plotted against the concentration values of BG dye in (Figure 2-7) .

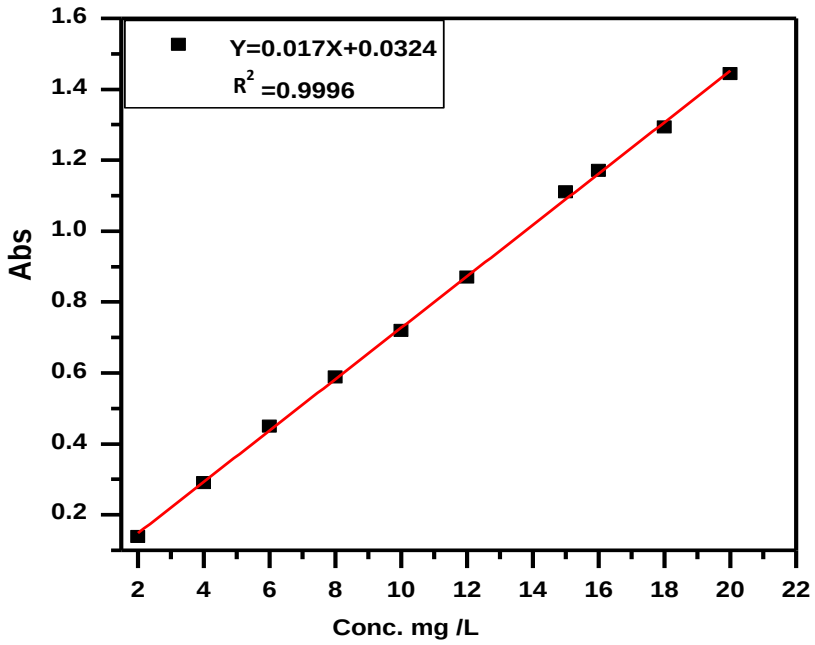

Figure (2-7): Calibration curve for Brilliant Green (BG)dye.

Table (2-3): Statistics data of calibration for different concentrations of Malachite green (MG), and Brilliant Green (BG) dye.

Parameters	Proposed Method MG	Proposed Method BG
λ_{max} (nm)	624	630
Beer's law limit ($mg.L^{-1}$)	2-30	2-20
Regression equation	(Y = m X + C) Y=0.0346X+0.05086	(Y = m X + C) Y=0.017X+0.0324)
Slope (m)	0.0346	0.017
Intercept (C)	0.05086	0.0324
Correlation coefficient (R^2)	0.9998	0.9996
Colour	Green	Blue

2-8 Effect of different parameters on the adsorption process

2-8-1 Effect of contact time

100 mL of two dyes solution (700 mg.L^{-1}) With different time periods(2-120) minute is prepared and put in a conical flask with adsorbent concentration (0.05 g/100 mL) of SA-g-P(ITA-co-VBS)/RC at 25°C and 220 rpm Shaking speed and kept separately in a shaker the water bath controlled temperature. Two dyes concentration to be estimated spectrophotometrically at the wavelength corresponding to maximum absorbance, λ_{max}, using a double beam UV-Visible spectrophotometer. The samples at different interval times are separated by the centrifugation process. The absorbance of the solution is then measured; the dyes concentration was measured after (2- 120) minute until equilibrium is reached.

The adsorption capacity was calculated from equation (2-2): [31]

$$\boldsymbol{Qe = \frac{(C_0 - C_e) * V_L}{m_g}} \qquad (\mathbf{2-2})$$

Where: Q_e = Amount of dyes adsorbed per unit mass of adsorbent (mg/g).

C_o= Initial concentration (mg.L^{-1}).

C_e= Equilibrium concentration (mg.L^{-1}).

m = Dose of adsorbent (g).

V_L= is the volume of solution (L).

The percentage removal (E%) of the dyes was calculated based on the reduction in absorbance at λ_{max} value of the dyes as follows:[31]

$$\boldsymbol{E\ \% = \frac{C_{o-}C_e}{C_o} * 100} \qquad (\mathbf{2-3})$$

Where: C_o and C_e are initial and equilibrium concentrations, respectively.

2-8-2 Effect of Dose of Adsorbent

The study was carried out with different doses (0.01, 0.025, 0.05, 0.08, and 0.1) g for (SA-g-P(ITA-co-VBS)/RC) .The concentrations of the samples were (700 $mg.L^{-1}$). The solutions were kept in the shaker water bath at (220 rpm) about (1hr.) at a fixed temperature (25 ^{o}C) and pH 7, the remaining dyes concentration in the aqueous phase was measured spectrophotometrically at the chosen wavelength**.**

2-8-3 Effect of Initial Concentration of Dye

A series of different concentrations of 100 mL of dyes has been used in this study (100- 1000) $mg.L^{-1}$, were added to a conical flask (Erlenmeyer) in the presence of (0.05g/100 mL) of SA-g-P(ITA-co-VBS)/RC at 25°C and 220 rpm shaking speed these series were putting in a shaker water bath for 1 hr. , after that the supernatant was separated by centrifuge and the remaining concentration of dyes in the aqueous phase was measured spectrophotometry for the chosen wavelength.

2-8-4 Effect of pH

The effect of dyes solution pH on the dyes removal is examined by varying the initial pH of the dyes solutions (3-10) using conical flasks (100 mL) container at (700 $mg.L^{-1}$) for each dye. The pH was adjusted by using (0.1N) HCl and/or (0.1N) sodium hydroxide (NaOH) and was measured using a pH meter. Then (0.05g/100 mL) of SA-g-P(ITA-co-VBS)/RC adsorbent was added in to each conical flask.

The flasks were put inside the shaker water bath (220 rpm fixed throughout the study) maintained at 25^{o}C and the final concentration of dyes was measured using a single beam UV-Vis spectrophotometer .

2-8-5 Effect of Temperature

The adsorption experiments were performed at different temperatures (15-35°C) in a thermostat water bath with a shaker. The effect of temperature was investigated with (0.05g) dose of adsorbent SA-g-P(ITA-co-VBS)/RC mixing with (100mL) aqueous solution of dye concentration (100-1000) $mg.L^{-1}$, and the samples was shaking at a period for (1 hr.), then measured the remaining dyes concentration in the aqueous phase is measured spectrophotometry for the chosen wavelength.

2-9 Determination of Point zero charge (pHpzc) of SA-g-P(ITA-co-VBS)/ RC Hydrogel Nanocomposite

Zero-point charge (pHpzc) of hydrogel surface is the point where its surface has potential zero charge. The pHpzc determination was carried out by pH titration procedure. The solution pH initial in each conical flask was adjusted to a value 2-10 by addition of 0.1 N NaOH and HCl solution . The hydrogel was immersed in the prepared solutions and shaken 220 rpm, at room temperature($25^{o}C$) for 24 h. and then pH of was recorded pH final. The value of pHpzc is the point where the curve pH final vs pH initial crosses the line pH initial = pH final.

2-10 Adsorbent Regeneration Experiments

To investigate the reusability of the adsorbent, 0.5g of SA-g-P(ITA-co-VBS)/RC adsorbent was added into 100 mL for each of (MG, BG) dyes solution of concentration 700 $mg.L^{-1}$ at $25^{o}C$ temperature and pH 7 to achieve saturated adsorption. The SA-g-P(ITA-co-VBS)/RC was regenerated in excess desorption studies were carried out using different desorption agents at concentration (0.01 N) such as H_2SO_4, NaOH, H_3PO_4 , HCl , HNO_3, and water to regenerate anionic binding sites and finally washed with excess distilled water prior to be used in the next adsorption

cycle. An adsorption and desorption cycle was repeated four additional times using 100 mL of dyes solution of concentration 700 mg/L at 25^{o}C temperature and pH of 7.

2-11 A Comparative Adsorption Between Different Surfaces

A sample of 100 mL of two dyes concentration (700 mg. L^{-1}) are used in this study, then added to a conical flask (Erlenmeyer) in the presence of 0.05g from prepared (hydrogel\RC, hydrogel, RC), and put in a shaker water bath for 1 hr., after that the supernatant was separated by centrifuge and measured the remaining concentration by using UV-Visible spectrophotometer for the chosen wavelength.

2-12 Removal of Pollutants (Dyes) by Using SA-g-P(ITA-co-VBS)/RC

A laboratory sample 100mL of dye pollutants containing (Brilliant Green(BG) , Congo red (CR), Methyl Violet (MV), Crystal Violet (CV), Methylene Blue (MB) , Brilliant Blue (BB) , Direct yellow (DY) ,Reactive blue (RB) with a riffle concentration were using in this study, then added to a conical flask (Erlenmeyer) in the presence of 0.05g from prepared SA-g-P(ITA-co-VBS)/RC, after that the mixture were putting in Shaker water bath for 1hr, after that the supernatant were separated by centrifuge and measured the remaining concentration by using UV-Visible spectrophotometer .

2-13 Bacterial Biological Activity Test

The types of Gram-positive bacteria (*Streptococcus pneumonia*) and Gram-negative bacteria (*Pseudomonas aeruginosa*), and fungus (A.F) were obtained from the Department of Life Sciences / College of Science for women - University of Babylon. Hinton agar and Mannitol salt agar as media for cultivation, isolation, and differentiation between positive and negative bacteria. And the fungus (Aspergillus flavus) was obtained from the Department of Life Science\ College of Science for Women - University of Babylon. and potato dextrose agar (pda) was used as a medium for cultivation and activation of the fungus.

2-13-1 Preparation of Standard Solutions For Bacteria

Mueller Hinton agar medium was prepared by dissolving (37 gm) of the culture medium in 1 liter of distilled water, the mixture was heated until the agar dissolved, then putting the culture medium in an autoclave at a temperature of 120 ^{o}C for 15 minutes). then pour the medium into sterilized glass dishes (Petri disk) at a rate of (15-20) milliliters per plate and left until solidification completes, then the dishes were placed in the incubator for (24 hrs.) at a temperature (37 ^{o}C) to make sure that there were no any contaminate it.

2-13-2 Preparation of Standard Solutions For Fungus

Potato dextrose agar medium was prepared by dissolving (37 gm) of the culture medium in 1 liter of distilled water, then heating the mixture until the agar dissolved, next putting the

culture medium in an autoclave at a temperature of 120 ^{o}C for 15 minutes). then pour the medium into sterilized glass dishes (Petri disk) at a rate of (15-20) milliliters per plate and left until solidification completes, then the dishes were placed in the incubator for (24 hrs.) at a temperature (37 ^{o}C) to make sure that there were no any contaminate it.

2-14 Treating Mice Wounds Using a Surface Prepared from SA-g-P(ITAc-co-VBS)/RC

Mice were obtained from the animal house of the College of Veterinary Medicine at Al-Qadisiyah University, where the rats were wounded with a wound of medium depth and this wound was bandaged by loading (0.1 g) of hydrogel and the rates of wound healing after surface loading were studied from (1-7) days depending on the superior surface hydrogel properties on wound healing and the ability to deliver it to the inside of the wound.

Chapter Three
Results and Discussion

3-Results and Discussion

3-1 Physicochemical characterization of adsorbents surfaces

3-1-1 FTIR Characterization for Adsorbent/Adsorbate

Fourier-transform infrared spectroscopy FTIR technique was used to analyses the surface functional groups responsible for two dyes (MG, and BG) adsorption. Adsorbent surfaces RC, SA-g-P(ITA-co-VBS), SA-g-P(ITA-co-VBS)/ RC, and dye-loaded adsorbent sample after adsorption was placed in an oven at 65 ˚C for 4 hr. Samples were made as pellet and then the infrared spectra of MG and BG dyes on adsorbents before and after the adsorption process was recorded in the range 4000–500 cm^{-1} on an Infrared spectrophotometer. Results are shown in figures (3-1) and (3-2).

Figures (3-1,3-2) shows a broad peak at 2500 to 3600 cm^{-1} in the spectrum of alginate and is attributed to the COOH groups, and little change was observed in peak intensity after modification of alginate with RC. [69]. The grafting of Itaconic acid(IA) on sodium alginate (SA) is supported by a new characteristic adsorption band 1720 cm^{-1}, assigned to C=O stretching of poly (Itaconic acid) in the spectrum of SA-g-P(ITA-co-VBS)/ RC. Moreover, the RC of broad band at 1600 cm^{-1} is assigned to the stretching band of (C= O) groups[70, 71]

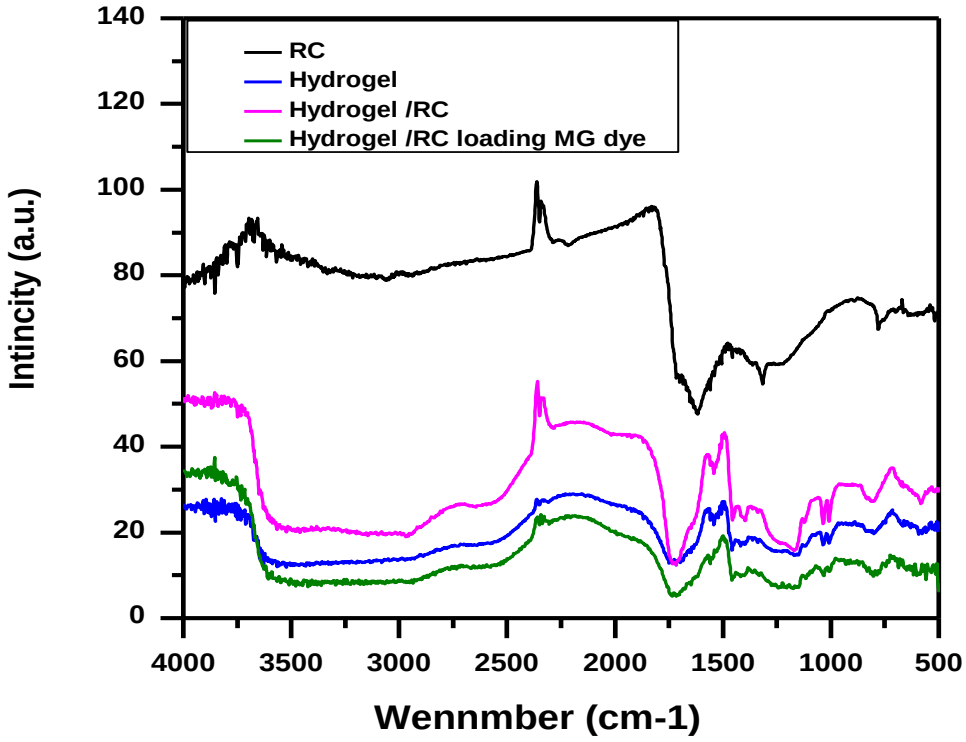

Figure (3-1) FT-IR spectra of RC, SA-g-P(ITA-co-VBS) and SA-g-P(ITA-co-VBS)/ RC) surface before, and after adsorption of MG dye .

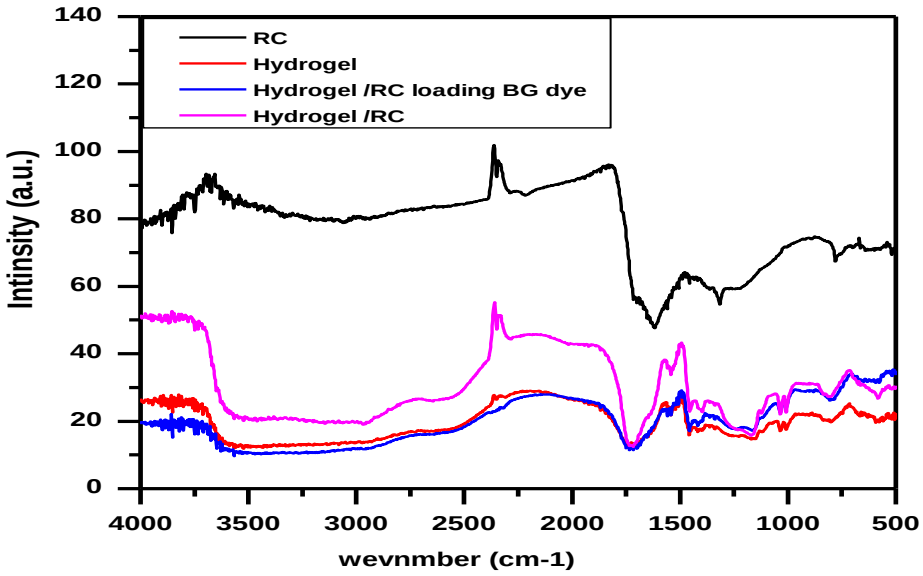

Figure (3-2): FT-IR spectra of RC, SA-g-P(ITA-co-VBS) and SA-g-P(ITA-co-VBS)/ RC) surface before, and after adsorption of BG dye .

3-1-2 Field Emission Scanning Electron Microscopy (FE-SEM) and, Energy Dispersive X-Ray (EDX) characterization for Adsorbent/Adsorbate

Field Emission Scanning Electron Microscopy (FESEM) was carried out to understand the particle size, shape, FESEM images of RC, (SA-g-P(ITA-co-VBS)) , (SA-g-P(ITA-co-VBS)/ RC) and (MG, and BG) dyes adsorbed (SA-g-P(ITA-co-VBS)/ RC) hydrogel nanocomposite are appear in Figure (3-3). The RC was found to have a homogeneous and smooth surface with no irregularities (Fig. 3-3 (a)). FESEM image of (SA-g-P(ITA-co-VBS) exhibited three-dimensional porous net-work structure with interconnected channels of pores and much rougher surface (Fig. 3-3 (b)). [72]It is clearly seen in the FESEM image of (SA-g-P(ITA-co-VBS)/ RC) that it has a layered morphology and appear comparatively less uniformity and more roughness after the attachment of RC with the hydrogel and the considerably high adsorption efficiency of (SA-g-P(ITA-co-VBS)/ RC) was due to the presence of these interconnected channels of pores in its structure (Fig. 3-3 (c)). After adsorption of MG dye, the surface area of hydrogel to become rough representing the successful surface adsorption (Fig. 3-3 (d)). EDX analysis was performed to investigate the elemental composition of (SA-g-P(ITA-co-VBS)/ RC). As observed from (Fig. 3-3 (f)), Ca, C, and O peaks confirm the formation of (SA-g-P(ITA-co-VBS)/ RC), Moreover, the Ca, C, and O contents were found to be 6.46%, 49.48%, and 44.04%, respectively [73, 74].

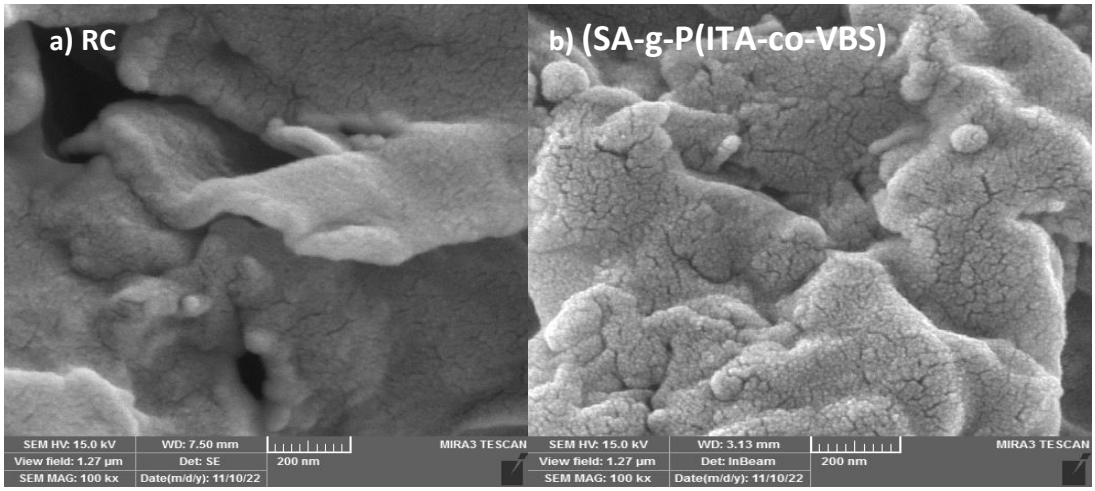

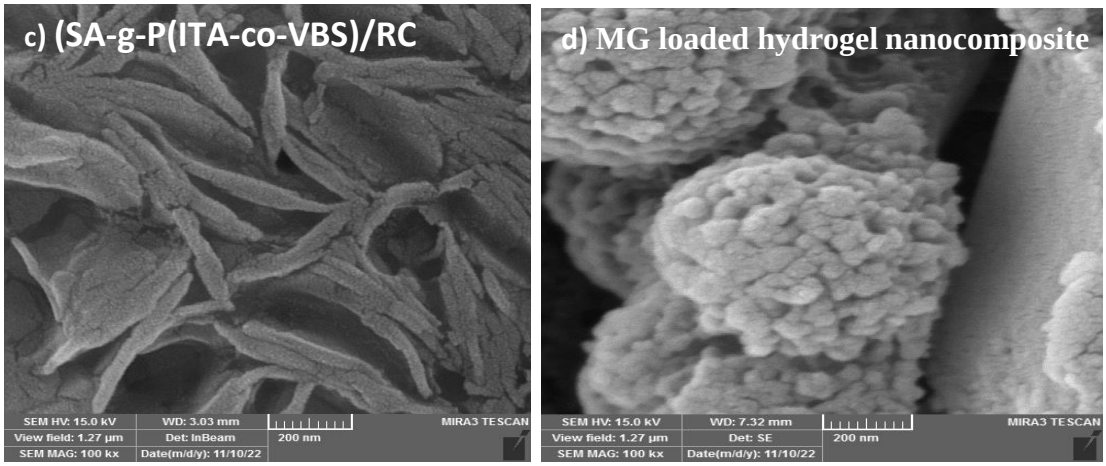

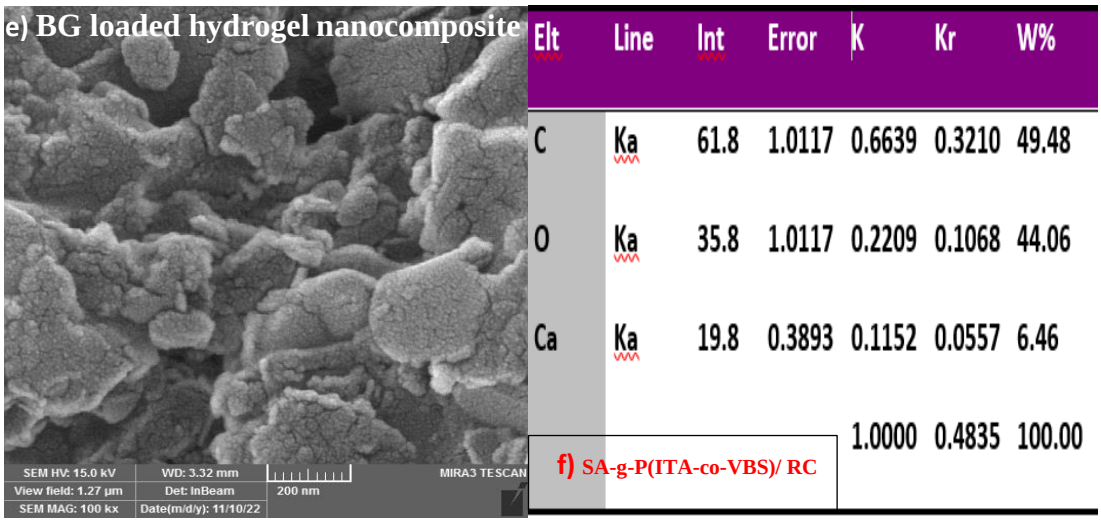

Elt	Line	Int	Error	K	Kr	W%
C	Ka	61.8	1.0117	0.6639	0.3210	49.48
O	Ka	35.8	1.0117	0.2209	0.1068	44.06
Ca	Ka	19.8	0.3893	0.1152	0.0557	6.46
				1.0000	0.4835	100.00

f) SA-g-P(ITA-co-VBS)/ RC

Figure (3-3): FESEM images of (a) RC, (b) (SA-g-P(ITA-co-VBS)) (c) , (SA-g-P(ITA-co-VBS)/ RC), (d) MG loaded (SA-g-P(ITA-co-VBS)/ RC), (e) BG loaded (SA-g-P(ITA-co-VBS)/ RC)and (f) EDX of (SA-g-P(ITA-co-VBS)/ RC).

3-1-3 Transmittance Electron Microscopy (TEM)

Transmittance Electron Microscopy TEM images appear the morphology of the surfaces RC , (SA-g-P(ITA-co-VBS) , and (SA-g-P(ITA-co-VBS)/ RC) hydrogel nanocomposites ; as shown in figure(a-b) (3-4) the cloud was more available and new geometry was created after decorated the RC on the surface of hydrogel nanocomposite , this may be attributed to the role of amount of RC on the hydrogel [75]. it can be seen that RC exhibited a spherical shape , show in Figure a(3-4) , also in Figure b(3-4) (SA-g-P(ITA-co-VBS) appear irregular balls along with some patchy shapes and has a tendency to form chain-like totals at 50 nm. moreover, the surface of the (SA-g-P(ITA-co-VBS)/ RC) is covered by a transparent layer, where RC was observed embedded inside the (SA-g-P(ITA-co-VBS)/ RC) and RC play pivotal role in improving stability and increase surface area as a requisite constituent of synthesize eco-friendly hydrogel nanocomposite as shown in Figure c(3-4) [76].

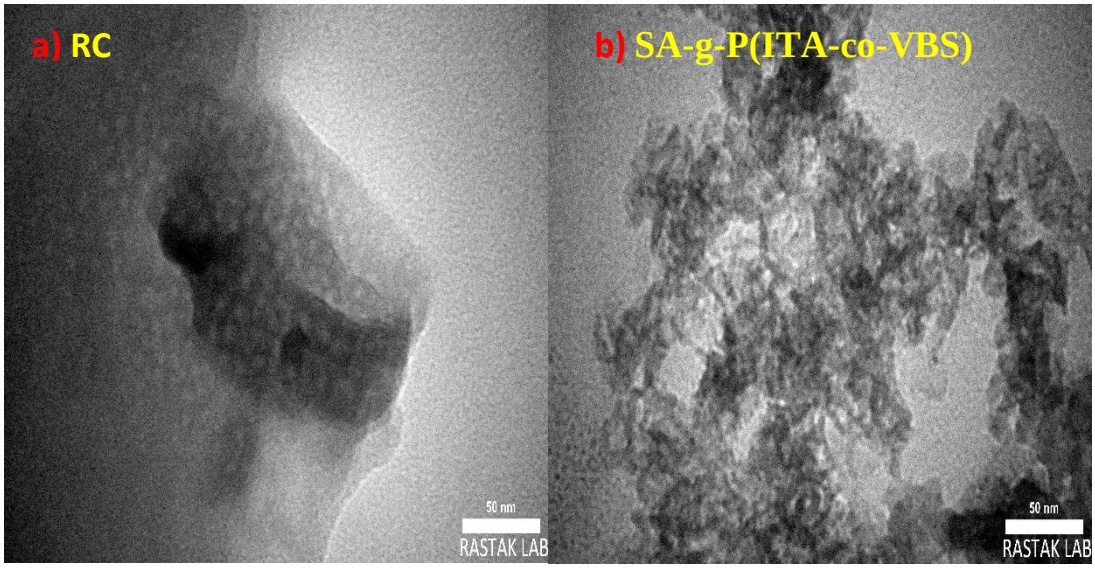

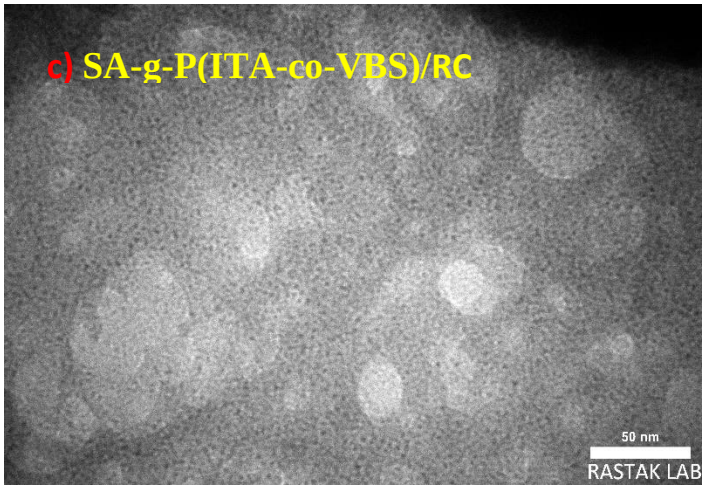

Figure (3-4): TEM Images of (a) RC , b) SA-g-P(ITA-co-VBS) , and c) (SA-g-P(ITA-co-VBS)/ RC)

3-1-4 Thermogravimetric Analysis (TGA)

The thermal gravimetric analysis of the hydrogel was investigated. TGA curves of the RC, SA-g-P(ITA-co-VBS), and SA-g-P(ITA-co-VBS)/ RC obtained at a heating rate of 5 ◦C/min up to 600 ˚C under a dry nitrogen flow is shown in (Figure 3-5 to 3-7); one can see that the degradation process is different. It is well- known that any weight loss below 200 ◦C is due to the loss of unbound water, while the loss in the range of 200− 600 ◦C is mainly due to the organic matter degradation. By analyzing the thermograms of RC, SA-g-P(ITA-co-VBS) and SA-g-P(ITA-co-VBS)/RC, it is quite clear that the incorporation of RC has an approving effect on the thermal stability of the biopolymer matrix since we have a decrease of the weight loss percentage. In fact, the virgin biopolymer lost about 85 % of its total weight, which implies that it is totally degraded up to 600 ◦C, unlike hydrogel supported RC of which the total weight loss is of the order of 42.1 % [77]. This means that there was a creation of a resistant path through the polymer matrix by RC to retard the decomposition process. Similarly, by examining the thermograms of

SA-g-P(ITA-co-VBS) and SA-g-P(ITA-co-VBS)/ RC , it can detected an enhancement in thermal stability attributed to the RC loading. It is very common that the nanocomposite's thermal degradation is affected by the presence of organic and inorganic materials at their surface. In fact, in our case the bonds at the biocomposite surface are originated from the interaction between RC and COO^- biopolymer groups. which gives rise to more stable complexes. Thusly, the latter ameliorates the SA-g-P(ITA-co-VBS)/ RC thermal stability [25, 76].

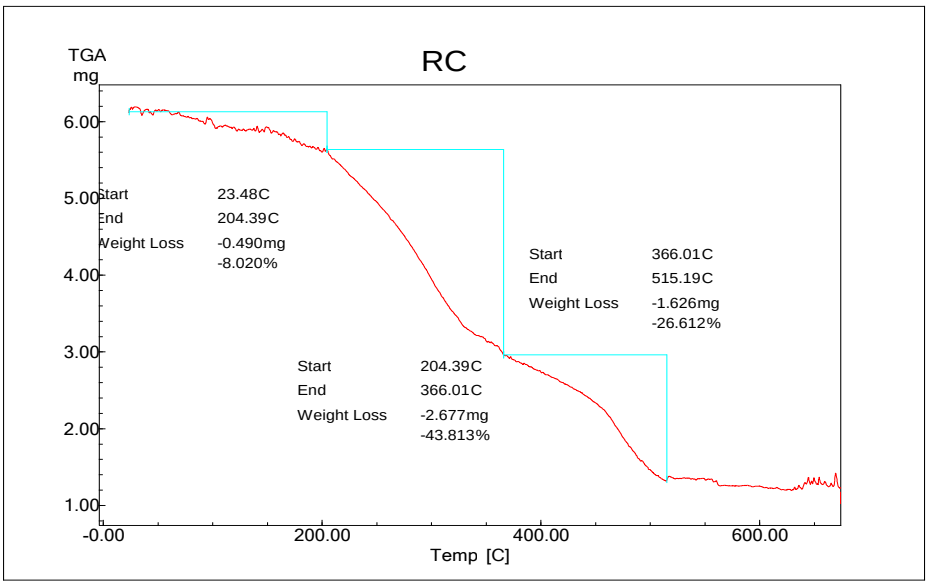

Figure (3-5): Thermal Gravimetric Analysis Curve of the RC.

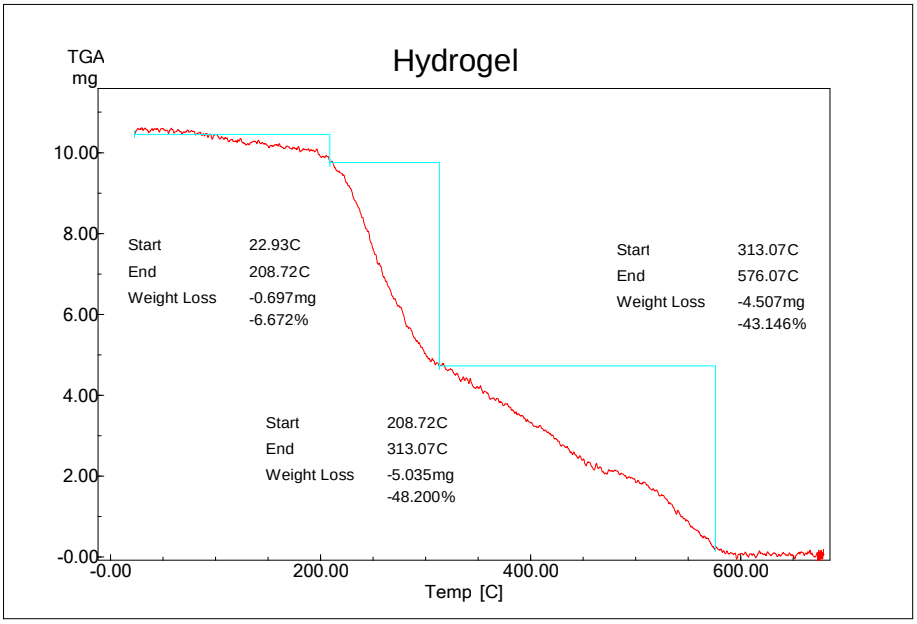

Figure (3-6): Thermal Gravimetric Analysis Curve of the SA-g-(PAAC-co-VBS)

.

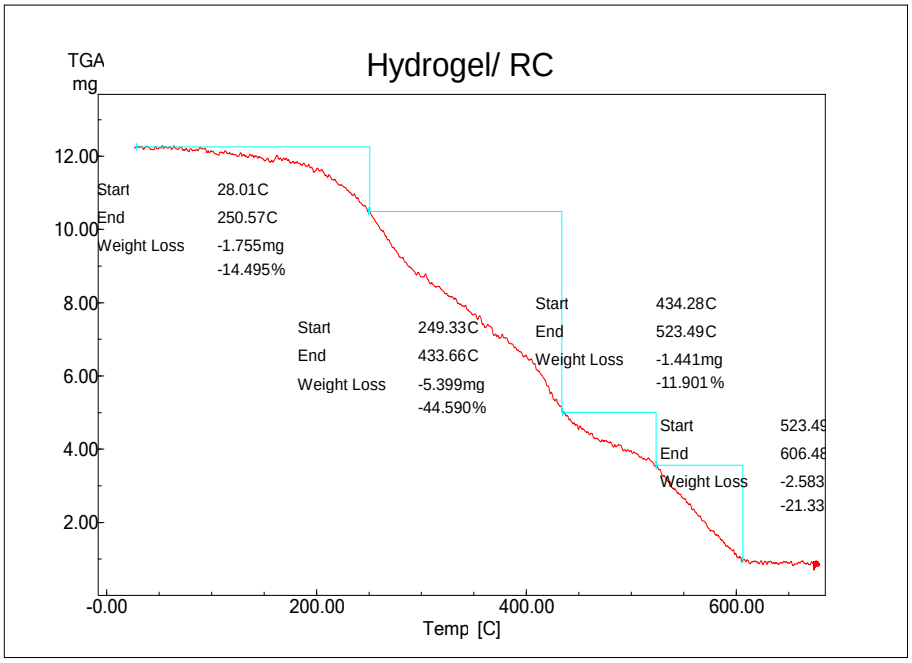

Figure (3-7): Thermal Gravimetric Analysis Curve of the SA-g-(PAAC-co-VBS)/RC .

3-1-5 X-Ray Diffraction (XRD)

X-ray diffraction is measured to study the crystal phases and the purity components of nanomaterials. It gives detailed information about the lattice parameter, lattice defects, lattice strain, crystallite size (in the case of nanoparticles), and the type of molecular bond of the crystalline phase. The XRD patterns of RC, (SA-g-P(ITA-co-VBS), and (SA-g-P(ITA-co-VBS)/ RC) are shown in Figure (3-8). RC appear one dispersion peak at $2\Theta = 18.6^{o}$ due to its semi-crystallinity [78]. thus (SA-g-P(ITA-co-VBS)/ RC), soft and weakened peaks appear at $2\Theta = 18.6^{o}$, and 20°. This shows the semi-crystallinity structure of the (SA-g-P(ITA-co-VBS)/ RC). These characteristic peaks disappeared in the XRD patterns of the (SA-g-P(ITA-co-VBS) and a new weak dispersion peak appeared at $2\Theta = \sim 21.0^{o}$, indicating that graft co-polymerization weakened the structure of hydrogel [79].

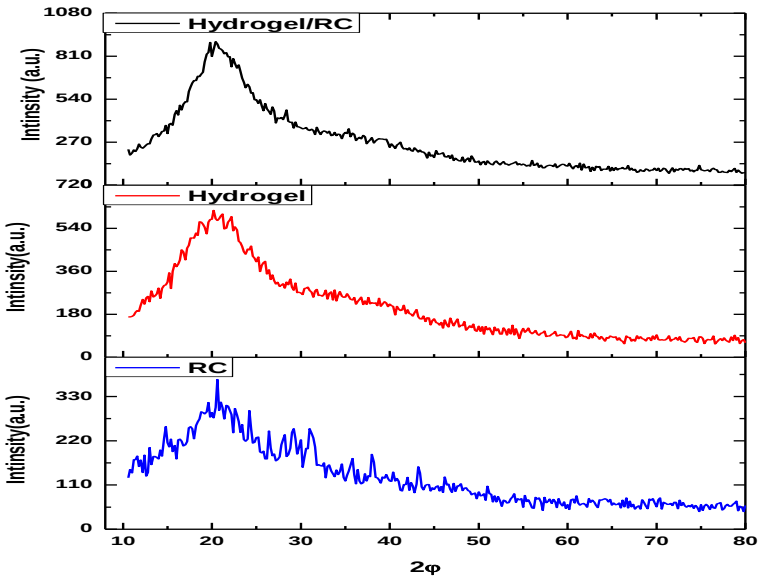

Figure(3-8):X-ray diffraction patterns for (a) RC, (b) (SA-g-P(ITA-co-VBS) ,(d) (SA-g-P(ITA-co-VBS)/ RC).

3-1-6 Surface Area Analyzer (BET)

The surface area and pore structure of (SA-g-P(ITA-co-VBS), and (SA-g-P(ITA-co-VBS)/RC) hydrogel nanocomposite is determined by employing the nitrogen isothermal adsorption technique. The nitrogen adsorption-desorption isotherms and pore size distributions of (SA-g-P(ITA-co-VBS), and (SA-g-P(ITA-co-VBS)/ RC) are represented in (Figure 3- 9 and 3-10). The isotherm profile of (SA-g-P(ITA-co-VBS), and (SA-g-P(ITA-co-VBS)/ RC) demonstrates a small hysteresis loop that can be categorized as type IV (Figure 3-9 and 3-10) [80]. The surface area, average pore diameter, and total pore volume were enhanced after the incorporation of carbon onto the grafted RC (Table 3-1 and 3-2). The interfacial interactions between hydrogel and hydrogel /RC have a great influence on the pore structure of the material as evident from this study. FE- SEM study well support this result as well-developed pores can be seen clearly in the surface morphology of (SA-g-P(ITA-co-VBS) ,and (SA-g-P(ITA-co-VBS)/ RC) hydrogel nanocomposite in comparison to hydrogel , i.e. surface area and pore volume of hydrogel were increased after the doping of RC [81-84]. The textural parameters of hydrogel \RC and hydrogel are summarized in (Tables 3-1 and 3-2) respectively.

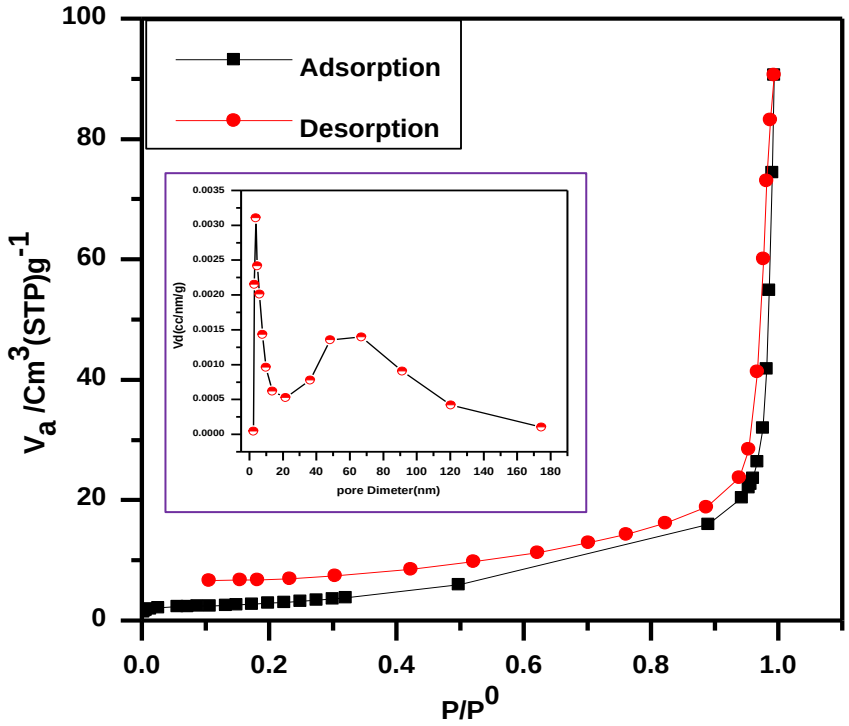

Figure(3-9): Nitrogen Adsorption-Desorption Isotherms and the Corresponding pore Size Distribution curve of Hydrogel /RC.

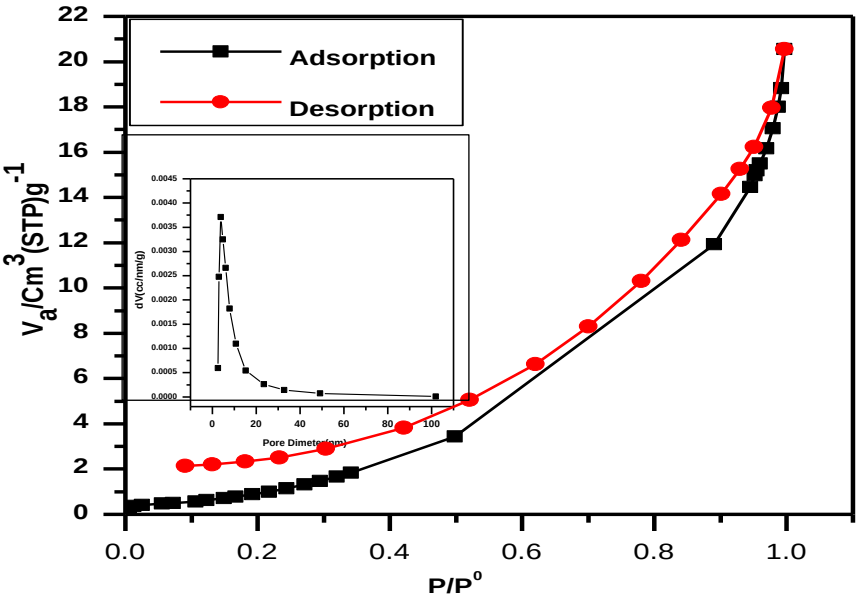

Figure(3-10): Nitrogen Adsorption-Desorption Isotherms and the Corresponding pore size Distribution Curve of Hydrogel

Table 3-1: Surface Physical Characteristics of Hydrogel /RC.

Surface physical parameters	Value
BET surface area ($m^2 g^{-1}$)	32.033
Langmuir surface area ($m^2 g^{-1}$)	182.94
Micro pore surface area ($m^2 g^{-1}$)	21.29
Cumulative pore volume ($cm^3 g^{-1}$)	0.0266
Micro pore volume ($cm^3 g^{-1}$)	0.0197

Table 3-2:Surface Physical Characteristics of Hydrogel

Surface physical parameters	Value
BET surface area ($m^2 g^{-1}$)	11.225
Langmuir surface area ($m^2 g^{-1}$)	105.36
Micro pore surface area ($m^2 g^{-1}$)	8.641
Cumulative pore volume ($cm^3 g^{-1}$)	1.936
Micro pore volume ($cm^3 g^{-1}$)	0.0037

3-2 Optimization of the Swelling Behavior for the Synthesis of (SA-g-P(ITA-co-VBS)/ RC) Hydrogel nanocomposite

3-2-1 Effect of RC Amount on the Swelling Behavior

The Figure 3-11 depicts the effect of RC amount on water absorption. Water absorption of hydrogel first increased and then decreased with the increase of RC amount from 0.1 wt. % to 2 wt. %. RC with a large number of hydrophilic groups could be chemically cross-linked with a polymer chain, forming a cross-linked polymer network with RC particles as the additional cross-linking points. The introduction of appropriate RC particles weakens the hydrogen-bonding interaction between carboxyl groups in the polymer and reduces the physical entanglement of the grafted polymer network chain. Nevertheless, with excessive RC (>1 wt %), the excess RC particles increased the degree of cross-linking, leading to a decrease of the penetration space of water molecules. Therefore, appropriate RC loading is critical to obtaining hydrogel with high water swelling capacity[85].

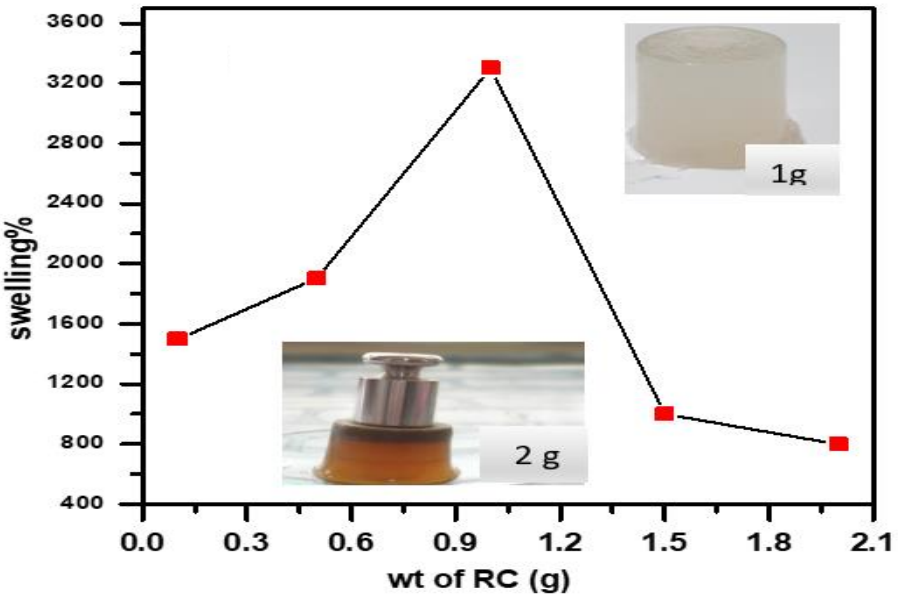

Figure 3-11 : Variation of Swelling percentage% with Amount of RC

3-2-2 Effect of VBS Amount on the Swelling Behavior

The percentage swelling and water absorbance efficiency in (SA-g-P(ITA-co-VBS)/ RC) hydrogel was examined by varying the monomer amount from (0.1-2.5 g), Water absorption of hydrogel increased as monomer increased from 1900 % to 3400%. (Figure 3-12). However, when VBS was higher than 3400 %, water absorption dropped significantly, attributed to the reaction of $-COO^-$ groups with excess Na^+, resulting in weakening of the repulsive force. The reduction in percentage swelling at high amount monomer could be assigned to the formation of homopolymers of ITA and increased viscosity which hindered the mobility of free radicals onto active sites .Also This might be due to the hydroxyl group (a weak hydrophilic group) which forms a hydrogen bond between two neighboring chains that causes shrinkage of the network[80]

.

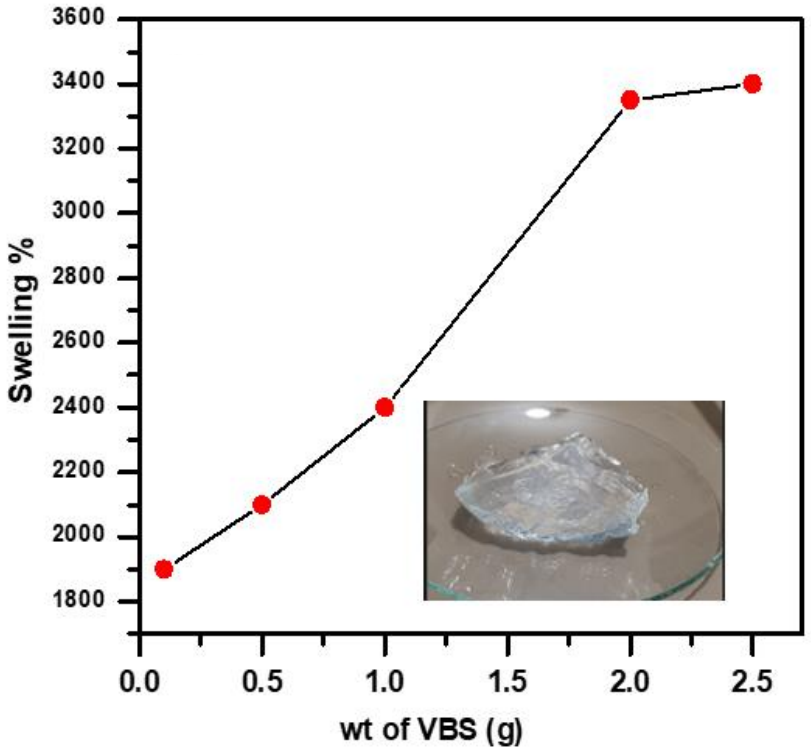

Figure 3-12 : Variation of Swelling percentage% with amount of monomer VBS.

3-2-3 Effect of Itaconic Acid Amount on the Swelling Behavior

SA-g-P(ITA-co-VBS)/ RC hydrogel nanocomposite swelling % was highest at the ITA amount of 1.0 g (Fig. 3-13). Increasing the ITA amount from 0.1 -1.5 g makes more ITA molecules available for the chain propagation sites on graft copolymer network, hydrogel swelling percentage, increased with ITA amount, and reached maximum (3400 %) at 1 g. attributed to enhanced hydrogel swelling percentage. ITA amount higher than 1.0 g led to increase the rate of homo-polymerization reaction, which enhanced the viscosity of the reaction mixture and hindered free radical movement. and a decrease in hydrogel swelling percentage[80] .

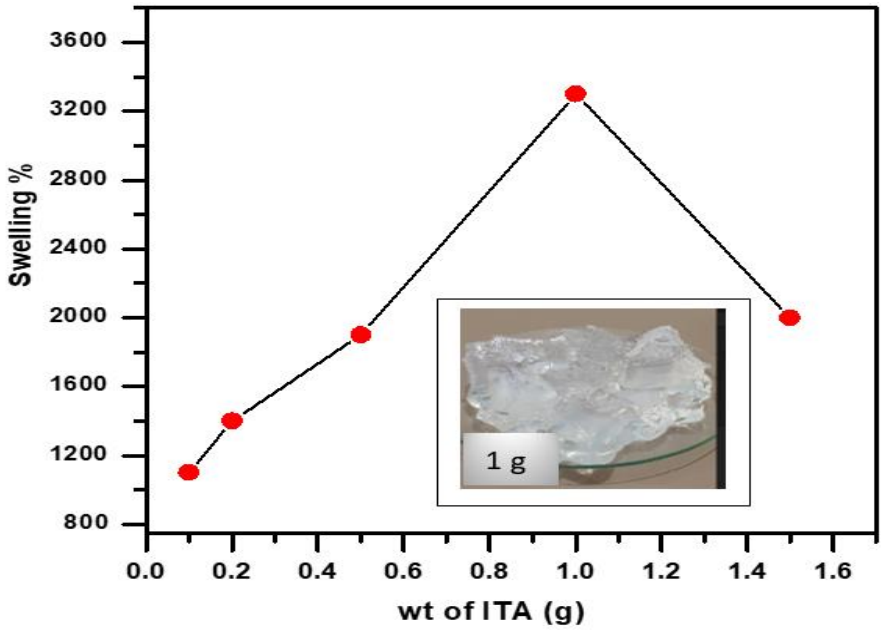

Figure 3-13 : Variation of Swelling percentage% with Amount of Monomer ITA.

3-2-4 Effect of Sodium Alginate Amount on the Swelling Behavior

The effect of SA amount on water absorption of hydrogel increased with increasing the amount of SA from 0.5 to 1.5 g and decreased with further increase in SA amounts. The highest swelling (3400 %) was obtained with a SA content of 1g . When the amount of SA was low, the

monomer was excess in the reaction system. The excess ITA, VBS turned to be a homo-polymer, which cannot contribute to the water swelling. The swelling was increased as homo-polymer content was decreased and SA amount was increased at fixed crosslinking density. On the other hand, when of SA amount was above 1g the viscosity of SA solution was increased shawed shown in figure (3-14), the initiation efficiency was decreased, and the reactive sites cannot be sufficiently formed. As a result, grafting ratio was decreased resulting in a decrease of the water swelling. With much higher SA content, sharply increased viscosity resulted in the system, restricting the monomer movement and reducing the conversion rate. Thus, a less developed 3D polymer network and suppressed water absorption capacity could be expected [72].

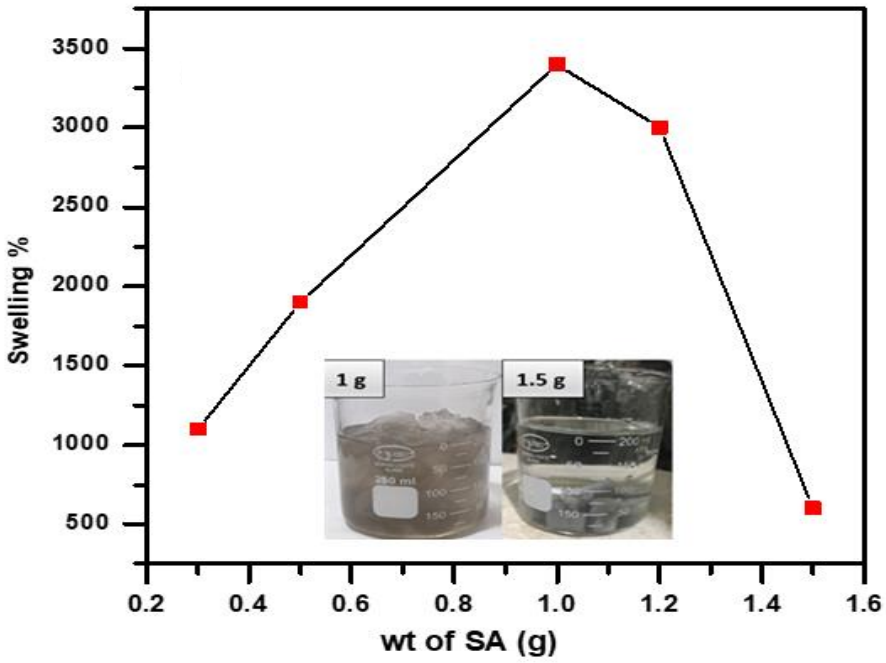

Figure 3-14 : Variation of Swelling percentage% with Amount of SA.

3-2-5 Effect of Cross-linker Amount on the Swelling Behavior

A Cross linker plays an important role in the synthesis of a SA-g-P(ITA-co-VBS)/ RC hydrogel nanocomposite due to prevention the dissolving of the hydrophilic polymer networks in an aqueous phase. and effectively makes the hydrogel insoluble. The presence of crosslinking chains is essential to controlling crosslinking density and fluid absorbency. SA-g-P(ITA-co-VBS)/ RC hydrogel nanocomposite swelling studies were carried out at different cross-linker (MBA) amount varying from 0.003-0.1 gm (Fig. 3-15). The hydrogel nanocomposite showed maximum swelling of 3400 % at 0.01 g . For crosslinker amount of more than 0.01 g , hydrogel swelling started to reduce. It could be because the hydrogel network developed a significant number of cross-linked chains, resulted stiff structure . On increasing the cross-linker amount, the cavities between polymer chains in the hydrogel were reduced, consequently, the amount of water retained in the composite cavities was decreased[86] .

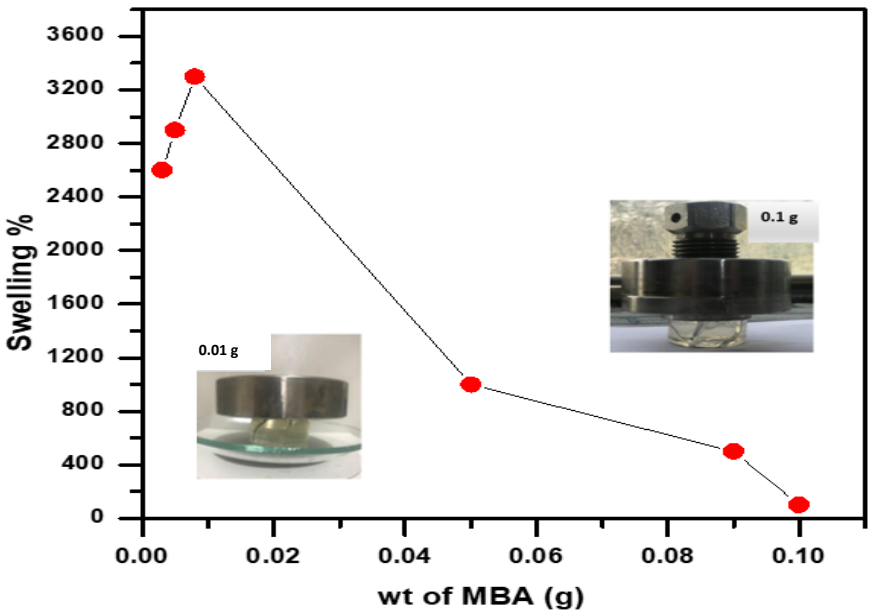

Figure 3-15: Variation of Swelling percentage% with Amount of Crosslinker (MBA)

3-2-6 Effect of Initiator Amount on the Swelling Behavior

The effect of initiator KPS amount on swelling percentage of SA-g-P(ITA-co-VBS)/ RC hydrogel nanocomposite was examined via change the initiator from (0.03 - 0.12) g as shown in(Figure 3-16). percentage Swelling was improved initially with increasing initiator amount up to 0.09 g , That after 0.09 g the swelling percent started decreasing. thus the best percent swelling (3400 %) at 0.09 g. On increasing the amount of KPS from (0.03 to 0.09)g , the swelling was increased from 1900 to 3400%. Further increase in the amount of KPS to 0.09 g, the swelling was decreased to 141 g/g. This increase might be attributed to the attack of the sulfate anion-radical to the Alginate chains. Further raise in KPS amount decreased the percentage swelling, which led to the termination of the reaction[72] .

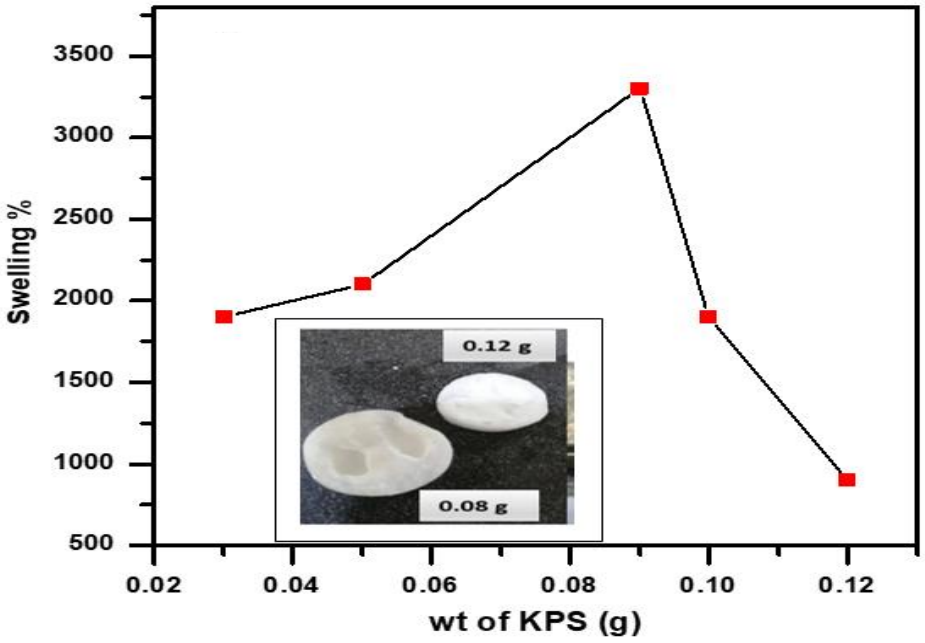

Figure 3-16: Variation of Swelling Percentage% with Amount of Initiator (KPS).

3-2-7 Effect of pH on the Swelling Behavior

The pH is a very important effect on the swelling ability of SA-g-P(ITA-co-VBS)/ RC hydrogel nanocomposite. In the range pH of 3–10, as shown Fig. 3-17). The charge density was balanced at pH neutral, leading to high swelling of SA-g-P(ITA-co-VBS)/ RC hydrogel nanocomposite. thus The best percentage swelling was found at pH 7 , hydrogel swelling was decrease with each low (acid)or high (base) pH . The protonation of groups COO^- at acid pH led to a decrease in electrostatic repulsions, the 3D structure of the hydrogel matrix got collapsed, hence low swelling. . Under the basic pH, carboxylic groups were ionized into groups COO^- and excess of groups COO^- caused the collapse of the 3D structure of hydrogel, resulted in low swelling[87] .

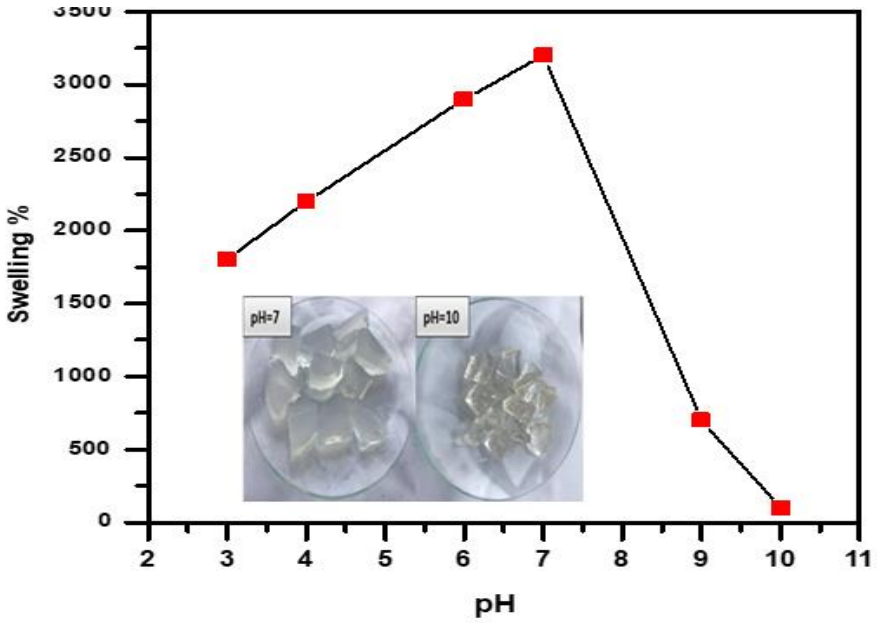

Figure 3-17: Variation of Swelling Percentage% with pH

3-2-8 Effect of Solvent on the Swelling Behavior

The grafting of ITA on to SA was influenced by solvent volume (17–50 ml) as shown in (Figure 3-18). Up to 20 ml of solvent volume, swelling percentage first increased and when beyond 20 ml volume of solvent ,swelling percentage decreased. The hydroxyl radical produced by water could be attributed to the propagation step in the polymerization reaction which caused an initial increase in swelling percentage . increase volume solvent led to the generation of excessive hydroxyl of water radicals, which were responsible for the termination of the reaction, which further obstructed the graft co-polymerization method[80] .

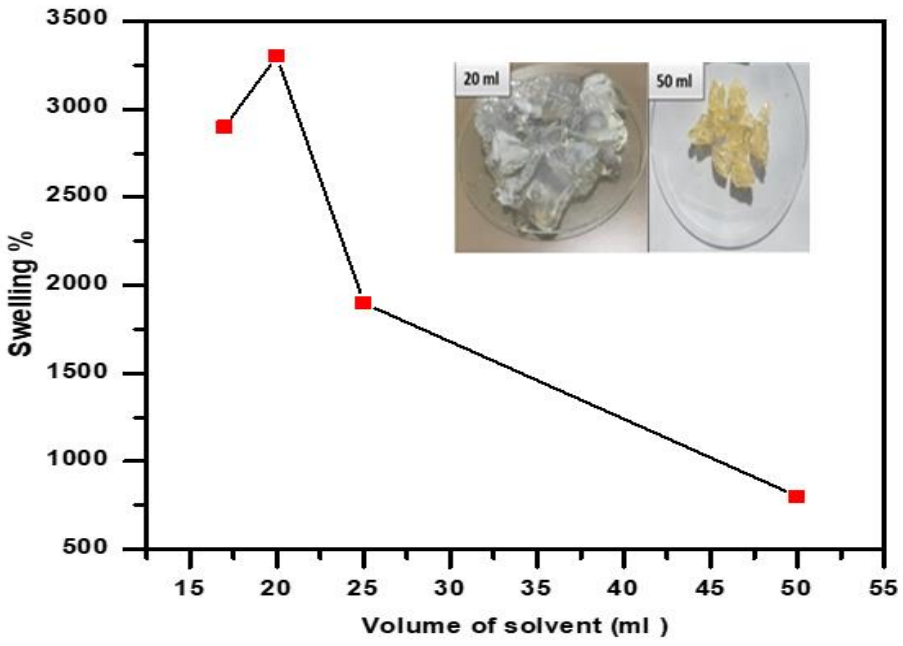

Figure 3-18: Variation of Swelling percentage% with solvent.

3-2-9 Effect of Temperature on the Swelling Behavior

The grafting of monomer onto backbone (SA) was investigated under several temperature from 60 - 90 ^{o}C as shown in (Figure 3-19). Enhanced the temperature of SA-g-P(ITA-co-VBS)/RC hydrogel nanocomposite swelling percentage at maximum temperature at 75 ^{o}C with values3400%.

The increase in percentage swelling up to temperature 75 ^{o}C is due to the improvement in the diffusion of the monomer as well as the activation. KPS was effectively decomposed at higher temperatures, and increased temperature promoted the activation of free radicals, which was ascribed to get better SA-g-P(ITA-co-VBS)/ RC hydrogel nanocomposite swelling. At temperatures beyond 75 ^{o}C, excessive cross-linking occurred, resulting in a more compact and stiff structure, leading to reduced swelling [85].

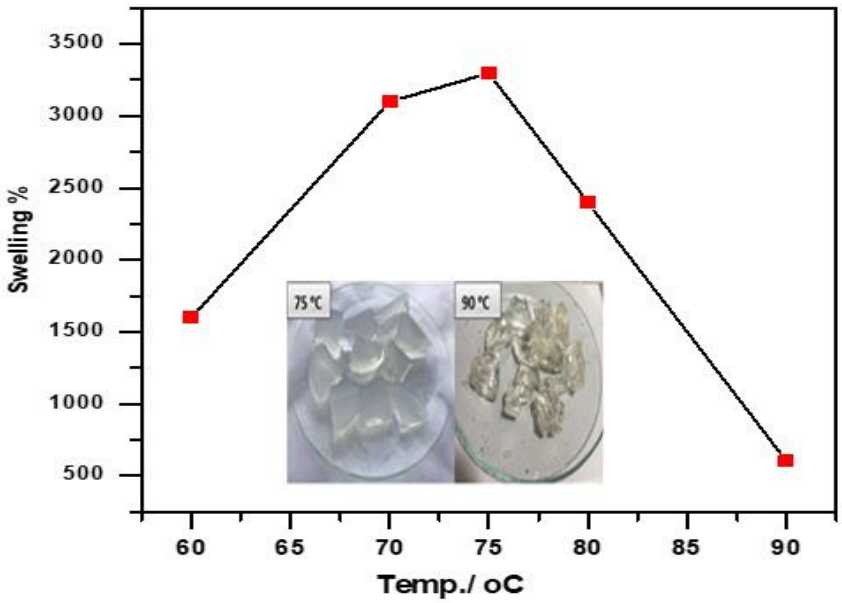

Figure 3-19: Variation of Swelling percentage% with temperature.

3-2-10 The Swelling Capacity of Hydrogel Over Time

The percentage swelling was boosted with time from 120 to 210 min and then dropped from 210 to 240 min (Figure 3-20). The initial increase in percentage swelling could be assigned to the formation of more active sites on SA and monomer via interaction between radical and substrate. The decline in percentage swelling after 210 min is ascribed to less availability of radical active sites and amount of radical active sites

diminishes. The results appear that the best equilibrium time was attained after 240 min [87].

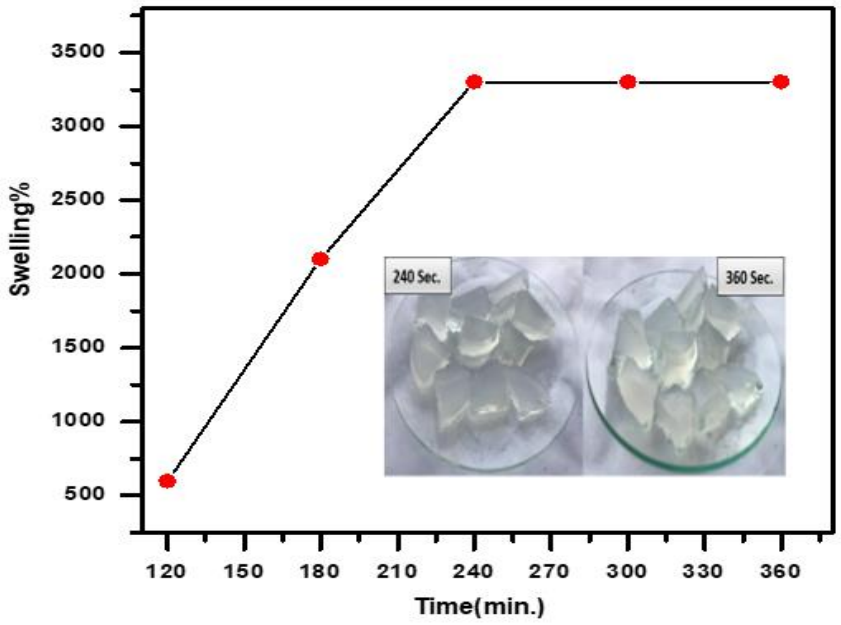

Figure 3-20: Variation of Swelling percentage% with reaction time.

3-3 Effect of different parameters on the adsorption process

3-3-1 Effect of Contact Time

The contact time is one of the important parameters for the assessment of the practical application of the adsorption process. The experimental results of adsorption of initial two dyes (MG, and BG) concentrations of 700 $mg.L^{-1}$ on the adsorbent surfaces of the SA-g-P(ITA-co-VBS)/ RC with contact time . The equilibrium data are shown in Figures (3-21) which reveal that the adsorption increased rapidly in the first 20 min, and after that gradually increased till the equilibrium [88]. Adsorption capacity increases with the increase in contact time to reach the equilibrium, because with a time of adsorption increased, the active sites of absorbent surfaces will saturate, indicating that an apparent equilibrium is reached, Where an acceptable efficiency was found at a

concentration of 700 mg.L^{-1} and contact time of one hour as the increase in time will have a slight effect on the removal rate due to the fullness of the active sites, this is because the adsorbents have a finite number of active binding sites. After a certain concentration, all such active sites were filled with dye molecules and the adsorbents became saturated [89, 90].

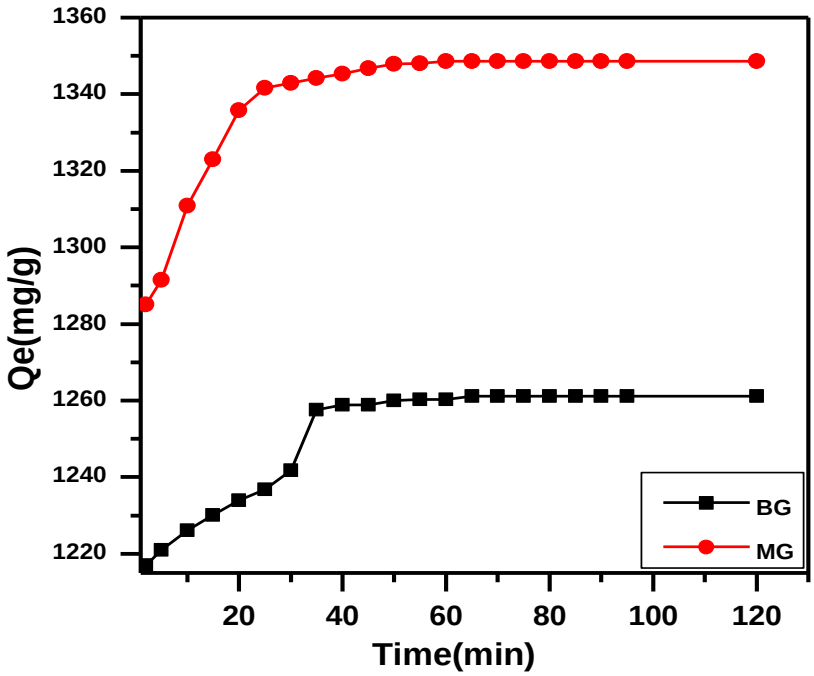

Figure (3-21): Effect of contact time on adsorption capacity for removal of (BG & MG) dyes by SA-g-P(ITA-co-VBS)/ RC at pH 7 , Temp. 25 ^{o}C and mass adsorbent 0.05 g

3-3-2 Adsorbent Dose

The effect of the amount of the adsorbents was necessary to observe the minimum possible amount, which shows the maximum adsorption stoichiometric. The amounts of the adsorbent was varied from 0.01 to 0.1 g/100 mL of SA-g-P(ITA-co-VBS)/ RC. The results are illustrated in Table (3-3) and shown in Figures (3-22) and (3- 23).

Table (3-3): Effect of adsorbent dose on the removal percentage of two dyes on to SA-g-P(ITA-co-VBS)/ RC .

WT	MG			BG		
	C_e/ mg/L	Q_e/ mg.g^{-1}	E%	C_e/ mg/L	Q_e/ mg.g^{-1}	E%
0.01	57.42775	6425.723	91.79604	175.7059	5242.941	74.89916
0.025	54.21965	2583.121	92.25434	137.8235	2248.706	80.31092
0.05	25.66474	1348.671	96.33361	69.82353	1260.353	90.02521
0.08	18.90173	851.3728	97.29975	52.82353	808.9706	92.45378
0.1	12.16763	687.8324	98.26177	39.82353	660.1765	94.31092

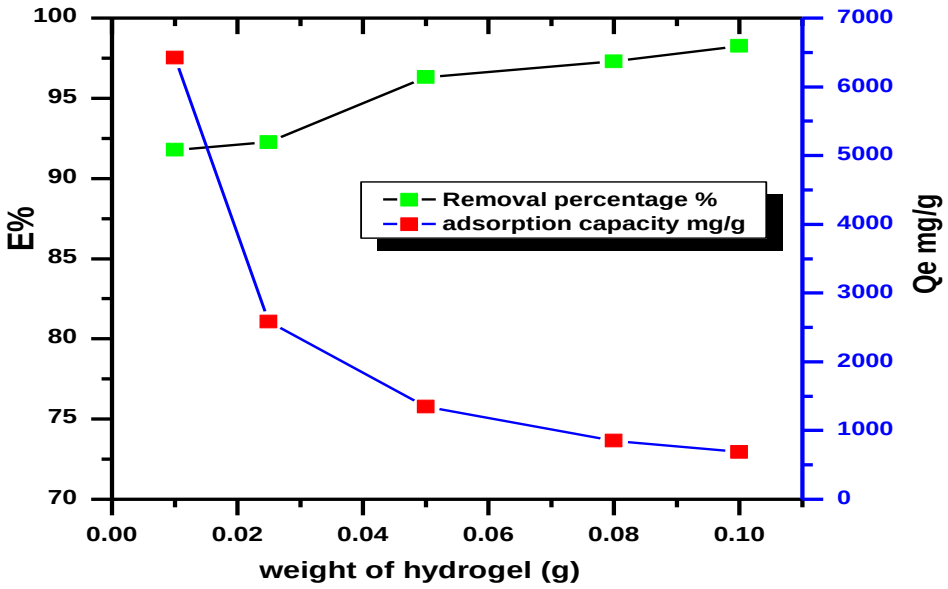

Figure (3-22): Effect of the mass amount of adsorbent SA-g-P(ITA-co-VBS)/ RC on the percent removal and amount of adsorbed MG dye, initial concentration = 700 mg.L^{-1}, Temp. = 25°C, contact time 1hr , pH=7.

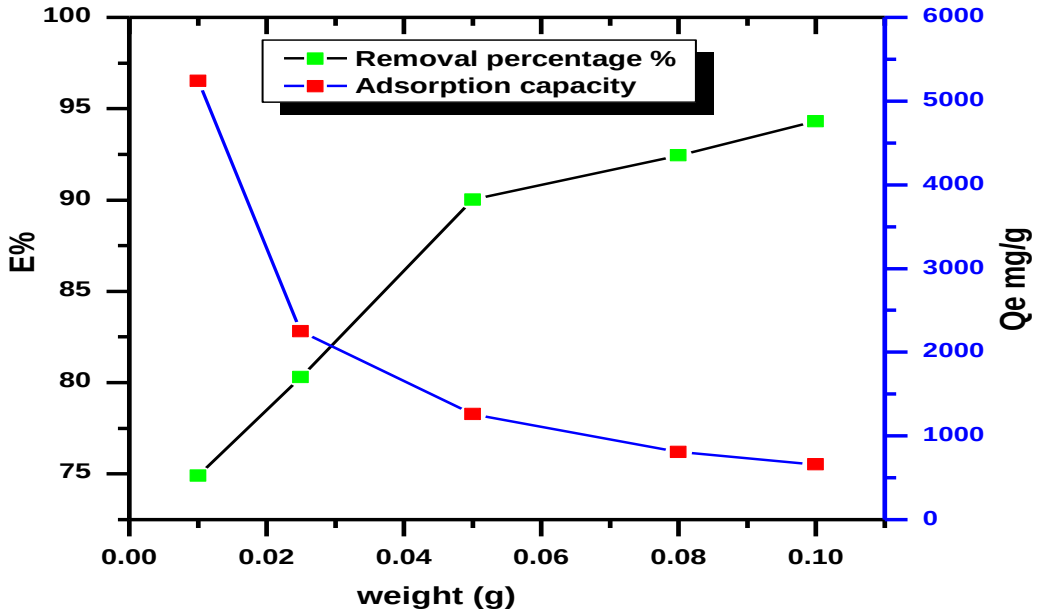

Figure (3-23): Effect of the mass amount of adsorbent (SA-g-P(ITA-co-VBS)/ RC) on the percent removal and amount of adsorbed BG dye, initial concentration = 700 mg.L^{-1}, Temp. = 25°C, contact time 1hr., pH=7 .

An increase in the percentage of the (MG , and BG) dyes removal with adsorbent mass was related to the increase in the adsorbent surface areas, enhancing the number of adsorption sites available for adsorption as reported already in other cases [19]. The increase in removal of dyes with adsorbent dose due to the introduction of more binding sites for adsorption [91]. The primary factor explaining this characteristic is that adsorption sites remain unsaturated during the adsorption reaction whereas the number of sites available for adsorption site increases by increasing the adsorbent dose[68].The increase of adsorbent amount about rang 0.01 - 0.1g, the percentage removal of MG and BG dyes increase from (91.7 - 98.2%) , (74.8 -94.3%) and adsorption capacity decrease from (6425.7 - 687.8 mg/g) , (5242.9 - 660.1 mg/g) onto (SA-g-P(ITA-co-VBS)/ RC) about 1h of adsorption time at the same order . This data is attributed to the increasing the number of active sites caused via increasing mass of adsorbent [21, 92].

3-3-3 Effect of pH

The effect of pH on the adsorption of MG, and BG dyes onto SA-g-P(ITA-co-VBS)/ RC was studied at a pH range of (3-10) in the presence of initial concentrations (700 $mg.L^{-1}$). Results are given in Table (3-4) and shown in Figures (3-24) and (3-25).

Table (3-4): Effect of solution pH on adsorption two pollutants (MG, BG) by SA-g-P(ITA-co-VBS)/ RC

pH	MG			BG		
	C_e/ mg/L	Q_e/ $mg.g^{-1}$	E%	C_e/ mg/L	Q_e/ $mg.g^{-1}$	E%
3	57.80058	1284.399	91.74277	169.1765	1061.647	75.83193
4	54.56647	1290.867	92.20479	130.7059	1138.588	81.32773
7	25.66474	1348.671	96.33361	69.82941	1260.341	90.02437
8	18.94509	1362.11	97.29356	54.97059	1290.059	92.14706
10	9.306358	1381.387	98.67052	26.14118	1347.718	96.26555

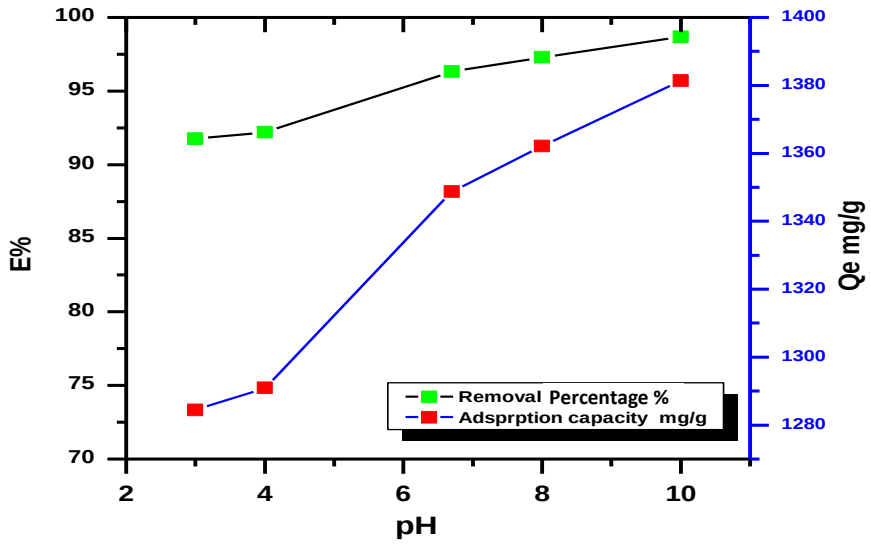

Figure (3-24): Effect of solution pH on the adsorption of MG dye on (SA-g-P(ITA-co-VBS)/ RC) (Exp. Condition: Temp. = 25°C, contact time 1 h, pH of solution 7 and mass adsorbent 0.05 g)

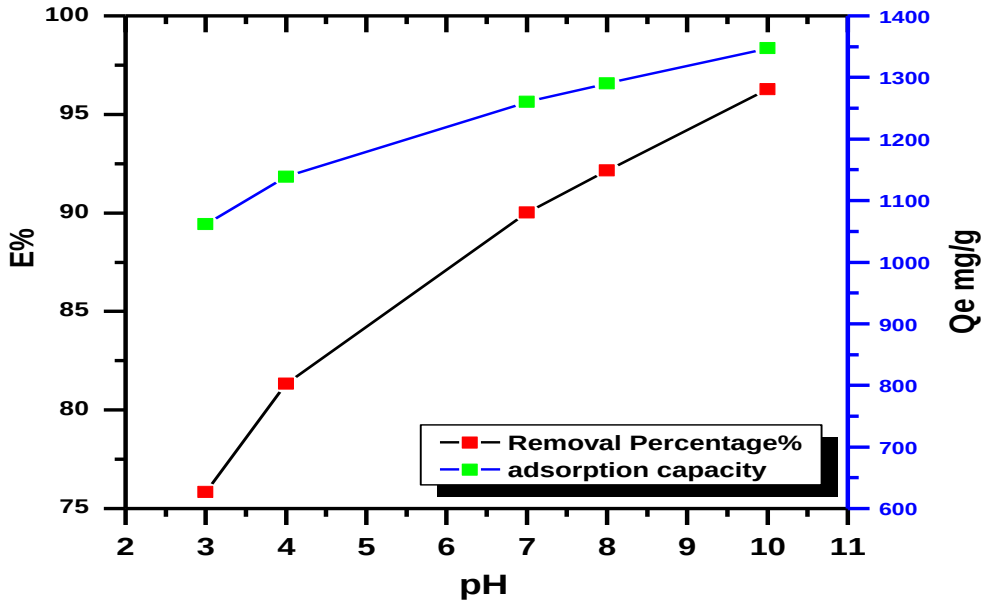

Figure (3-25): Effect of solution pH on the adsorption of BG dye on (SA-g-P(ITA-co-VBS)/ RC) (Exp. Condition: Temp. = 25°C, contact time 1 h, and pH of solution 7).

The equilibrium sorption capacity of MG , and BG dyes on (SA-g-P(ITA-co-VBS)/ RC) was very little in acid medium at pH 3. The adsorption capacity (Qe $mg.g^{-1}$) at pH 3 (1284.3 $mg.g^{-1}$) and (1061.6 $mg.g^{-1}$) for MG , and BG dyes , which suggests that (SA-g-P(ITA-co-VBS)/ RC) is excellent adsorbents for MG , and BG dyes dye removal from large volumes of aqueous solutions[39, 93]. When the pH is greater than 7 the adsorption capacity (Qe $mg.g^{-1}$) of MG and BG dyes on (SA-g-P(ITA-co-VBS)/ RC) capacity (Qe $mg.g^{-1}$) increases with increasing pH. Lower adsorption of dyes at acidic pH is probably due to the presence of excess H^+ ions competing with the cation groups on the dye for adsorption sites . At higher pH, the surface may get positively charged, which enhances the negatively charged dye anion through electrostatic forces of attraction [94, 95] .

3-3-3-1 point of zero charge (pHpzc)

The pH drift method was utilized for the pHpzc estimation. Generally, the pH pzc is the point where the curve of pH final vs. pH initial crosses the line pH initial = pH final, with the value for the nanocomposite being 4.2 (Figure 3-26). At pH < pHpzc, the nanocomposite hydrogel displays a net positive charge, whereas at pH > pHpzc the surface is negatively charged. At alkaline pHs (pH > pHzpc) the amount of OH^- ion in aqueous solution increases and the functional groups in the structure of adsorbers have a negative charge which can be effective in the process of elimination of pollutant. [79, 96].

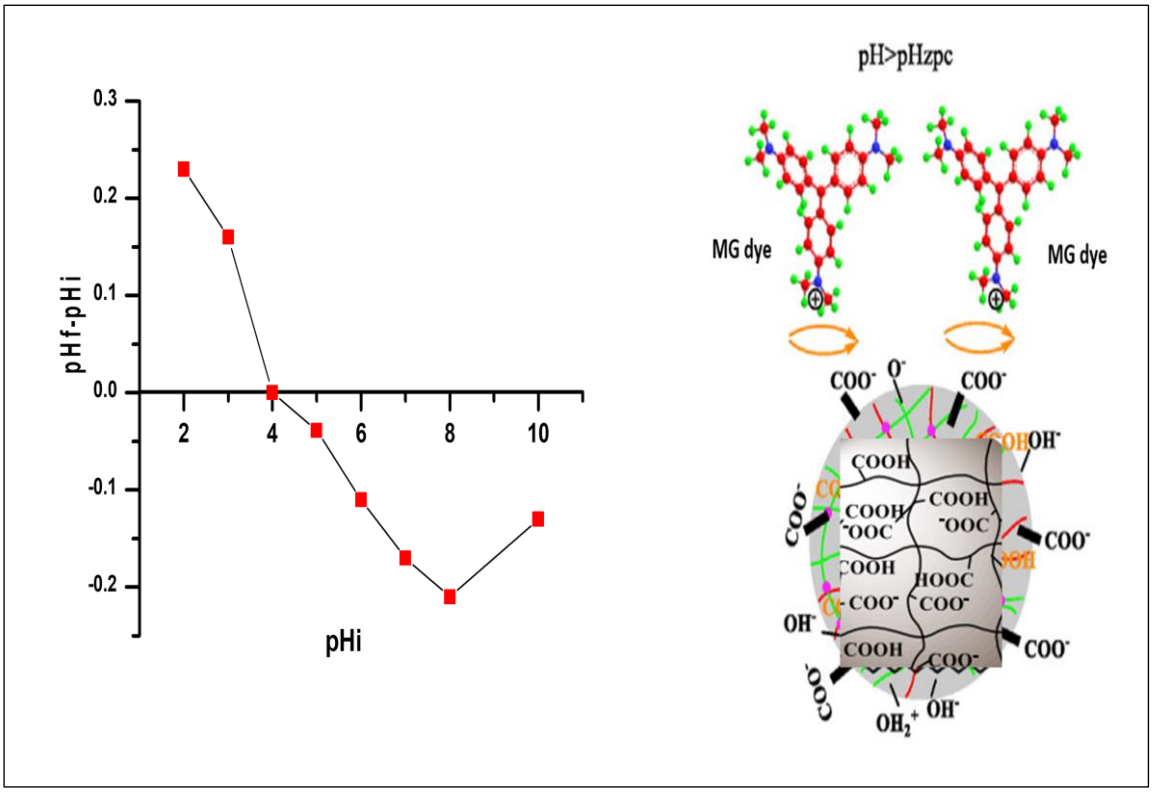

Figure 3-26: Point Zero charge of SA-g-P(ITA-co-VBS)/ RC Exp. Condition: Temp. = 25°C, contact time 24 h, and mass adsorbent 0.05 gm/ 100 ml).

3-3-4 Effect of Temperature

To determine whether the ongoing adsorption process was endothermic or exothermic. The adsorption isotherms were determined for various pollutants-adsorbent systems. The removal of MG, and BG dyes has been studied at different temperature (15- 35 ^{o}C) in the presence of various initial concentrations (100-1000 mg.L^{-1}) results are illustrated in Tables (3-5 & 3-6), and presented in Figures (3-27 & 3-28) .

Table (3-5): Adsorption Isotherm for Adsorption of MG dye on the SA-g-P(ITA-co-VBS)/ RC at Different Temperatures. (pH 7, mass adsorbent 0.05 gm/ 100 ml, contact time 1hr).

	15 ^{o}C		25 ^{o}C		35 ^{o}C	
C_0 mg.L^{-1}	Q_e mg.g^{-1}	E%	Q_e mg.g^{-1}	E %	Q_e mg.g^{-1}	E%
100	199.9358	99.96792	199.7994	99.89971	199.9936	99.99682
200	394.9711	98.74277	394.8555	98.71387	395.6069	98.90173
300	593.0058	98.8343	593.5838	98.93064	594.2775	99.04624
400	782.5896	97.8237	787.7457	98.46821	794.1618	99.27023
500	978.8439	97.88439	982.0173	98.20173	991.0983	99.10983
600	1167.89	97.32418	1172.329	97.69412	1180.734	98.39451
700	1348.671	96.33361	1355.723	96.83732	1364.035	97.43105
800	1529.364	95.58526	1553.688	97.10549	1558.318	97.39487
1000	1921.387	96.06936	1935.775	96.78873	1949.335	97.46676

Table (3-6): Adsorption Isotherm for Adsorption of BG dye on the SA-g-P(ITA-co-VBS)/ RC at Different Temperatures. (pH 7, mass adsorbent 0.05 gm/ 100 ml, contact time 1hr).

C_0 mg.L^{-1}	15 °C		25 °C		35 °C	
	Q_e mg.g^{-1}	E %	Q_e mg.g^{-1}	E %	Q_e mg.g^{-1}	E%
100	194.824	97.4118	198.694	99.3471	195.766	97.8829
200	389.424	97.3559	396.235	99.0588	394.235	98.5588
300	584.176	96.3627	585.094	97.5157	583.529	97.2549
400	746.553	93.3191	773.612	96.7015	773.612	96.7015
500	896.941	89.6941	920.235	92.0235	908.471	90.8471
600	1045.76	87.1471	1083.88	90.3235	1081.06	90.0882
700	1253.53	89.5378	1260.35	90.0252	1242.12	88.7227
800	1405.18	87.8235	1366.12	85.3824	1415.65	88.4779
1000	1738.82	86.9412	1661.18	83.0588	1751.65	87.5824

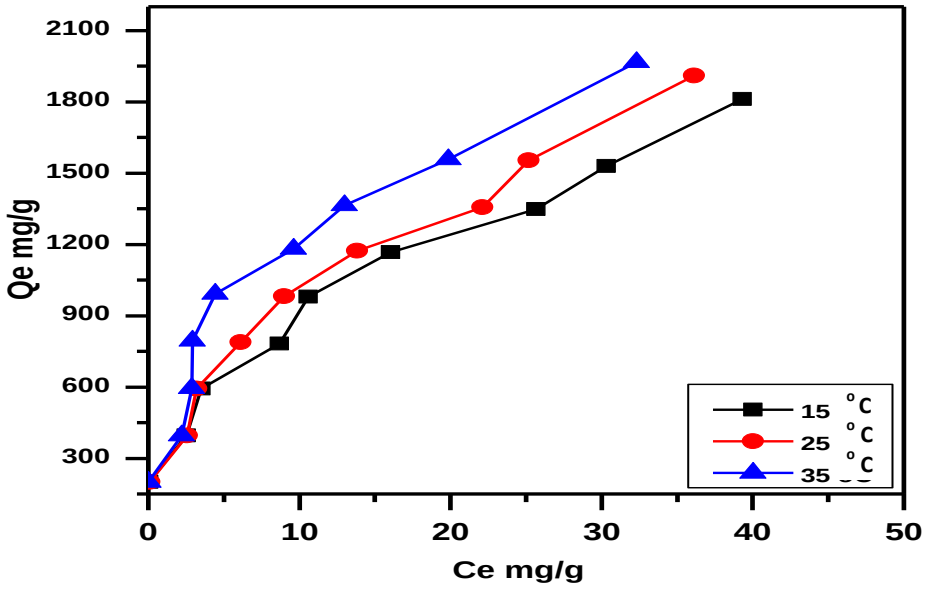

Figure (3-27) Effect of Temperature on the Adsorption of MG dye on the Surface of SA-g-P(ITA-co-VBS)/ RC . (pH 7, mass adsorbent 0.05 gm/ 100 ml).

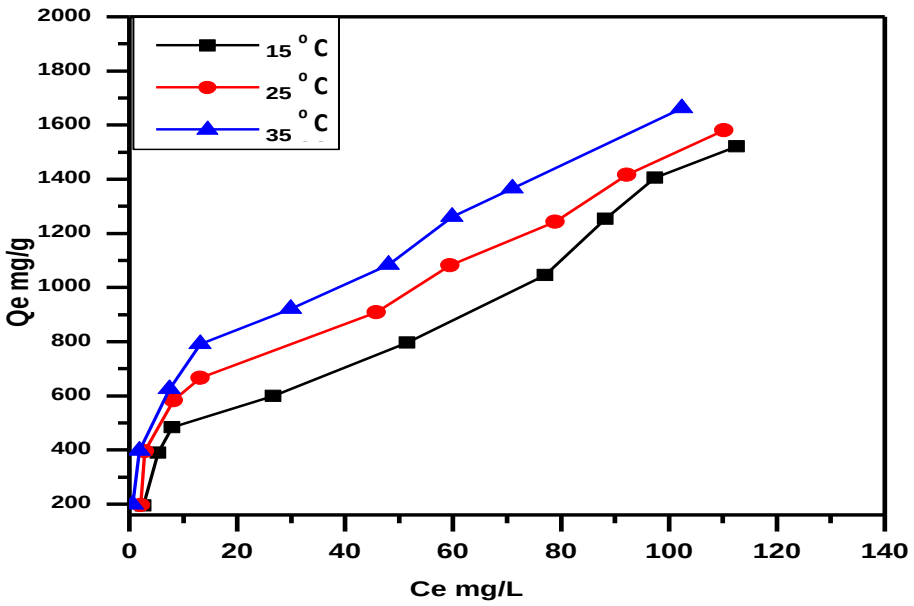

Figure (3-28) Effect of temperature on the adsorption of BG dye on the surface of SA-g-P(ITA-co-VBS)/ RC. (pH 7, mass adsorbent 0.05 gm/ 100 ml).

The result shows that the equilibrium adsorption capacity of MG , and BG dyes was increased while increasing the solution temperature for all initial dyes concentrations. The adsorbent's capacity of adsorption changes with temperature. Hence, the parameter of temperature is important as a physicochemical process. An endothermic adsorption process involves a directly proportional increase of adsorption with temperature, caused by an increase in active adsorption sites and dye molecule's mobility with rising temperatures[97]. It was found that the rising temperature causes a decrease in aqueous phases viscous forces resistance, thereby leading to the dye molecule's faster diffusion across adsorbent particles' external boundary, as well as, internal pores. The removal process was also significantly affected by the change in adsorbate molecules' solubility in some cases. At high temperatures, pore size enlargement also causes increased adsorption[68, 98].

The study of the temperature effect on adsorption will also help in the calculation of the basic thermodynamic functions such as

Gibbs free energy (ΔG), change enthalpy (ΔH), and change entropy (ΔS) of the adsorption process [91]. The equilibrium constant (K_e) of the adsorption process at each temperature, was calculated from the equations (3-1) [99]:

$$\boldsymbol{K_e = \frac{(Q_{max}) * Wt\ (0.05\ gm)}{(C_e) * V(0.1L)} \times 1000} \qquad (3-1)$$

Where Q_{max} is the amount adsorbed in ($mg.gm^{-1}$), C_e is the equilibrium concentration of the adsorbent expressed in ($mg.L^{-1}$), 0.05gm represents the weight of the (SA-g-P(ITA-co-VBS)/ RC) adsorbent, and 0.1L represents the volume of the MG and BG dyes solution used in the adsorption process [100]. The change in the free energy could be determined from the equation (3-2) :[100]

$$\boldsymbol{\Delta G = -RT \ln K_e} \qquad (3-2)$$

Where ΔG: Gibbs free energy ($J.K^{-1}.mol.^{-1}$), R is the gas constant (8.314 $J.K^{-1}.mole^{-1}$), T is the absolute temperature in Kelvin.

The enthalpy of adsorption may be obtained from the following equation (3-3) [81]:

$$\boldsymbol{\ln X_m = -\frac{\Delta H^{\circ}}{RT} + Cons.} \qquad (3-3)$$

When $X_{m:}$ is the maximum value of adsorption at a certain value of equilibrium concentration (Ce). Table (3-7) and (3-8) gives X_m values at different temperatures MG dye. Plotting $\ln X_m$ versus (1/T) should produce a straight line with a slope -ΔH/R as shown in Figures (3-29) and (3-30) The value of ΔH and ΔS can be calculated from the slope and intercept respectively [101].

Table (3-7): Maximum adsorption quantity Xm values of MG dye onto SA-g-P(ITA-co-VBS)/ RC surfaces at different temperatures.

T(K)	1000/T(K^{-1})	C_e = 32.5	
		X_m	ln X_m
288	3.472	1590	7.371
298	3.355	1780	7.484
308	3.246	1950	7.575

Table (3-8): Maximum adsorption quantity Xm values of BG dye onto SA-g-P(ITA-co-VBS)/ RC surfaces at different temperatures.

T(K)	1000/T(K^{-1})	C_e =100.11	
		X_m	ln X_m
288	3.472	1425	7.261
298	3.355	1537	7.337
308	3.246	1610	7.383

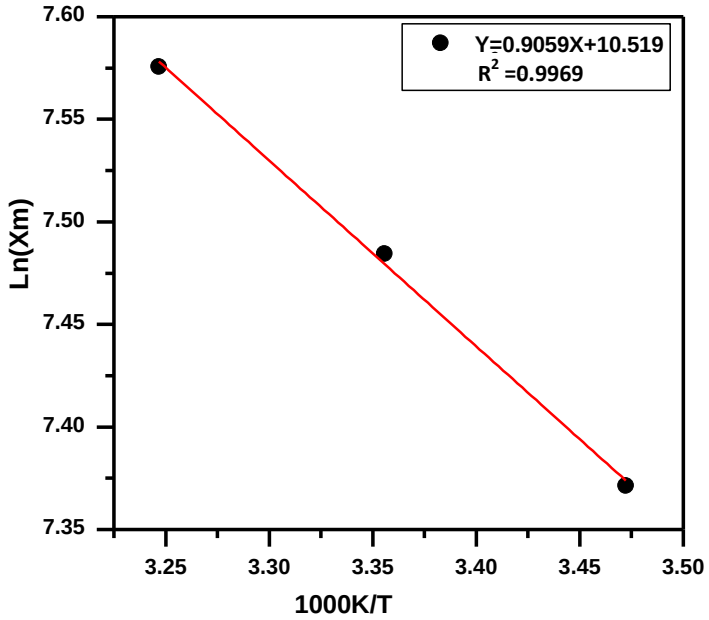

Figure (3-29): Plot ln X_m against the absolute temperature. of the adsorption (MG dye) onto SA-g-P(ITA-co-VBS)/ RC.

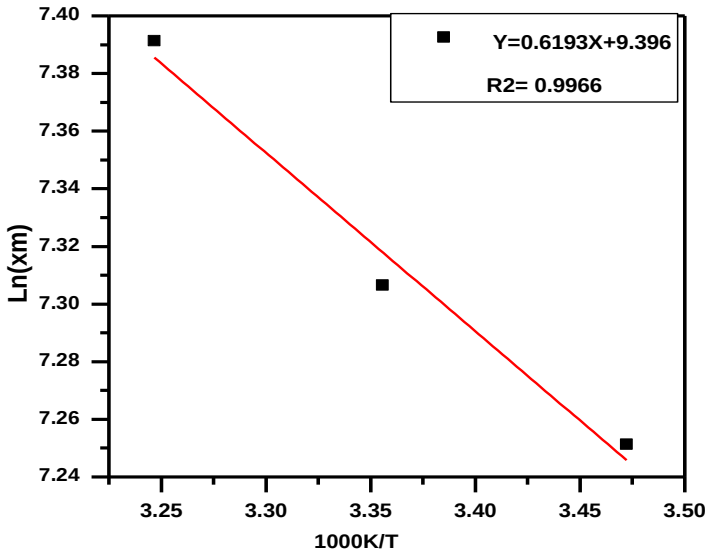

Figure (3-30): Plot ln X_m against the absolute temperature. of the adsorption (BG dye) onto SA-g-P(ITA-co-VBS)/ RC .

The quantitative thermodynamic data of MG and BG on the adsorbent surfaces SA-g-P(ITA-co-VBS)/ RC are presented in Table 3-9. The Table 3.9 shows the ΔH values of MG and BG are positive indicating that the adsorption process is endothermic reaction. All process of adsorption considered spontaneous from the negative value of ΔG. While, ΔS have positive value for MG and BG that refer the interaction of molecules caused random of the total system [102, 103]

From the results of Table 3-9, the enthalpy change ΔH and entropy change ΔS for adsorption are assumed to be temperature independent The enthalpy of the adsorption ΔH is a measure of the energy barrier that must be overcome by reacting molecules [104, 105].

Table 3-9: Thermodynamic functions ΔG, ΔS and, ΔH of MG and BG adsorbed on the SA-g-P(ITA-co-VBS)/ RC.

SA-g-P(ITA-co-VBS)/ RC adsorbent/ MG adsorbate				
Thermodynamics parameters / T/K	K_e	ΔG/ kJ.mol^{-1}	ΔH/ kJ.mol^{-1}	ΔS/ J.K^{-1}.mol^{-1}
288	48.92308	-9.15322	7.531	87.45497
298	54.76923	-9.75163		
308	60	-10.3142		
SA-g-P(ITA-co-VBS)/ RC adsorbent/ BG adsorbate				
Thermodynamics parameters / T/K	K_e	ΔG/ kJ.mol^{-1}	ΔH/ kJ.mol^{-1}	ΔS/ J.K^{-1}.mol^{-1}
288	14.2343	-6.2483	5.146	77.819
298	15.3531	-6.653		
308	16.082	-6.997		

3-4 A Comparative adsorption between different surfaces to removal pollutant

A Comparative study between (Ricinus communis (RC), SA-g-P(ITA-co-VBS), SA-g-P(ITA-co-VBS)/ RC), surfaces as Adsorbents wear carried out. A sample of 100 mL of (MG, and BG) dyes at concentration (700 mg.L^{-1}) are used in this study, then added to a conical flask (Erlenmeyer) in the presence of 0.05g from prepared (Ricinus communis (RC), SA-g-P(ITA-co-VBS), SA-g-P(ITA-co-VBS)/ RC), and put in a shaker water bath for 1 hr., after that the supernatant was separated by centrifuge and measured the remaining concentration by using UV-Visible spectrophotometer at the λmax nm.

The best results of the percentage of removal (E%) for (BG , MG) dyes the order increasing: (SA-g-P(ITA-co-VBS)/ RC) > (SA-g-P(ITA-co-VBS)), > RC as shown in Figure (3-31) .

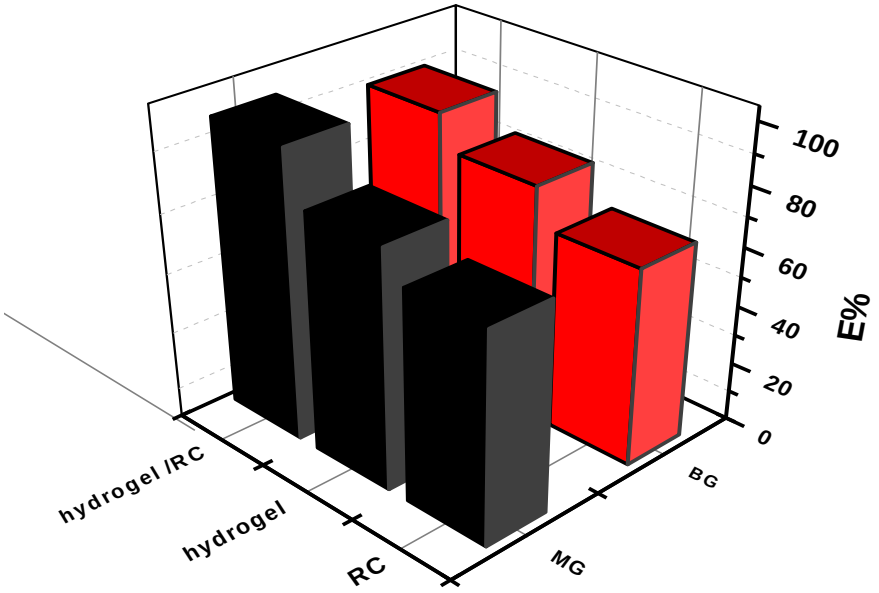

Figure (3-31): Effect comparative between (hydrogel/RC , hydrogel and RC (Exp. Condition: mass of absorbent 0.05 g, conc. 700 mg.L^{-1} Temp. = 25°C, contact time 1 h)

Also Comparative study between (Natural Ricinus Communis (RC) , Activated untreated - acid Ricinus Communis Pericarp(ACRC) and acid-treated Ricinus Communis Pericarp (AACRC)) surfaces as adsorbents was carried out. A sample of 100 mL of (MG and BG dyes) concentration (100 mg.L^{-1}) are used in this study, then added to a conical flask of 0.05g ,and put in a shaker water bath for one hour., after that the supernatant was separated by centrifuge and measured the residual dye concentration by using UV-Visible spectro-photometer at the λ_{max} . The best results of the percentage of removal (E%) for (MG and BG dyes) the order increasing: (RC > ACRC > AACRC) as shown in Figure 3-32.

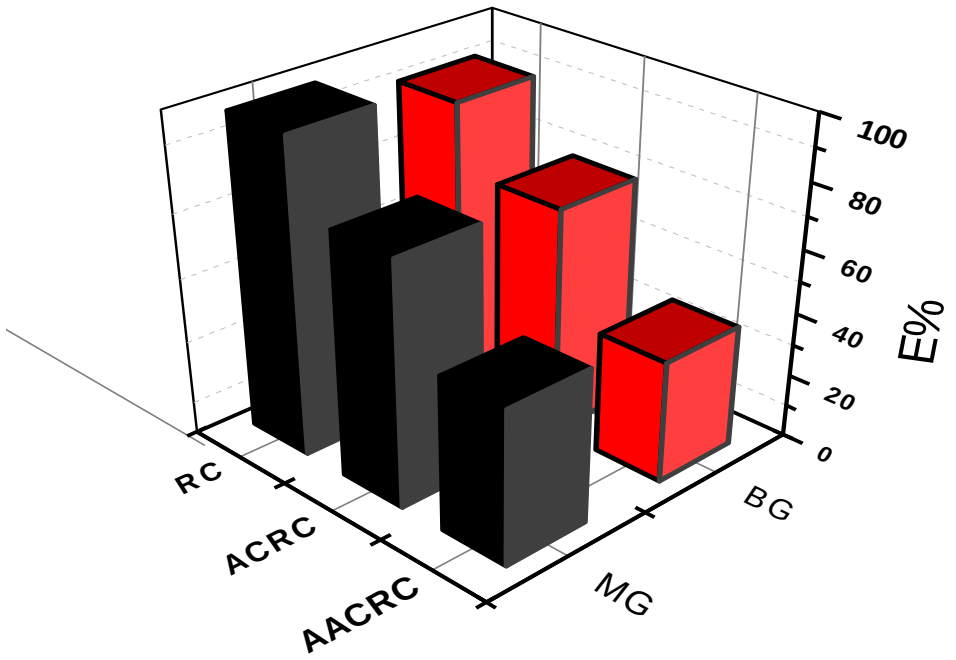

Figure 3-32 : Effect comparative between (RC , ACRC , AACRC (Exp. Condition: mass of absorbent 0.05 g, conc. 100 mg.L^{-1} Temp. = 25°C, contact time 1 h)

3-5 Removal of laboratory sample Aqueous Pollutants by Using SA-g-P(ITA-co-VBS)/ RC

A laboratory sample 100 mL of pollutants (dyes) with a refry concentration were using in this study, then added to a conical flask (Erlenmeyer) in the presence of 0.05 g from prepared SA-g-P(ITA-co-VBS)/ RC , after that the mixture was putting in a Shaker water bath for 2 h, after that the supernatant were separated by centrifuge and measured the remaining concentration was measured by using UV-Visible spectrophotometer[106, 107] the result shows in figures (3-33 , and 3-34).

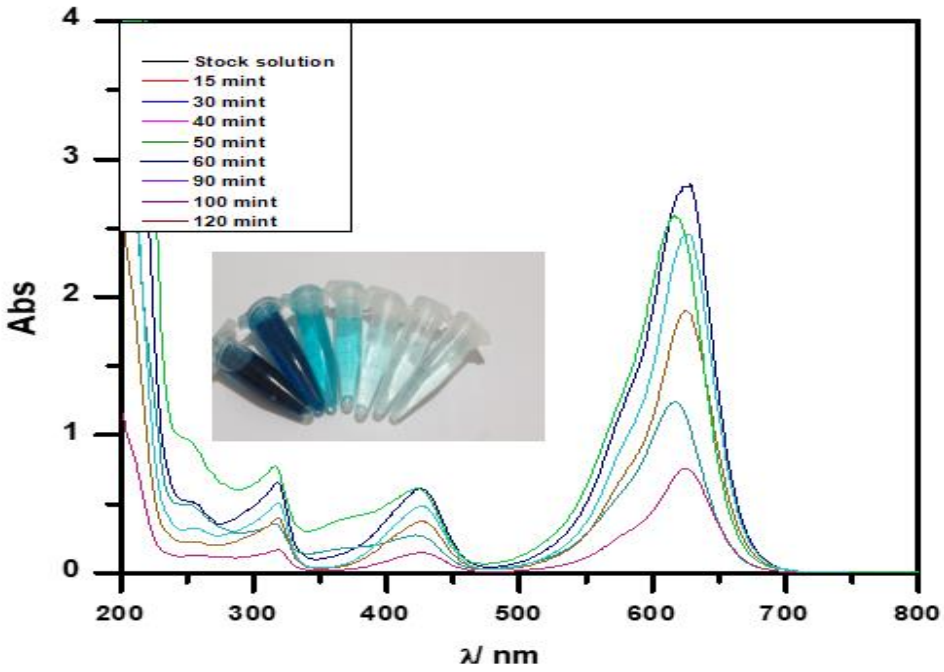

Figure (3-33): Spectra of removal Two dyes (MG and BG) by using (SA-g-P(ITA-co-VBS)/ RC) , (Exp. Condition: Temp. = 25°C, contact time 2 h, and mass absorbent 0.05g).

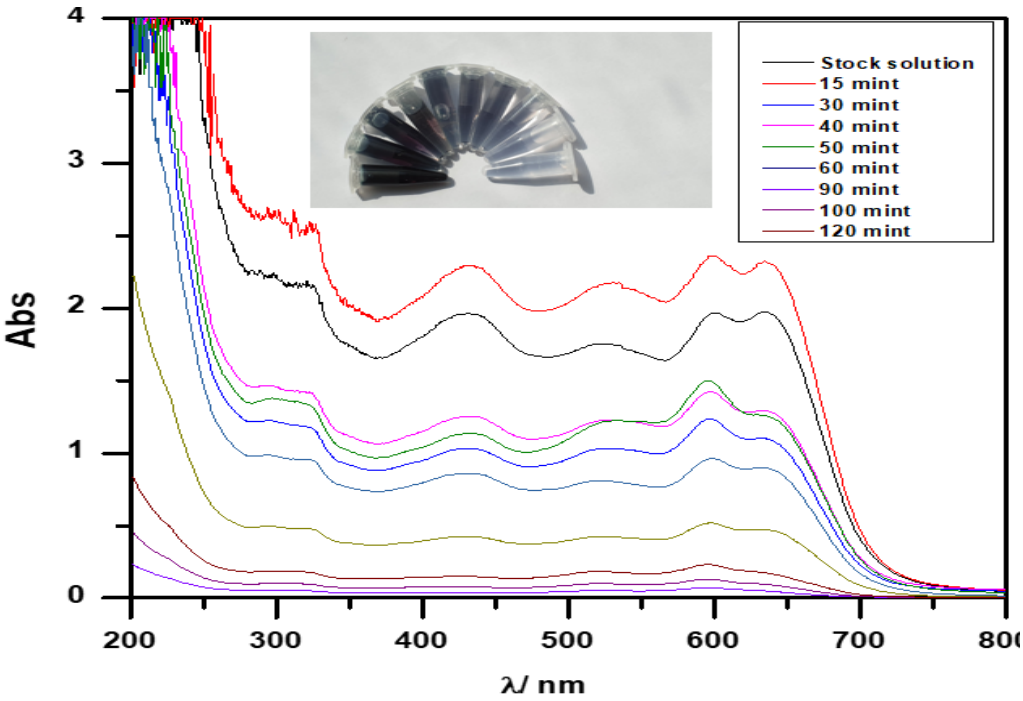

Figure (3-34): Spectra of removal dyes by using (SA-g-P(ITA-co-VBS)/ RC) , (Exp. Condition: Temp. = 25°C, contact time 2 h, and mass absorbent 0.05g).

3-6 Regeneration and Reactivation of (SA-g-P(ITA-co-VBS)/ RC)

The regeneration of hydrogels, after sorption, is one of the significant economic parameter for the treatment method. It helps in elucidating the mechanism of removal two dyes (MG, and BG) from dye -loaded adsorbent, regeneration mechanism and recycling of spent adsorbents, which in turn may reduce operational cost and protect the environment from secondary pollution. Dyes desorption studies were carried out using different desorption agents at concentration (0.01 N) such as H_2SO_4, NaOH, H_3PO_4 , HCl , HNO_3, and water [108-111] . The (SA-g-P(ITA-co-VBS)/ RC) , was regeneration with 100% can be desorbed in diluted HCl solution because the -COO^- is converted into –COOH in acidic solutions, and correspondingly, the electrostatic interactions between (SA-g-P(ITA-co-VBS)/ RC) and two dyes are weakened .The performance and reuse of (SA-g-P(ITA-co-VBS)/ RC) by using HCl solution in the dyes adsorption process was investigated up to 4 steps under optimal conditions . After the 4 cycles of using (SA-g-P(ITA-co-VBS)/ RC), the efficiency is still significant (>80%) and this shows (SA-g-P(ITA-co-VBS)/ RC), is probable renewable adsorber [112, 113] as shown in Figure (3-35), and (3-36) .

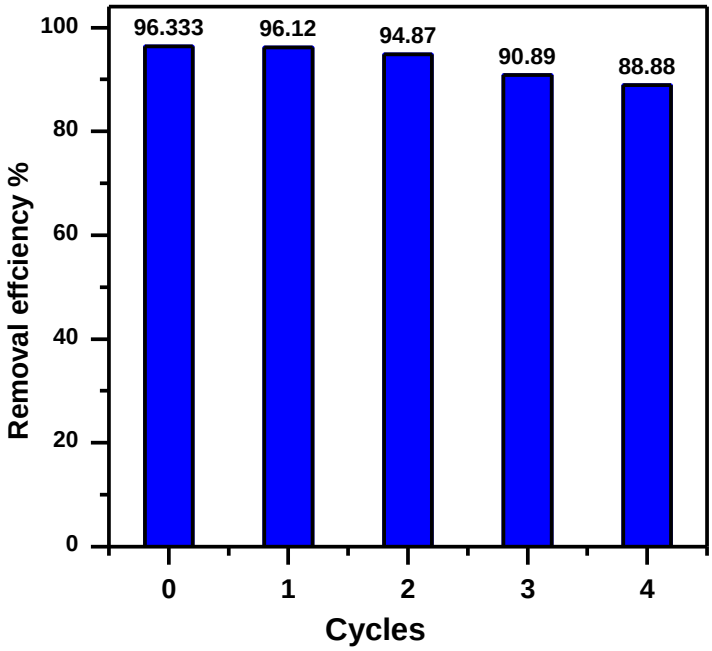

Figure 3-35: multi-cycle use of SA-g-P(ITA-co-VBS)/ RC for MG dye adsorption using HCl as desorption medium.

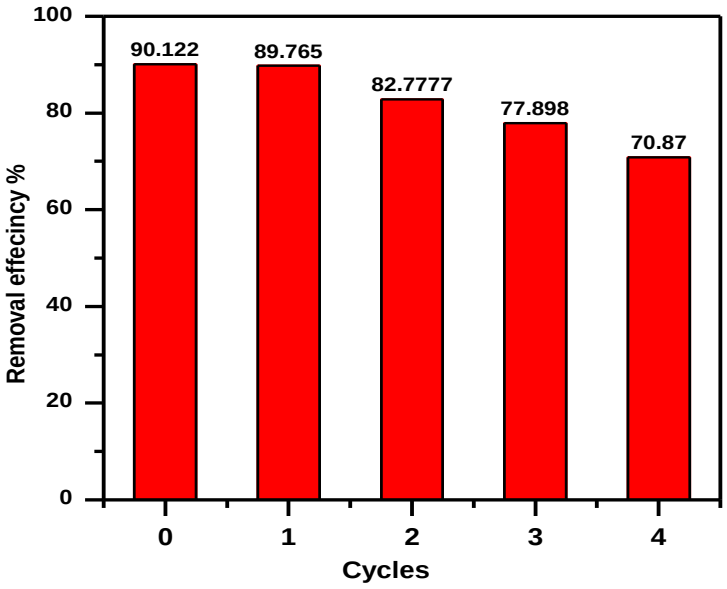

Figure 3-36: multi-cycle use of SA-g-P(ITA-co-VBS)/ RC for BG dye adsorption using HCl as desorption medium.

3-7 Adsorption Isotherms

3-7-1 Freundlich Isotherm

The Freundlich isotherm is defined through the following equation 3-4 [114].

$$\boldsymbol{Q_e = K_f C_e^{1/n}} \qquad (3-4)$$

Q_e: Amount adsorbed per unit weight of adsorbent at equilibrium ($mg.g^{-1}$) , (mol/g), C_e: Equilibrium concentration of adsorbate in solution after adsorption ($mg.L^{-1}$), ($mol.L^{-1}$), K_f: Empirical Freundlich constant or capacity factor ($L.mg^{-1}$) or the dye quantity adsorbed for unit equilibrium concentration, 1/n: Freundlich exponent, if the value of n is equal to unity, the adsorption is linear; if below to unity, then adsorption process is chemical and if the value is above unity, then adsorption is a physical process[115, 116].

3-7-2 Langmuir Isotherm

The Langmuir isotherm is mostly used for pollutants adsorption from liquid solutions. The nature of the adsorption process was derived by Langmuir alternative equation 3-5

$$\boldsymbol{Q_e = \frac{q_m K_L C_e}{1 + K_L C_e}} \qquad (3-5)$$

Q_e: amount adsorbed per unit weight of adsorbent at equilibrium (mg/g), C_e: equilibrium concentration of adsorbent in solution after adsorption ($mg.L^{-1}$), qm: Empirical Langmuir constant which represents maximum adsorption capacity ($mg.g^{-1}$) of the total number of surface sites per mass of adsorbent and it may vary among different compounds because of

differences in adsorbate sizes, K_L: empirical Langmuir constant ($L.mg^{-1}$) or the equilibrium constant of the adsorption reaction [117].

The coefficients of determination (R^2) and isotherm parameters from the nonlinear regressive method were listed in Table (3-10). A comparison of nonlinear fitted curves from experimental data and two different isotherms at 25 ^oC .

A plot of q_e versus C_e Figures (3-37 &3-38) where the values of K_F and 1/n are obtained from the intercept and slope of the linear regressions (Table 3-10 to 3-11).

the correlation coefficient, R^2 values for the Freundlich model at tempracher 25 ^oC are (R^2=0.9959) and (R^2=0.9780) of MG and BG onto SA-g-P(ITA-co-VBS)/ RC [118, 119].

Table 3-10: Different Parameters Isotherm Models for the Adsorption Study of MG dye on to (SA-g-P(ITA-co-VBS)/ RC).

(SA-g-P(ITA-co-VBS)/ RC)			
Freundlich	K_f	292.65	±47.44
	1/n	0.4879	±0.0502
	R^2	0.9959	
Langmuir	q_m (mg/g)	235.66	±31.702
	K_L (L/mg)	0.06	±0.021
	R^2	0.9300	

Table 3-11: different parameters isotherm models for the adsorption study of BG dye on to (SA-g-P(ITA-co-VBS)/ RC)

(SA-g-P(ITA-co-VBS)/ RC)			
Freundlich	K_f	200.39375	28.88134
	1/n	0.43052	0.03425
	R^2	0.9780	
Langmuir	q_m (mg/g)	1843.23246	281.349
	K_L (L/mg)	0.03251	0.01446
	R^2	0.8961	

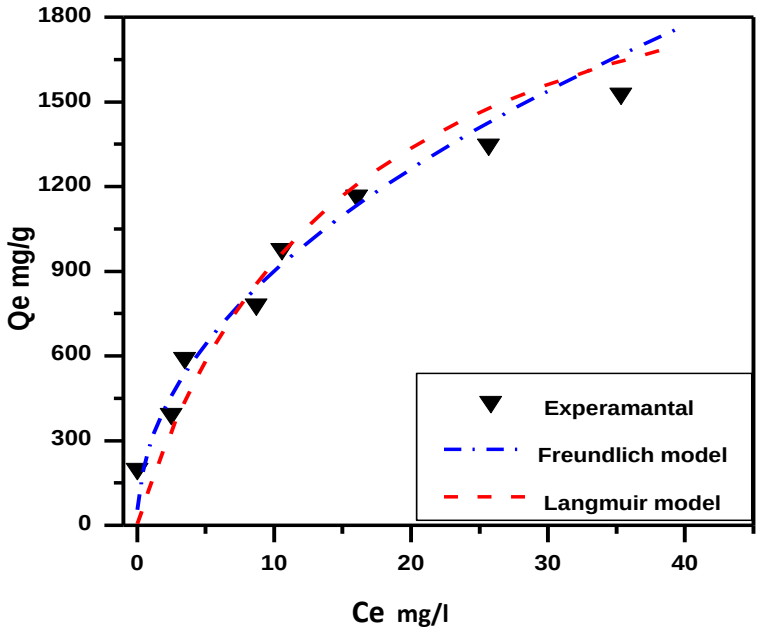

Figure 3-37: Several adsorptions models nonlinear fit of adsorption MG dye onto SA-g-P(ITA-co-VBS)/ RC at temperatures 25 ^{o}C , conc. = 700 mg. L^{-1}, pH of solution 7 and weight of surface 0.05 g/100ml).

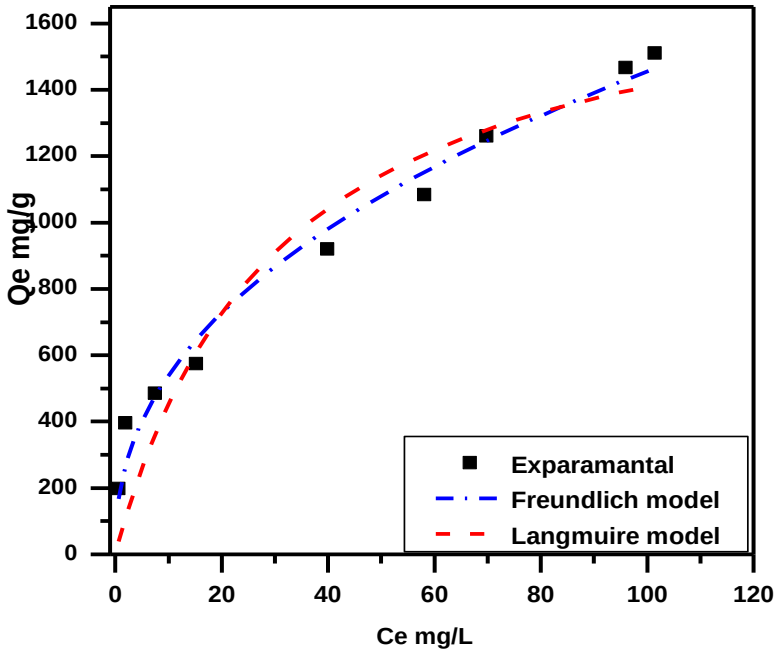

Figure 3-38: Several adsorptions models nonlinear fit of adsorption BG dye onto SA-g-P(ITA-co-VBS)/ RC at temperatures 25 ^{o}C , conc. = 700 mg. L^{-1}, pH of solution 7 and weight of surface 0.05 g/100ml).

3-8 Kinetic study

The mechanism of adsorbate–adsorbent interaction is best described by studying the rate expression for dye adsorption on (SA-g-P(ITA-co-VBS)/ RC); this can be shown by examining the effect of time on the adsorption process and fitting the experimental findings to different conventional models. The agreed function for model suitability for good prediction of experimental data at different times , which is validated by a low relative error among the orchid and experimental adsorption potential [81]. The rate expression can be calculated by analyzing the adsorption data with three different kinetic models: Lagergren first-order ,pseudo-second-order , and Chemisorption [120] . The fitting results are seen in Table 3-12 to 3-13 .

A simple kinetic description of adsorption (pseudo-first-order equation) is as follows in equation (3-6) :

$$q_t=q_e[1-\exp(k_f t)] \quad (3\text{-}6)$$

where qt is the total amount of adsorbate adsorbed at time t (mg^{-1}), q_e is the equilibrium adsorption potential (mg g^{-1}), k_f is the pseudo-first-order rate constant (min^{-1}), and t is the contact time (min).

Lagergren's usability deviates from its linear form, according to the results. This means that the new kinetic model is inadequate for forecasting pseudo-first order sorption kinetics on (SA-g-P(ITA-co-VBS)/ RC). We wanted to apply the experimental data to models because the first-order kinetic model failed to represent the sorption effects [39].

The following is an example of a pseudo-second-order equation based on adsorption equilibrium capacity in equation (3-7):

$$qt=\frac{K2qe2t}{1+K2qet} \quad (3\text{-}7)$$

k_2 and qe were estimated from qt versus t; shows the pseudo-second-order plot; it can be seen that the sorption data maintains its linear profile over the entire period; however, higher values of correlation coefficients and qe determined using the pseudo-second-order model were more compatible with the experimental data[41, 104].

Both of these findings indicate that the model can be used to describe adsorption data over time. Furthermore, the model supports the theory that the sorption process is caused by chemisorption.

The non-linear structure of the Elovich (Chemisorption kinetic formula) model equation is usually written in equation (3-8):

$$qt=\frac{1}{\beta}1\beta\ln(\alpha\beta)+\frac{1}{\beta}\ln t \quad (3-8)$$

The kinetic data from the Elovich model. The nonlinear plots of qt versus t for various initial concentrations demonstrated good consistency between the experimental and calculated qe values. Furthermore, the pseudo-second-order kinetic model has higher correlation coefficients than the Chemisorption model. As a result, the adsorption is best suited to the pseudo-second-order model than the Chemisorption kinetic model. Adsorption kinetics are associated with the intraparticle diffusion concept [81].

The gap in two dye adsorption on (SA-g-P(ITA-co-VBS)/ RC) with shaking time (2–120 min) and initial solution concentration (700 mg/L). Although two dye adsorption were initially very high, the rate of adsorption slowed over time and gradually reached a constant value, as shows in Figure (3-39 and 3-40) (equilibrium time). As the concentration rose, this process was gradually repeated. The initial faster rate may be due to the adsorbents' exposed surface region being available [101, 116, 121].

Table 3-12 : Pseudo first-order, pseudo-second-order, and Elovich including correlation coefficients for (MG dye) adsorption onto SA-g-P(ITA-co-VBS)/ RC.

Type	Parameters	Value	Stand. Error	R^2
Pseudo-First-order	q*e* (mg g^{-1})	1247.36	2.2653	0.3768
	k*f* (min^{-1})	8.184	1.0118	
pseudo-second-order	q*e* (mg g^{-1})	1339.83	3.3684	0.9857
	ks (gmg^{-1} min^{-1})	1.589	0.1363	
Elovich	α (mg g^{-1} min^{-1})	40.765	3.1005	0.8777
	β (g min^{-1})	5.369	1.3407	

Table 3-13 : Pseudo first-order, pseudo-second-order, and Elovich including correlation coefficients for (BG dye) adsorption onto SA-g-P(ITA-co-VBS)/ RC.

Type	Parameters	Value	Stand. Error	R^2
Pseudo-First-order	qe (mg g^{-1})	1233.833	3.3864	0.377
	kf (min^{-1})	1.5806	0.1363	
pseudo-second-order	qe (mg g^{-1})	1247.365	0.0213	0.9303
	ks (gmg^{-1} min^{-1})	6.1233	0.121	
Elovich	α (mg g^{-1} min^{-1})	42.651	2.113	0.895
	β (g min^{-1})	3.346	1.012	

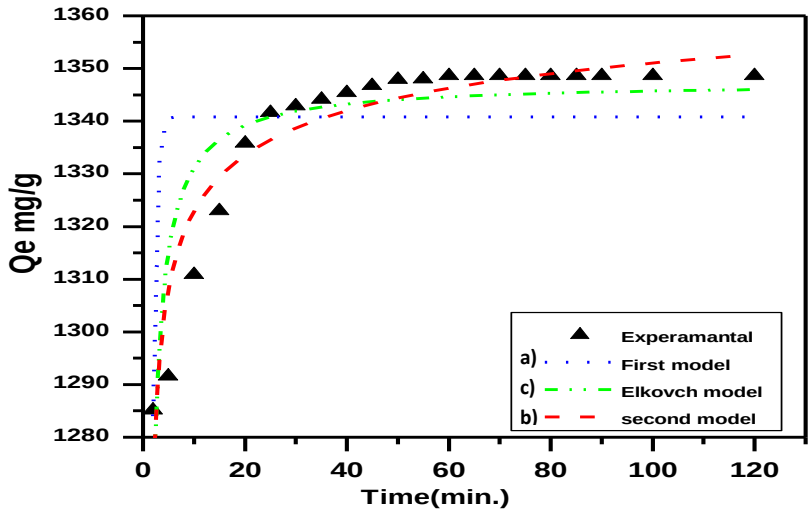

Figure 3-39 : Adsorption rate curve models fitted to experimental MG dye adsorption on the surface of (SA-g-P(ITA-co-VBS)/ RC). a) first-order kinetic; b) second-order kinetic; and c) Elkovich kinetic (pH 7, Temp. 25 ^{o}C , mass dosage 0.05 g).

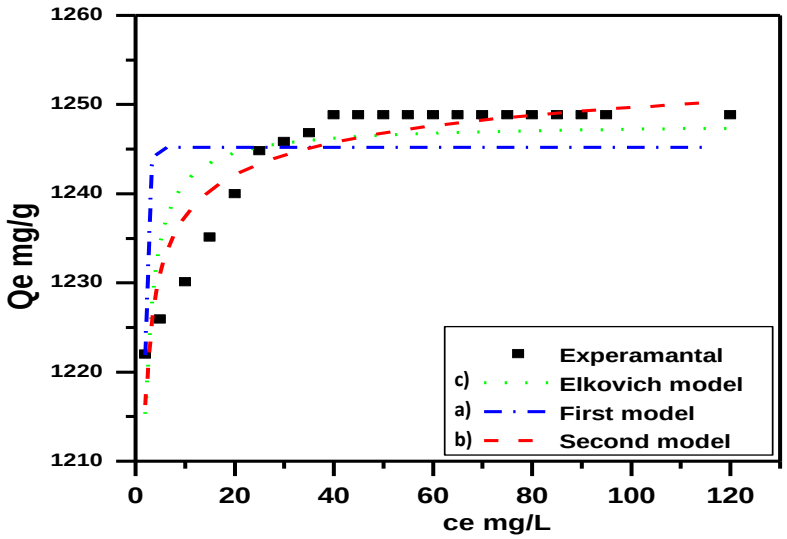

Figure 3-40 : Adsorption rate curve models fitted to experimental BG dye adsorption on the surface of (SA-g-P(ITA-co-VBS)/ RC). a) first-order kinetic; b) second-order kinetic; and c) Elkovich kinetic (pH 7, Temp. 25 ^{o}C , mass dosage 0.05 g).

3-9 Biological Activity of Bacterial Test

In this study, one type of Aspergillus flavus and two types of bacteria were Gram-positive bacteria (*staphylococcus*) and Gram-negative bacteria (*Pseudo monas*), using four isolates depending on the method of disc diffusion, where concentrations (0.1, 0.2, 0.3, and 0.4 gm) from the three surfaces RC, SA-g-P(ITA-co-VBS); and (SA-g-P(ITA-co-VBS)/ RC). The results showed the zones of inhibition that the surface of the RC showed high antibacterial activity (1.3cm) for a concentration (0.16 mg/L) against (*Pseudo monas*) and (ZERO) against *Streptococcus*, meaning that it was resistant and had no effect. But when the (SA-g-P(ITA-co-VBS) was used, this surface showed antibacterial activity at (1.1 cm) for a concentration of 0.16 mg/L against Gram negative bacteria. (*Pseudo monas*) and (2.4 cm) against *Streptococcus*, meaning that it had a higher effect on negative bacteria. But when the (SA-g-P(ITA-co-VBS)/

RC); was used, this surface showed a very high antibacterial activity at (3 cm) at the same concentration against Gram negative bacteria. *(Pseudo monas)* and (1.6 cm) against *Streptococcus*, meaning that it had less effect on positive bacteria. This is a clear indication that the process of loading (RC) on the hydrogel increases the efficiency of the surface in the biological activity. [122, 123]. as shown in the Figure 3-41 .

Also, the biological activity of one type of fungus (Aspergillus flavus) was studied using three RC surfaces, SA-g-P (ITA-co-VBS); And (SA-g-P (ITA-co-VBS) / RC) using four isolates, at different concentrations and times, as the results shown in Figure 3-42 showed an increase in fungal inhibition occurs with increasing time and concentration. Also, a comparison of the efficiency of the three RC surfaces, SA-g-P (ITA-co-VBS) was performed; And (SA-g-P (ITA-co-VBS) / RC) where it was observed that (SA-g-P (ITA-co-VBS) / RC) was highly efficient in inhibiting fungi, where the order of increase of fungal inhibition (SA-g-P (ITA-co-VBS) / RC)> SA-g-P (ITA-co-VBS)>RC [124, 125] .

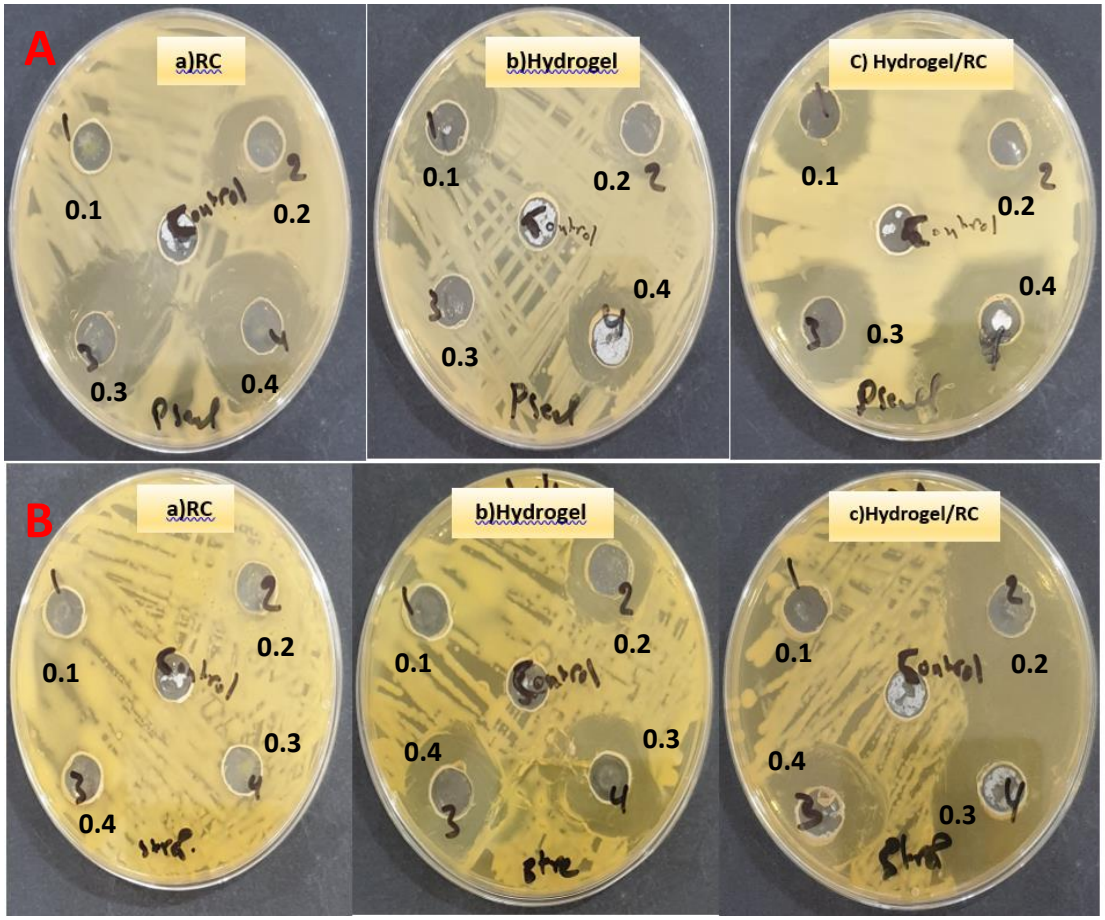

Figure 3-41: Anti-bacterial activities of the (A) Gram- negative bacteria, (B) Gram-positive bacteria using disc diffusion method.

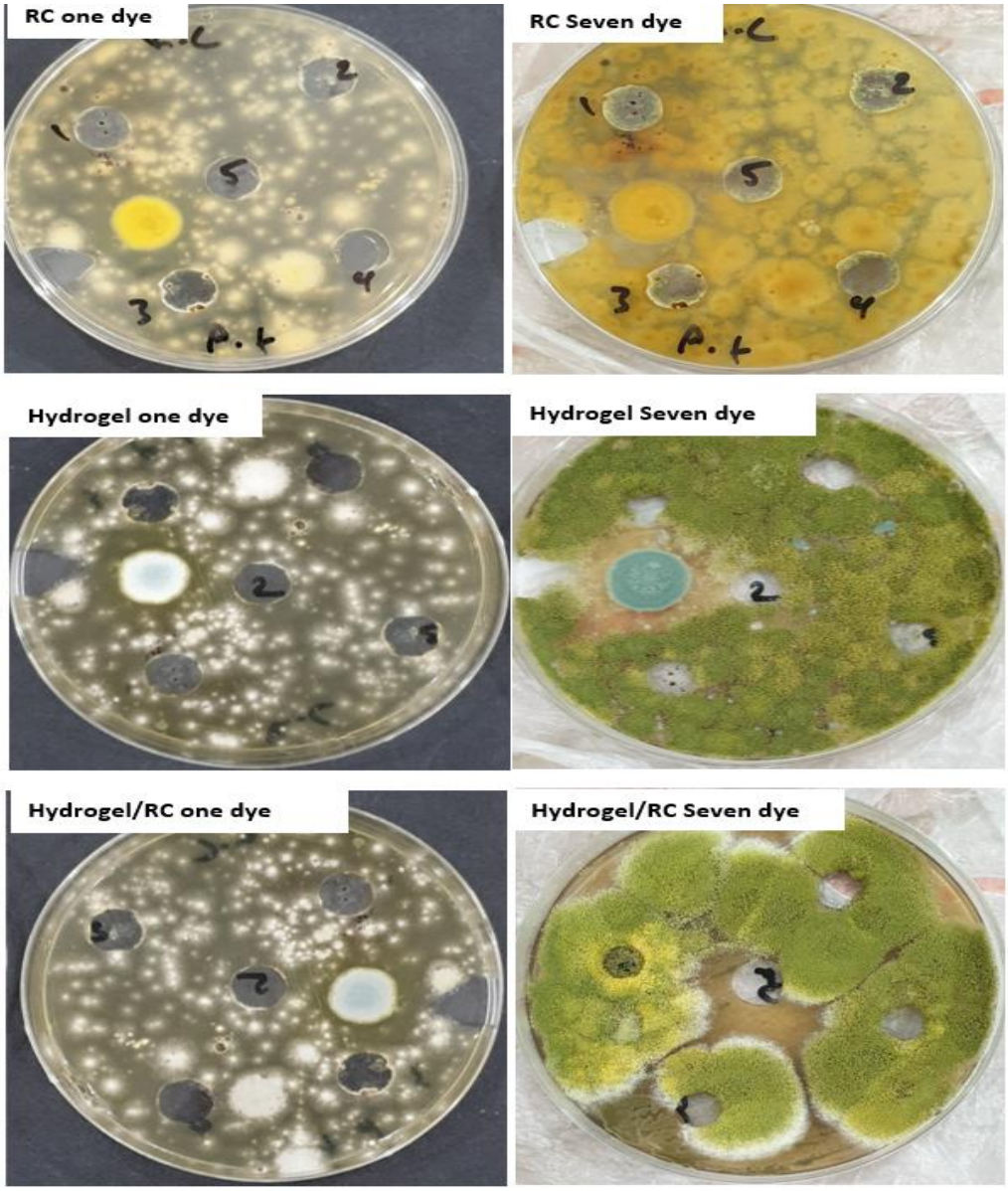

Figure 3-42: biological activity of fungus (Aspergillus flavus) onto three surfaces RC, hydrogel ; and hydrogel/ RC)

3-10 Surface Efficacy in Mice Healing

It was processed about (0.1 g) from the surface prepared from (RC), and (SA-g-P(ITA-co-VBS) hydrogel as shown in the image (A). On the second day, a very slight improvement was observed in the treatment of wounds, as the rate of healing and improvement of the wounds was at its beginning, as shown in the picture (B). In the third to seven days, an improvement was observed in the wound, where the rate of healing and wound improvement was very clear, with some redness in the skin surrounding the wound, as shown in images (C-E). On the fourteen day, according to the results shown in picture (F), there is healing The wound is completely healed and the skin returns to its natural color, with a slight burn effect remaining. The reason for healing is due to the fact that the leaves RC and hydrogel have high efficiency in treating and healing wounds, and are environmentally friendly, non-toxic, and anti-inflammatory. and the results were obtained as shown in Figure (3-43) and Figure (3-44) .

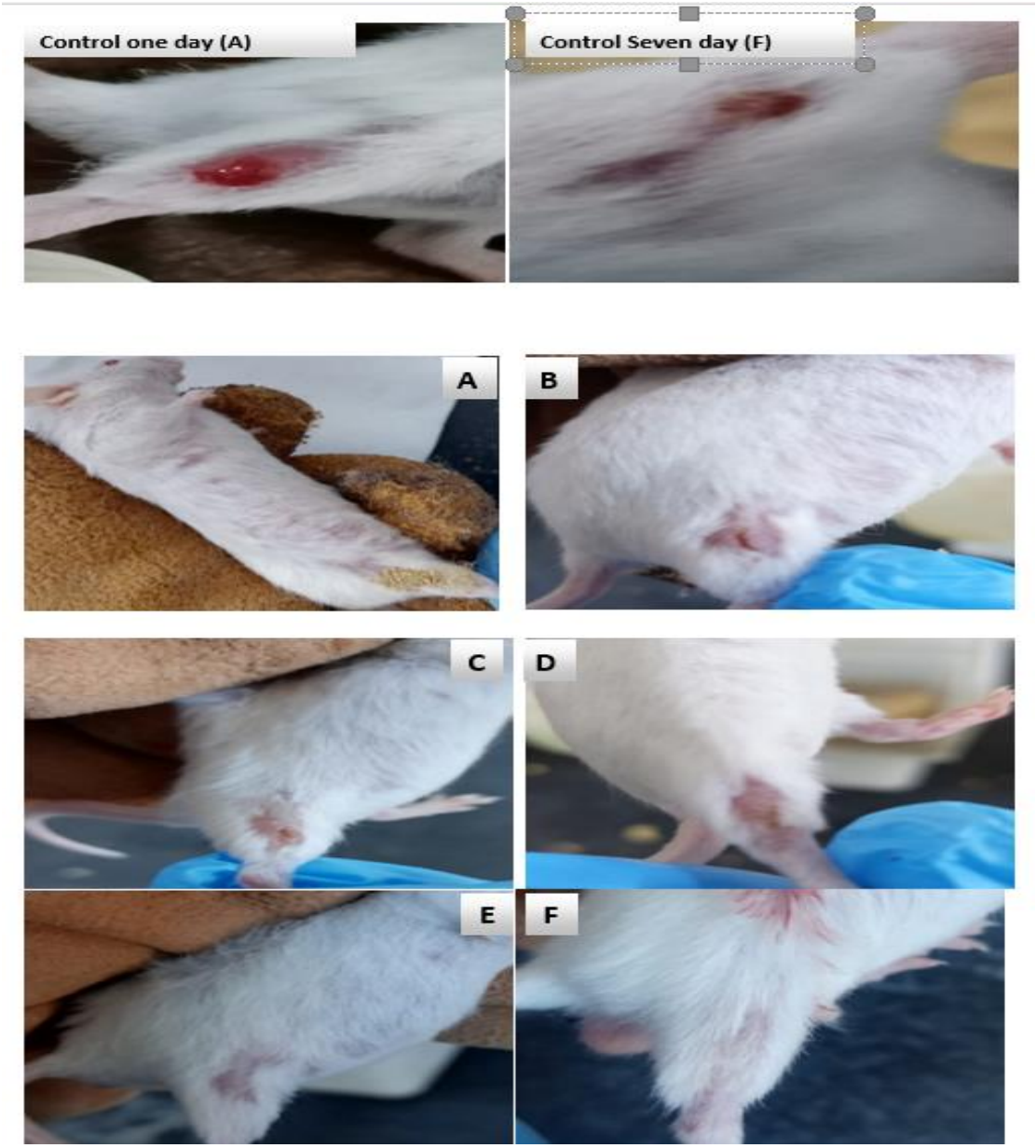

Figure 3-43: Effect of the surface RC on the wound healing of mice during fourteen days.

Figure 3-44: Effect of the surface hydrogel on the wound healing of mice during fourteen days.

However, when using a hydrogel loaded with RC, an increase in the wound healing efficiency of rats was observed during the first days of the wound. As shown in Figure 3-45 .

On the first day, mice were clearly injured on the first day of wounding, and they were treated with about (0.1 gm) from the surface (SA-g-P(ITA-co-VBS)/ RC) as shown in image (A) .On the Second to third day, an improvement was observed in the mice, where the rate of healing and improvement of mice was very clear, with some redness in the skin surrounding the mice as shown in image (C, b) .On the four and five day, the clear results in image showed a clear healing of the mice and the return of the skin to its natural pink color, a clear evidence of the surface's efficiency in mice healing, as shown in image (D, E)

On the seventh day, and according to the results shown in the image (F), there is a complete recovery of the mice and the return of the skin to its normal color, with a noticeable disappearance of the burn scar. This is due to the fact that (SA-g-P(ITA-co-VBS)/ RC) have high efficiency in treating and healing the mice. It is environmentally friendly, non-toxic and also considered an anti-inflammatory. In addition, there is biocompatibility with mammalian cells [126-128].

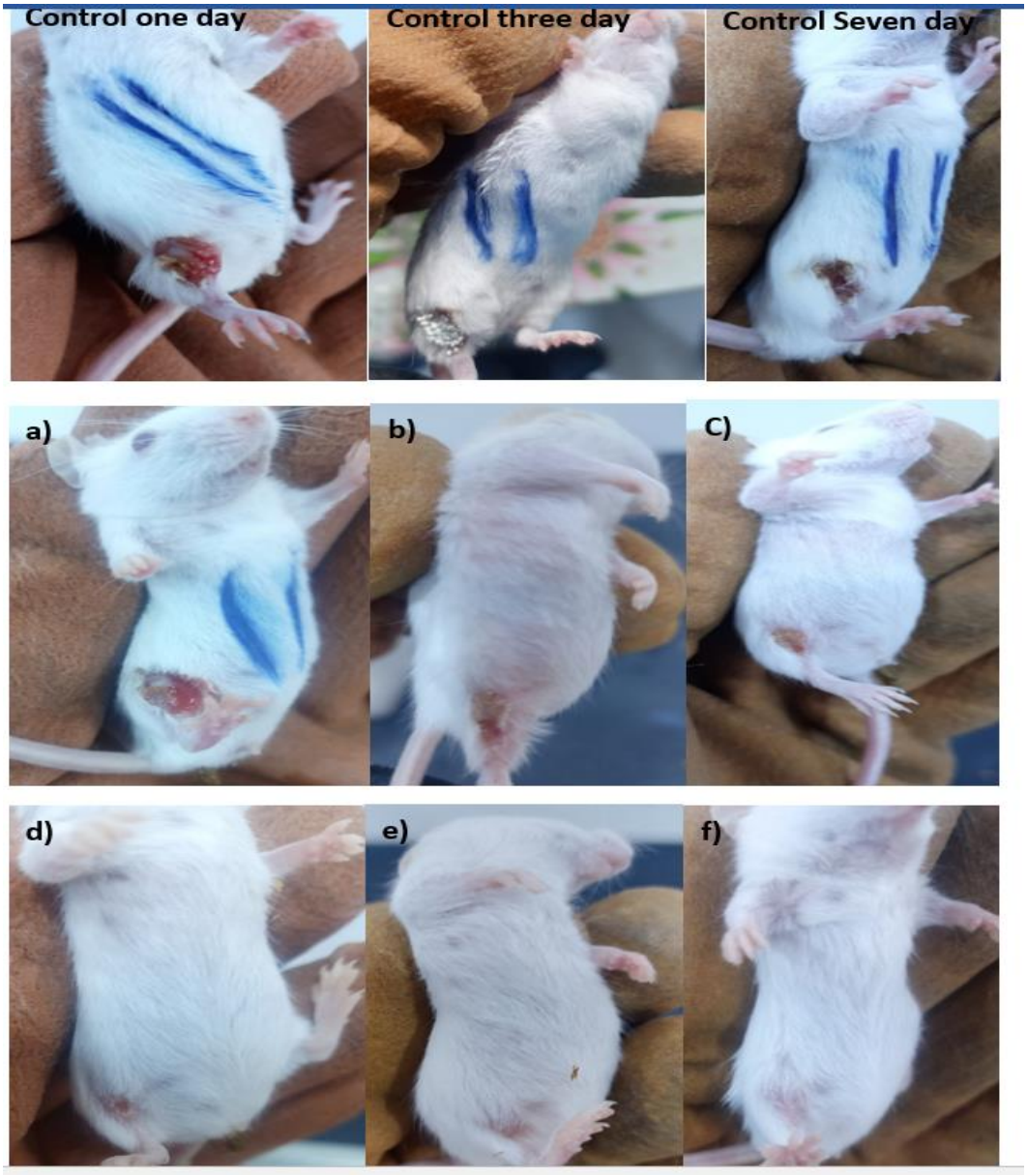

Figure 3-45: Effect of the surface hydrogel\RC nanocomposite on the wound healing of mice during seven days.

Conclusions

Studies have been conducted to gain understandings and generic knowledge of the equilibrium aspects of adsorption of adsorbents, (SA-g-P(ITA-co-VBS)/ RC), SA-g-P(ITA-co-VBS), RC surfaces. Removal of two dyes (Brilliant green BG dye , Malachite green MG dye) from aqueous solutions by adsorption with , (SA-g-P(ITA-co-VBS)/ RC) surfaces have been experimentally determined. The best results have been found in temperature 25 ^{o}C, and adsorbent dosage 0.05gm of, (SA-g-P(ITA-co-VBS)/ RC) for both studying adsorption capacity and removal percentage and the following observations are made:

1. The adsorption capacity and percentage of two dyes removal increase with increasing contact time, surface area, and temperature. But adsorption capacity has decreased with the increase of adsorbent dosage.
2. The optimum contact time for equilibrium to be achieved is found to be 1 hr. It is basically due to saturation of the active site which does not allow further adsorption to take place.
3. For MG and BG dyes on adsorbent surfaces, maximum adsorption was found to be at pH = 7 .
4. The negative value of ΔG confirms the spontaneous nature adsorption process. The positive value of ΔS showed the increased randomness at the solid-solution interface during adsorption and the positive value of ΔH indicated the adsorption process was endothermic.
5. The interaction between dose and initial concentration showed a significant effect on the adsorption process. Adsorbent showed fits better to Freundlich isotherm which suggests that adsorption is heterogeneous.

6. The adsorption efficiency for removal of two dyes (SA-g-P(ITA-co-VBS)/ RC) surface was found better than the SA-g-P(ITA-co-VBS) and RC .
7. Removal of laboratory aqueous pollutants (dyes) by using (SA-g-P(ITA-co-VBS)/ RC) to give low absorbance (0.0001) by using UV-Visible spectrophotometer at a chosen wavelength for 120 minutes.
8. The chemisorption, pseudo-first-order, and pseudo-second-order kinetic models were applied to test the experimental data. The pseudo-second -order exhibited the best fit for the kinetic studies.
9. The (SA-g-P(ITA-co-VBS)/ RC) was regeneration with 100% can be desorbed in diluted HCl solution in the two dyes (MG and BG) adsorption process was investigated up to 2 steps under optimal conditions.
10. (SA-g-P(ITA-co-VBS)/ RC) had high antibacterial activity, that is, it had a higher effect on the Gram-positive bacteria than on the Gram-negative bacteria.
11. In two to seven days, according to the results, there is complete healing of the mice and the return of the skin to its natural color.

Future Works

A study of adsorption of two dyes using (SA-g-P(ITA-co-VBS)/ RC) hydrogel nanocomposite work needs to be done to further understand the science behind the adsorption processes.

1- The possibility of using these surfaces (SA-g-P(ITA-co-VBS)/ RC) hydrogel nanocomposite and (SA-g-P(ITA-co-VBS) to remove many contaminants such as heavy elements and pesticides and herbicides.

2- Preparing new surfaces that are inexpensive, environmentally friendly, and the possibility of replacing RC with Zinc oxide, Titanium dioxide.

3- Synthesizing new polymeric complexes adsorbent on the Cay, CNT and Activated carbon surfaces.

Reference

Reference

1. Romero, F., et al., *Desiccation events change the microbial response to gradients of wastewater effluent pollution.* Water research, 2019. **151**: p. 371-380.
2. Berradi, M., et al., *Textile finishing dyes and their impact on aquatic environs.* Heliyon, 2019. **5**(11): p. e02711.
3. Aljeboree, A.M., A.N. Alshirfy, and A.F. Alkaim, *Removal of textile dyes form aqueous solutions by using coconut as a source of activated carbon: As a model of equilibrium and thermodynamic studies.* Plant Archives, 2020. **20**(1): p. 3187-3195.
4. Aljeboree, A.M., et al., *Adsorption of textile dyes in the presence either clay or activated carbon as a technological models: A review.* Journal of Critical Reviews, 2020. **7**(5): p. 620-626.
5. A. Demirbas, *Agricultural based activated carbons for the removal of dyes from aqueous solutions: a review* J. Hazard. Mater., 2009. **167**: p. 1-9.
6. Pinar Ilgina, H.O., Ozgur Ozay, *Selective adsorption of cationic dyes from colored noxious effluent using a novel N-tert-butylmaleamic acid based hydrogels.* Reactive and Functional Polymers 2019. **124**: p. 189–198.
7. Muhammad Saif UrRehmanb, M., Muhammad Ashfaqa Naim Rashid ,Muhammad FaizanNazaraMuhamm,DanishaJong-InHan, *Adsorption of Brilliant Green dye from aqueous solution onto red clay*. Chemical Engineering Journal, 2020. **228** p. 54-62.
8. Mane, V.S. and P.V.V. Babu, *Studies on the adsorption of Brilliant Green dye from aqueous solution onto low-cost NaOH treated saw dust.* Desalination, 2011. **273**: p. 321-329.
9. R. A. Mansour, A.E.S., A. Attia,Mokhtar S. Beheary, *Brilliant Green Dye Biosorption Using Activated Carbon Derived from Guava Tree Wood.* International Journal of Chemical Engineering, 2020. **2**: p. 190.
10. Jasim, L.S., N.D. Radhy, and H.O. Jamel, *Synthesis and characterization of poly (acryl amide - Maleic acid) hydrogel: Adsorption kinetics of a malachite green from aqueous solutions.* Eurasian Journal of Analytical Chemistry, 2018. **13**(1).
11. S. Nethaji a, b., A. Sivasamya,, G. Thennarasua, S. Saravananb, *Adsorption of Malachite Green dye onto activated carbon derived from Borassus aethiopum flower biomass.* Journal of Hazardous Materials, 2010. **181** p. 271–280.
12. Liang Y, Zhao X, and M. PX, *pH-responsive injectable hydrogels with mucosal adhesiveness based on chitosan grafted-*

dihydrocaffeic acid and oxidized pullulan for localized drug delivery. J Colloid Interf Sci, 2019. **536**: p. 224-234.
13. Ahmed EM, *Hydrogel: preparation, characterization, and applications: a review*. J Adv Res 2019. **6**(2): p. 105-121.
14. Makhado E and Hato M *Preparation and characterization of sodium alginate-based oxidized multi-walled carbon nanotubes hydrogel nanocomposite and its adsorption behaviour for methylene blue dye.* . Front Chem, 2021. **9**: p. 576913.
15. Li J, Ma J, and C. S, *Adsorption of lysozyme by alginate/graphene oxide composite beads with enhanced stability and mechanical property*. Mater Sci Eng C, 2019. **89**: p. 25-32.
16. Nompumelelo Malatji, E.M., Kwena D Modibane, Kabelo E Ramohlola,Thabiso C Maponya,Gobeng R Monama , Mpitloane J Hato, *Removal of methylene blue from wastewater using hydrogel nanocomposites: A review*. Nanomaterials and Technologies for Environmental Applications 2021. **11**: p. 1-27.
17. Thakur S, Pandey S, and Arotiba O, *Development of a sodium alginate-based organic/inorganic superabsorbent composite hydrogel for adsorption of methylene blue.* . Carbohydr Polym 2019. **135**: p. 34-46.
18. Xu J, Liu X, and Ren X, *The role of chemical and physical crosslinking in different deformation stages of hybrid hydrogels.* . Eur Polym J 2019. **100**: p. 86-95.
19. Wang, W., Wang, A *Synthesis and swelling properties of pH sensitive semi-IPN superabsorbent hydrogels based on sodium alginate-g-poly (sodium acrylate) and polyvinylpyrrolidone*. Carbohydr Polym 2020. **80**(4): p. 1028-1036.
20. Makhado E, P.S.R.J.M.a., *synthesis of xanthan gum-cl-poly (acrylic acid) based reduced graphene oxide hydrogel composite for adsorption of methylene blue and methyl violet from aqueous solution*. Int J Biol Macromol 2018. **119**: p. 255-269.
21. Mohammed A. Jawad, A.J.K., Nadher D. Radia, *Role of Sodium Alginate-g-poly (Acrylic acid-fumaric acid) Hydrogel for Removal of Pharmaceutical Paracetamol from Aqueous Solutions by Adsorption* International Journal of Pharmaceutical Quality Assurance, 2021. **12**(3): p. 202-205.
22. Nompumelelo A Malatji, E.B.M., Kwena D Modibane,Kabelo E Ramohlola,Thabiso C Maponya,Gobeng R Monama,Mpitloane J Hato, *Removal of methylene blue from wastewater using hydrogel nanocomposites: A review*. Nanomaterials and Nanotechnology, 2021. **11**: p. 1-27.

23. Ahmed, E.M., *Hydrogel: Preparation, characterization, and applications: A review.* Journal of Advanced Research, 2019. **6**(2): p. 105-121.
24. Issa Katime, E.R., *Absorption of metal ions and swelling properties of poly(acrylic acid-co-itaconic acid) hydrogels.* Journal of Macromolecular Science, 2022. **2**: p. 22-25.
25. Parvin Naderi, K.K., Reza Jahanmardi , Mohammad Jalal Zohuriaan-Mehr, *Preparation of itaconic acid bio-based cross-linkers for hydrogels.* Journal of Macromolecular Science, Part A, 2022. **12**: p. 12-18.
26. Teow, Y.H. and A.W. Mohammad, *New generation nanomaterials for water desalination: A review.* Desalination, 2019. **451**: p. 2-17.
27. Zhang, W., D. Zhang, and Y. Liang, *Nanotechnology in remediation of water contaminated by poly-and perfluoroalkyl substances: A review.* Environmental pollution, 2019. **247**: p. 266-276.
28. Salman, J.M. and A.M. Aljeboree, *Adsorption, Modeling, Thermodynamic, and Kinetic Studies of Removal of Textile-dye using Low-Cost Adsorbents.* International Journal of Drug Delivery Technology, 2022. **12**(3): p. 1400-1405.
29. Fu, L.-H., et al., *Cellulose/vaterite nanocomposites: sonochemical synthesis, characterization, and their application in protein adsorption.* Materials Science and Engineering: C, 2019. **96**: p. 426-435.
30. Aseel M. Aljeboree, H.Y.A.-G., Ali T. Bader,Ayad F. Alkaim, *ADSORPTION OF TEXTILE DYES IN THE PRESENCE EITHER CLAY OR ACTIVATED CARBON AS A TECHNOLOGICAL MODELS: A REVIEW.* Journal of Critical Reviews, 2020. **7**(5).
31. Tariq J. AlMusawi, N.M., Mahmoud Taghavi, Samaneh Mohebi, Davoud Balarak, *Activated carbon derived from Azolla fliculoides fern: a high adsorption capacity adsorbent for residual ampicillin in pharmaceutical wastewater.* Biomass Conversion and Biorefnery 2021. **1**: p. https://doi.org/10.1007/s13399-021-01962-4.
32. Hazem Hassan , A.S., Ahmed K. El-ziaty , Mohamed El-Sakhawy, *New chitosan/silica/zinc oxide nanocomposite as adsorbent for dye removal.* International Journal of Biological Macromolecules 2019. **131**: p. 520-526.
33. A.Nemr, O. Abdelwahab, A. Khaled, and A. El Sikaily, *Biosorption of Direct Yellow 12 from aqueous solution using green alga Ulva lactuca.* Chemistry and Ecology, 2006. **22**(4): p. 253–266.

34. P. Vieira, A.A. Santana, W.B. Bezerra, Hildo A.S. Silva, A.P. Chaves, C.P. de Melo, C.da Silva Filho, and C. Airoldi *Kinetics and thermodynamics of textile dye adsorption from aqueous solutions using babassu coconut mesocarp.* J.Hazard.Mater., 2009. **166**: p. 1272-1278.
35. Aseel M Aljeboree, R.A.M., Makarim A. Mahdi, Layth S. Jasim, Ayad F. Alkaim, *Synthesis, Characterization of P(CH/AA-co-AM) and Adsorptive Removal of Pb (II) ions from Aqueous Solution: Thermodynamic Study.* NeuroQuantology 2021. **19**(7): p. 137-143.
36. Abbas, N.K.L., S. Jasim *Synthesis and Characterization of Poly (CH/AA-co-AM) Composite: Adsorption and Thermodynamic Studies of Benzocaine on from Aqueous Solutions* International Journal of Drug Delivery Technology 2019. **9**(4): p. 558-562.
37. Naghdi, M., et al., *Pine-wood derived nanobiochar for removal of carbamazepine from aqueous media: Adsorption behavior and influential parameters.* Arabian Journal of Chemistry, 2017: p. https://doi.org/10.1016/j.arabjc.2016.12.025.
38. Xiong, J., et al., *Hexagonal boron nitride adsorbent: Synthesis, performance tailoring and applications.* Journal of Energy Chemistry, 2019. **40**: p. 99-111.
39. Saeed U J, A.A.K., Saad M, Iftikhar A, Guohua S, Cheng-Meng C, Rashid A, *Removal of azo dye from aqueous solution by a low-cost activated carbon prepared from coal: adsorption kinetics, isotherms study, and DFT simulation.* Environmental Science and Pollution Research, 2020. **1**: p. https://doi.org/10.1007/s11356-020-11344-4.
40. Langmuir, I., *The adsorption of gases on plane surfaces of glass, mica and platinum.* Journal of the American Chemical society, 1918. **40**(9): p. 1361-1403.
41. Del Mar Orta, M., Martn, Julia,Medina-Carrasco, Santiago,Santos, Juan Luis,Aparicio, Irene,Alonso, Esteban, *Adsorption of propranolol onto montmorillonite: Kinetic, isotherm and pH studies.* Applied Clay Science, 2019. **173**: p. 107-114.
42. Freundlich, H., *Over the adsorption in solution.* J. Phys. Chem, 1906. **57**(385471): p. 1100-1107.
43. Y.S. Ho, J.F. Porter, and G. McKay, *Individual response profiles of male Wistar rats in animal models for anxiety and depression.* Water Air Soil Pollut., 2002. **141**: p. 1-12.
44. Rosch, T.H.D.a.J.W., *JMM Profile: Streptococcus pneumoniae: sugar-coated captain of the men of death.* Journal of Medical Microbiology, 2021. **70**(001): p. 446.

45. Zheng Pang, R.R., Bernard R. Glick, Tong-Jun Lin, Zhenyu Cheng., *Antibiotic resistance in Pseudomonas aeruginosa: mechanisms*

and alternative therapeutic strategies. Biotechnology Advances, 2018. **11**(0): p. 13.

46. KLICH, M.A., *Aspergillus flavus: the major producer of aflatoxin.* MOLECULAR PLANT PATHOLOGY, 2007. **8**(6): p. 713–722.

47. Bengyella Louis1, 3*, Sayanika Devi Waikhom1, et al., *Invasion of Solanum tuberosum L. by Aspergillus terreus: a microscopic and proteomics insight on pathogenicity.* Louis et al. BMC Research Notes, 2014. **7**: p. 350.

48. Aseel M. Aljeboree1*, H.K.A., et al., *Synthesis, characterization, and applicability of an acrylic acid-grafted sodium alginate- based Zinc oxide hydrogel nanocomposite for crystal violet dye removal.* research square, 2022.

49. Anwar R. Karim, N.D.R., *Synthesis and Characterization of Sodium Alginate-G-Poly (AAC-AAM)/BC Nanocomposite Hydrogel and its Application for Dyes.* HIV Nursing 2022. **22**(2): p. 1945-1949.

50. Nadher D Radia, A.B.M., Ghufran A. Mohammed, Abeer Sajid4, Usama S. Altimari5, Marwah A. Shams6, Aseel M. Aljeboree7, Firas H. Abdulrazzak, *Removal of Rose Bengal Dye from Aqueous Solution using Low Cost (SA-g-PAAc) Hydrogel: Equilibrium and Kinetic Study.* RESEARCH ARTICLE, 2022. **12**(3).

51. Hadeel K. Albdairi , A.M.A., *Crystal Violet Dye Removal by Low-Cost Nano-Superabsorbent Hydrogel: Thermodynamic and Isotherm Model.* Journal of Medicinal and Chemical Sciences 2022. **6**(2): p. 186-194.

52. Rafid Q. Kmal, A.M.A., Layth S. Jasim, Nadher D. Radia, Ayad F. Alkaim, *Removal of Toxic Congo Red Dye from Aqueous Solution Using a Graphene Oxide/Poly (Acrylamide-Acrylic acid) Characterization, Kinetics and Thermodynamics Studies.* Journal of Chemical Health Risks, 2022. **12**(4): p. 609-619.

53. Zainab D. Alhattab1 , A.M.A., *Modification, Preparation, and Characterization, Low-Cost Hydrogel Nano/Micro Composite: Regeneration and Isotherm Models.* Journal of Medicinal and Chemical Sciences, 2022. **6**(1): p. 152-159.

54. Essa2, M.R.N.S.M., *Adsorption Kinetics and Thermodynamics of a Malachite Green from Aqueous Solutions by Novel Nanocomposite*

Hydrogel Ntadbrp-Poly (Aac-Co-Ca). HIV Nursing, 2022. **22**(2): p. 3740-3746.

55. Aljeboree, A.M.R., Nadher D;Jasim, Layth Sameer ;Alwarthan, Abdulrahman A.;Khadhim, Mustafa M.;Washeel Salman, Abbas ;Alkaim, Ayad F., *Synthesis of a new nanocomposite with the core TiO2/hydrogel: Brilliant green dye adsorption, isotherms, kinetics, and DFT studies.* Journal of Industrial and Engineering Chemistry, 2022. **109**: p. 475 - 485.
56. Tong Gao, G.G., Xuejun Wang, Tao Lou, *Electrospun molecularly imprinted sodium alginate/polyethylene oxide nanofibrous membranes for selective adsorption of methylene blue.* International Journal of Biological Mactomiolecules, 2022. **207**: p. 62-71.
57. Hanif Subhan, S.A., Luqman Ali Shah, Noor Saeed Khattak, Ivar Zekker, *Sodium alginate grafted hydrogel for adsorption of methylene green and use of the waste as an adsorbent for the separation of emulsified oil.* Journal of Water Process Engineering, 2022. **46**(1): p. 102546.
58. Ziging Tang, H.G., Jianyu Xu, Zongjin Li, Guoxing Sun, *Cationic poly(diallyldimethylammonium chloride) based hydrogel for effective anionic dyes adšorption from aqueous solution.* Reactive and Functional Polymers, 2022. **174**: p. 105-239.
59. Sourbh Thakur , J.C., Abhishek Thakur, Oguzhan Gunduz, Walaa F. Alsanie,Charalampos Makatsoris, Vijay Kumar Thakur, *Highly efficient poly(acrylic acid-co-aniline) grafted itaconic acid hydrogel: Application in water retention and adsorption of rhodamine B dye for a sustainable environment.* Chemosphere, 2022. **303**: p. 134917.
60. Hanif Subhan, et al., *Sodium alginate grafted poly(N-vinyl formamide-co-acrylic acid)-bentonite clay hybrid hydrogel for sorptive removal of methylene green from wastewater.* Colloids and Surfaces A: Physicochemical and Engineering Aspect, 2021. **611**: p. 125853.
61. SH H Wared, R., N.D, *Synthesis and Characterization of Sodium Alginate-g-polyacrylic Acid Hydrogel and its Application for Crystal Violet Dye Adsorption.* RESEARCH ARTICLE, 2021. **11**(2).
62. Nadher D Radhy, L.S.J., *A novel economical friendly treatment approach: Composite hydrogels.* Caspian Journal of Environmental Sciences, 2021. **19**(5): p. 841-852.
63. Edwin Makhado, S.P.b.c.K.D.M., Misook Kang , Mpitloane Joseph Hato, *Sequestration of methylene blue dye using sodium alginate*

poly(acrylic acid)@ZnO hydrogel nanocomposite: Kinetic, Isotherm, and Thermodynamic Investigations. International Journal of Biological Macromolecules, 2020. **162**: p. 60-73.

64. Priya, A.K.S.a., Balbir Singh Kaitha, Vaishali Tanwara, Jaspreet Kaur Bhatiab, Nisha Sharmaa, Sakshi Bajaja, Sagar Panchal, *RSM-CCD optimized sodium alginate/gelatin based ZnS-nanocomposite hydrogel for the effective removal of biebrich scarlet and crystal violet dyes.* 2019.
65. Thakur, S., *Synthesis, characterization and adsorption studies of an acrylic acid-grafted sodium alginate-based TiO2 hydrogel nanocomposite.* Adsorption Science & Technology, 2017. **0**: p. 1-20.
66. Jasim, L.S. and N.D.R. , Hayder O. Jamel *Synthesis and Characterization of Poly (Acryl Amide - Maleic Acid) Hydrogel: Adsorption Kinetics of a Malachite Green from Aqueous Solutions.* Eurasian Journal of Analytical Chemistry, 2018. **13**(1b): p. 74.
67. Ray, H.M.A.M.S.S., *Gum karaya based hydrogel nanocomposites for the effective removal of cationic dyes from aqueous solutions.* Applied Surface Science, 2015.
68. Aljeboree, A.M., A.N. Alshirifi, and A.F. Alkaim, *Kinetics and equilibrium study for the adsorption of textile dyes on coconut shell activated carbon.* Arabian Journal of Chemistry, 2017. **10**: p. S3381-S3393.
69. Zhao Ying, C.Y., Zhao Jian, Tong Zongrui, Jin Shaohua, *Preparation of SA-g-(PAA-co-PDMC) polyampholytic superabsorbent polymer and its application to the anionic dye adsorption removal from effluents.Ultrasonics Sonochemistry* 2020. **25**: p. 12-18.
70. Mohammad, N., Atassi, Y., & Tally, M., *Synthesis and swelling behavior of metal-chelating superabsorbent hydrogels based on sodium alginate-g-poly (AMPS-co-AA-co-AM) obtained under microwave irradiation.* Polymer Bulletin, 2019. **74**(11): p. 4453-4481.
71. Akeem Adeyemi Oladipo, M.G., *Enhanced removal of crystal violet by low cost alginate/acid activated bentonite composite beads: Optimization and modelling using non-linear regression technique.* journal of Water Process Engineering, 2019. **2**: p. 43-52.
72. Thakur, S., *Synthesis, characterization and adsorption studies of an acrylic acid-grafted sodium alginate-based TiO2 hydrogel nanocomposite.* Adsorption Science & Technology 2018. **36**(1-2): p. 458–477.

73. Wared S.H.H, R.N.D., *Synthesis and characterization of sodium alginate-g-polyacrylic acid hydrogel and its application for crystal violet dye adsorption.* International Journal of Drug Delivery Technology, 2021. **11**(2): p. 556 - 565.
74. Bo Gao, H.Y., Jingya Wea , Hongju Zeng, Ting Liang, Fang Zuo, Changjing Cheng, *Super-adsorbent poly(acrylic acid)/laponite hydrogel with ultrahigh mechanical property for adsorption of methylene blue.* Journal of Environmental Chemical Engineering, 2021. **21**: p. 01323-3.
75. Alloush, S.S. and N.D. Radia, *Adsorption of Brilliant Cresyl blue from Aqueous Solution by Superadsorbent Hydrogel Nanocomposite.* HIV Nursing, 2022. **22**(2): p. 1253-1256.
76. Aljeboree, A.M., et al., *Synthesis of a new nanocomposite with the core TiO2/hydrogel: Brilliant green dye adsorption, isotherms, kinetics, and DFT studies.* Journal of Industrial and Engineering Chemistry, 2022. **109**: p. 475-485.
77. ParisaMohammadzadeh , P.J., PeighambardoustaRauf, ForoutanaNasserArsalanib, HassanAghdasinia, *Decontamination of Fuchsin dye by carboxymethyl cellulose-graft-poly(acrylic acid-co-itaconic acid)/carbon black nanocomposite hydrogel.* International Journal of Biological Macromolecules, 2022. **222**(1): p. 2083-2097.
78. Ali M. El Shafey, M.K.A.-L., H.M. Abd El-Salam, *The facile synthesis of poly(acrylate/acrylamide) titanium dioxide nanocomposite for groundwater ammonia removal.* Desalination and Water Treatment, 2021. **212** p. 61–70.
79. Hemant Mittal , A.A.A., Pranay P. Morajkar , Saeed M. Alhassan, *Graphene oxide crosslinked hydrogel nanocomposites of xanthan gum for the adsorption of crystal violet dye.* Journal of Molecular Liquids 2021. **323**: p. 115034.
80. Sourbh Thakur , J.C., Abhishek Thakur , Oguzhan Gunduz ,Walaa F. Alsanie , Charalampos Makatsorisf ,Vijay Kumar Thakur, *Highly efficient poly(acrylic acid-co-aniline) grafted itaconic acid hydrogel: Application in water retention and adsorption of rhodamine B dye for a sustainable environment.* Chemosphere 2022. **303**: p. 134917.
81. Abdalghaffar M Osman, A.H.H., Tawfik A.Saleh, *Simultaneous adsorption of dye and toxic metal ions using an interfacially polymerized silica/polyamide nanocomposite: Kinetic and thermodynamic studies.* Journal of Molecular Liquids, 2020. **314**(15): p. 113640.
82. Urooj Kamran, Y.-J.H., Ji Won Lee, Soo-Jin Park, *Chemically modified activated carbon decorated with MnO2 nanocomposites*

for improving lithium adsorption and recovery from aqueous media. Journal of Alloys and Compounds 2019. **794**: p. 425e434.

83. Fatemeh Ansari , M.G., Mehdi Taghdiri , Arash Asfaram, *Application of ZnO nanorods loaded on activated carbon for ultrasonic assisted dyes removal: Experimental design and derivative spectrophotometry method.* Ultrasonics Sonochemistry 2016. **33**: p. 197-209.
84. Wenyan Jiang, L.Z., Xiaoming Guo, Mei Yang, Yiwen Lu, Yijun Wang, Yousen Zheng & Guangtao Wei, *Adsorption of cationic dye from water using an iron oxide/activated carbon magnetic composites prepared from sugarcane bagasse by microwave method.* Environmental Technology, 2019. **2**: p. DOI: 10.1080/09593330.
85. Mengna Chen , X.C., Caiyan Zhang , Baozheng Cui , Zewen Li , Dongyu Zhao , Zhe Wang, *Kaolin-Enhanced Superabsorbent Composites: Synthesis, Characterization and Swelling Behaviors.* Polymers 2021. **13**: p. 1204. https://doi.org/10.3390/polym13081204.
86. Xiaoning Shi, W.W., Yuru Kang, Aiqin Wang, *Enhanced Swelling Properties of a Novel Sodium Alginate-Based Superabsorbent Composites: NaAlg-g-poly(NaA-co-St)/APT.* Journal of Applied Polymer Science, 2012. **125**: p. 1822–1832
87. El-RefaieKenawy, M.M.A., Esraa M.El-nshar, *Sodium alginate-g-poly(acrylic acid-co-2-hydroxyethyl methacrylate)/montmorillonite superabsorbent composite: Preparation, swelling investigation and its application as a slow-release fertilizer.* Arabian Journal of Chemistry, 2019. **12**(6): p. 847-856.
88. Zheng, M.C., K.; Chen, M.; Zhu, Y.; Zhang, L.; Zheng, B. , *pH-responsive poly(gellan gum-co-acrylamide-co-acrylic acid) hydrogel: Synthesis, and its application for organic dye removal.* Int. J. Biol. Macromol. , 2020. **153**: p. 573-582.
89. Hossein Esmaeili, R.F., Dariush Jafari , Mohammad Aghil Rezaei *Effect of interfering ions on phosphate removal from aqueous media using magnesium oxide@ferric molybdate nanocomposite.* Korean Journal of Chemical Engineering 2021. **37**: p. 804-814.
90. León, G., Saura, F., Hidalgo, A.M.; Miguel, B. , *Activated Olive Stones as a Low-Cost and Environmentally Friendly Adsorbent for Removing Cephalosporin C from Aqueous Solutions.* Int. J. Environ. Res. Public Health 2021. **18**: p. 4489.
91. Yahya A. Faleh , N.D.R., *Removal of Metformin hydrochloride from Aqueous Solutions by using Carboxymethyl cellulose-g-poly(acrylic acid-co-acrylamide) Hydrogel: Adsorption and*

Thermodynamic Studies. IOP Conf. Series: Earth and Environmental Science 2021. **790**: p. 012062.

92. Mohammed A. Jawad, A.J.K., Aseel M. Aljeboree, *Removal of Direct Dye from Aqueous Solution by a Low-cost Hydrogel: Adsorption Kinetics, and Isotherms Study.* International Journal of Pharmaceutical Quality Assurance 2021. **12**(3): p. 191-195.
93. Farabi Temel , M., SezenKucukcongar, *Removal of methylene blue from aqueous solutions by silica gel supported calix[4]arene cage: Investigation of adsorption properties.* European Polymer Journal, 2020. **125**(15): p. 109540.
94. Hemant Mittal , A.A., Pranay P. Morajkar , Saeed M. Alhassan *Graphene oxide crosslinked hydrogel nanocomposites of xanthan gumm for the adsorption of crystal violet dye.* Journal of Molecular Liquids, 2021. **323**: p. 115034.
95. Aseel M Aljeboree, A.Y.A.-B., Saifaldeen M Abdalhadi, Ayad F Alkaim, *Investigation Study of Removing Methyl Violet Dye From Aqueous Solutions Using Corn-Cob as A Source of Activated Carbon.* Egyptian Journal of Chemistry, 2021: p. DOI: 10.21608/EJCHEM.2021.55274.3159.
96. Sevda Pashaei-Fakhri , S.J.P., Rauf Foroutan ,Nasser Arsalani ,Bahman Ramavandi, *Crystal violet dye sorption over acrylamide/graphene oxide bonded sodium alginate nanocomposite hydrogel.* Chemosphere 2021. **270**: p. 129419.
97. Abdalghaffar Mohammad , O.A.H.H., Tawfik A.Saleh, *Simultaneous adsorption of dye and toxic metal ions using an interfacially polymerized silica/polyamide nanocomposite: Kinetic and thermodynamic studies.* Journal of Molecular Liquids, 2020. **314**(15): p. 113640.
98. Aljeboree, A.M., A.F. Alkaim, and A.H. Al-Dujaili, *Adsorption isotherm, kinetic modeling and thermodynamics of crystal violet dye on coconut huskbased activated carbon.* Desalination and Water Treatment, 2014. **21**(02): p. http://www.tandfonline.com/loi/tdwt20.
99. A. F. AlKaim, A. N. AlShirifi, and A. H. AlDujaili, *Kinetic study of adsorption of phenol on the novel polymer prepared AUFP from aqueous solution.* National Journal of Chemistry, 2007. **27**: p. 428-455.
100. Huda Salim Al-Niaeem , A.A., Whidad Hanoosh, *Preparation of Semi IPNs-Hydrogel Composite for Removing Congo Red and Bismarck Brown Y from Wastewater: Kinetic and Thermodynamic Study.* Egypt. J. Chem., 2022. **56**(1): p. 19 - 34.
101. Nasseh, N., Barikbin, Behnam,Taghavi, Lobat,Nasseri, Mohammad Ali, *Adsorption of metronidazole antibiotic using a*

new magnetic nanocomposite from simulated wastewater (isotherm, kinetic and thermodynamic studies). Composites Part B: Engineering, 2019. **159**: p. 146-156.

102. Abdalghaffar M. , O.A.H., Tawfik A.S *Simultaneous adsorption of dye and toxic metal ions using an interfacially polymerized silica/polyamide nanocomposite: Kinetic and thermodynamic studies.* Journal of Molecular Liquids, 2020. **314**(15): p. 113640.
103. Adheem, H.M., Jasim, L.S., *Preparation and Characterization of a three-component hydrogel composite and study of kinetic and thermodynamic applications of adsorption of some positive and negative dyes from their aqueous solutions.* IOP Conference Series: Materials Science and Engineering, 2020. **928**(5): p. 052027.
104. Shumei Zhao, Y.Z., Xinyi Wan, Shuangjiang He, Xulin Yang, Jiaxin Hu, Guiyuan Zhang, *Selective and efficient adsorption of anionic dyes by core/shell magnetic MWCNTs nano-hybrid constructed through facial polydopamine tailored graft polymerization: Insight of adsorptionmechanism, kinetic, isotherm and thermodynamic study.* Journal of Molecular Liquids 2020. **319**: p. 1-6.
105. Sakin, O.A., H. M. ;Belal , H. M.;Arbi,M, *Adsorption thermodynamics of cationic dyes (methylene blue and crystal violet) to a natural clay mineral from aqueous solution between 293.15 and 323.15 K.* Arabian Journal of Chemistry, 2019. **11**(5): p. 615-623.
106. Xiong, J., et al., *Hexagonal boron nitride adsorbent: Synthesis, performance tailoring and applications.* Journal of Energy Chemistry, 2020. **40**: p. 99-111.
107. Shoaib Nawa , M.S., Romana Khan, Nadia Riaz, Ummara Waheed ,Irum Shahzadi , Asmat Ali, *Ultrasound-Assisted Hydrogen Peroxide and Iron Sulfate Mediated Fenton Process as an Efficient Advanced Oxidation Process for the Removal of Congo Red Dye.* Pol. J. Environ. Stud, 2022. **31**(3): p. 1-13.
108. Zhang, G., Feizbakhshan, Mohammad,Zheng, Shuilin,Hashisho, Zaher,Sun, Zhiming,Liu, Yangyu, *Effects of properties of minerals adsorbents for the adsorption and desorption of volatile organic compounds (VOC).* Applied Clay Science, 2019. **173**: p. 88-96.
109. Hoppen, M.I., Carvalho, K. Q.,Ferreira, R. C.,Passig, F. H.,Pereira, I. C., Rizzo-Domingues, R. C. P.,Lenzi, M. K.,Bottini, R. C. R., *Adsorption and desorption of acetylsalicylic acid onto activated carbon of babassu coconut mesocarp.* Journal of Environmental Chemical Engineering, 2019. **7**(1): p. 102862.

110. Al-Bayati, R.A., *Adsorption-desorption isotherm of one of antidibetic drug from aqueous solutions on some pharmaceutical adsorbents.* Eur. J. Sci. Res., 2020. **40**: p. 580-588.
111. Sevda Pashaei-Fakhri , S.J.P., Rauf Foroutan ,Nasser Arsalani , Bahman Ramavandi, *Crystal violet dye sorption over acrylamide/graphene oxide bonded sodium alginate nanocomposite hydrogel, 2021*. Chemosphere **270**: p. 129419.
112. Hemant Mittal , A.A.A., Pranay P. Morajkar , Saeed M. Alhassan, *Graphene oxide crosslinked hydrogel nanocomposites of xanthan gum for the adsorption of crystal violet dye.* ournal of Molecular Liquids 2021. **323**: p. 115034.
113. Sukul, P., Lamsh, Marc,Zhlke, Sebastian,Spiteller, Michael, *Sorption and desorption of sulfadiazine in soil and soil-manure systems.* Chemosphere, 2019. **73**(8): p. 1344-1350.
114. Freundlich H, W., *The Adsorption of cis- and trans-Azobenzene* J Am Chem Soc, 1939. **61**: p. 2228-2230.
115. Yongde Liu, Y.C., Yahui Shi, Dongjin Wan, Jing Chen, Shuhu Xiao, *Adsorption of toxic dye Eosin Y from aqueous solution by clay/carbon composite derived from spent bleaching earth. Journal of Hazardous Materials,*, 2019. **1**: p. 4656-5544.
116. Kim, Y.-S., Kim, Jin-Hyun, *Isotherm, kinetic and thermodynamic studies on the adsorption of paclitaxel onto Sylopute.* The Journal of Chemical Thermodynamics, 2019. **130**: p. 104-113.
117. Zaheer, Z., Al-Asfar, Aisha,Aazam, Elham Shafik, *Adsorption of methyl red on biogenic Ag@Fe nanocomposite adsorbent: Isotherms, kinetics and mechanisms.* Journal of Molecular Liquids, 2019. **283**: p. 287-298.
118. Nadavala Siva Kumar , M.A., Anesh Manjaly Poulose , Madala Suguna and Mansour I. Al-Hazza, *Equilibrium and Kinetic Studies of Biosorptive Removal of 2,4,6-Trichlorophenol from Aqueous Solutions Using Untreated Agro-Waste Pine Cone Biomass.* processes, 2019. **1**: p. 22-33.
119. E. Alipanahpour Dil , M.G., A.M. Ghaedi , A. Asfaram, A. Goudarzi , S. Hajati , M. Soylak, Shilpi Agarwal, Vinod Kumar Gupt *Modeling of quaternary dyes adsorption onto ZnO-NR-AC artificial 3 neural network: Analysis by derivative spectrophotometry* Journal of Industrial and Engineering Chemistry 2015. **1**: p. 22.
120. Aseel M. Aljeboree , A.B.M., *Synthesis highly active surface of ZnO/AC nanocomposite for removal of pollutants from aqueous solutions: thermodynamic and kinetic study.* Applied Nanoscience, 2021: p. https://link.springer.com/article/10.1007%2Fs13204-021-01946-w.

121. Arif Chowdhury, S.K., Afaq Ahmad Khan, M. Ravi Chandra, and Sahid Hussain, *Activated carbon loaded with Ni-Co-S nanoparticle for Superior Adsorption Capacity of Antibiotics and Dye from Wastewater: Kinetics and Isotherms.* Journal Pre-proof, 2020. **1**: p. https://doi.org/10.1016/j.colsurfa.2020.125868.
122. Asmaa H. Hammadi, S.A.H., Lena Fadhil Al-Jibouri, Falah H. Hussien, *Synthesis, Characterization and Biological Activity of Zinc Oxide Nanoparticles (ZnO NPs).* Sys Rev Pharm 2020. **11**(5): p. 431 439.
123. Adam, A.M.A., *Structural, thermal, morphological and biological studies of proton-transfer complexes formed from 4-aminoantipyrine with quinol and picric acid.* Spectrochimica Acta Part A: Molecular and Biomolecular Spectroscopy, 2010. **104**: p. 1-13.
124. R.V. Mundra, X.W., J. Sauer, J.S. Dordick, R.S. Kane, *Nanotubes in biological applications.* Curr. Opin. Biotechnol.,, 2014. **28**: p. 25-32.
125. Mukha IP, E.A., Smirnova NP, Mikhienkova AI, Korchak GI, Gorchev VF, *Antimicrobial activity of stable silver nanoparticles of a certain size.* Appl Biochem Microbio, 2019. **49** p. 199-206.
126. Dehui Xu, S.W., Bing Li, Miao Qi, Rui Feng, Qiaosong Li, Hao Zhang, Hailan Chen, and Michael G Kong, *Effects of Plasma-Activated Water on Skin Wound Healing in Mice.* Microorganisms, 2020. **7**(8): p. 1091.
127. Evelina Vågesjö, E.Ö., Anneleen Mortier, Hava Lofton, Fredrik Huss, Paul Proost, Stefan Roos, Mia Phillipsona,, *Accelerated wound healing in mice by on-site production and delivery of CXCL12 by transformed lactic acid bacteria.* National Center for Biotechnology Information, 2018. **7**(8): p. 1-9.
128. Samia Afrin , M.S., Papia Haque , Md. Sazedul Islam , Shafiul Hossain ,Taslim Ur Rashid , Tanvir Ahmed , Makoto Takafuji , Mohammed Mizanur Rahman *Advanced CNC/PEG/PDMAA Semi-IPN Hydrogel for Drug Delivery Management in Wound Healing.* Gels, 2022. **8**: p. 340.

الخلاصة

تحضير بوليمر جديد فائق الامدصاص ، الجينات الصوديوم- مطعم - بولي (حامض ايتكونيك-صوديوم 4-فينيل بنزين سلفونات) / اوراق نبات الخروع ، (SA-g-P(ITA-co-VBS)/ RC) الهلام المائي النانوي ، تم تحضيره بواسطة البلمرة المشتركة بتطعيم الجذو الحرة ، لإزالة الصبغتين الملكيت الخضراء (MG) وصبغة الاخضر اللامعة (BG) كنموذج للأصباغ الموجبة السامة .في هذا العمل ، تم تحضير مادة ماصة جديدة صديقة للبيئة وبسيطة ومستقرة حيث اعتمد تحضير سطحين ، الأول SA-g-P (ITA-co-VBS) الهلام المائي والثاني السطح بعد تحميل اوراق نبات الخروع (RC) على الهيدروجل SA-g-P (ITA- co-VBS) /RC, وهذه الأسطح الجديدة تم تحضيرها بالاعتماد على مونمرات مختلفة هي(ITA و VBS). تمت دراسة الخصائص الفيزيائية لهذه المواد المحضرة التي تم الحصول عليها باستخدام تقنيات مختلفة مثل باستخدام التحليل الطيفي للأشعة فوق البنفسجية المرئية (UV-Vis) ، مطيافية الاشعة تحت الحمراء (FT-IR) ، التحليل الحراري الوزني (TGA) ، المجهر الكتروني الماسح ذو المجال المنبعث (FESEM) ، المجهر الإلكتروني النافذ (TEM) ، الأشعة السينية المشتتة للطاقة (EDX) حيود الاشعة السينية (XRD) .

تضمنت التجارب العملية حساب الطول الموجي الاعظم ودراسة تحسين ظروف التحضير التي أنتجت الهلام المائي النانوي مع أعلى نسبة انتفاخ مثل: تأثير كمية RC ، تأثير كمية VBS ، تأثير حامض إيتاكونيك ، تأثير ألجينات الصوديوم ، تأثيرالعامل المشابك ، وتأثير البادئ ، وتأثير الأس الهيدروجيني ، وتأثير المذيب ، وتأثير درجة الحرارة ، وتأثير الزمن . أيضا ، دراسة الظروف المثلى لمعاملات الامتزاز هي: تأثير زمن الاتزان ، تأثير وزن السطح ، تأثير محلول الأس الهيدروجيني ، شحنة نقطة الصفر ، تأثير درجة الحرارة ، اعادة تنشيط السطح ،مقارنة الامتزاز بين الأسطح المختلفة إزالة الصبغتين ، إزالة الملوثات المائية للعينة مختبرية ، النشاط البيولوجي البكتيري ، اختبار الفطريات وعلاج جروح الفئران باستخدام ثلاثة أسطح محضرة من RC ، الهلام المائي (SA-g-P (ITA-co-VBS) و (SA-g-P (ITA-VBS) /RC) الهلام المائي النانوي.

تظهر نتائج دراسة الامتزاز أن نسبة الإزالة تزداد مع زيادة وزن السطح وزمن الاتزان . حيث كانت الظروف المثلى لزمن الاتزان 1 ساعة. وبعد ذلك يصبح الامتزاز ثابتا. زيادة كمية السطح حوالي (0.1 g-0.01)، وزيادة النسبة المئوية لإزالة صبغة MG وصبغة BG و من (99.8% –90.11%) ، (% 95.99 - 75.88%)على التوالي , وكفاءة الامتزاز تقل من (

(SA-g-P(ITA-co-VBS)/ RC) على (695 - 5020 mg/g) ، (mg/g 995 - 6695 هيدروجل بنفس الترتيب. تم دراسة الدوال الثرموديناميك ، حيث تكون قيمة الانثالبي ΔH موجبة مما يشير إلى أن عملية الامتزاز هي تفاعل ماص للحرارة. تعتبر جميع عمليات الامتزاز تلقائية من قيمة تغير طاقة جبس الحرة لـ ΔG. في حين أن الانتروبي ΔS لها قيمة موجبة تشير إلى تفاعل الجزيئات الناتج بشكل عشوائي من النظام الكلي ، كما تم دراسة ايزوثيرمات الامتزاز Freundlich و Langmuir. لقد وجد أن جميع النتائج تتبع موديل Freundlich في وجود الصبغتين . . تمت دراسة حركيات الامتزاز لصبغتين على (/ (ITAC-co-VBS) SA-g-P RC)باستخدام ثلاثة نماذج حركيه

تم دراسة مقارنة بين (اوراق نبات الخروع (RC) ، اوراق نبات الخروع المنشط غير المعالج - حامض (ACRC) واوراق نبات الخروع المنشط المعالج بحامض.(AACRC)) يتم ترتيب أفضل النتائج لنسبة الإزالة (E٪)لصبغتين بالترتيب (RC> ACRC> AACRC). أيضا تم دراسة مقارنة بين الاسطح المحضرة ((ITA-co-VBS) / RC) SA-g-P)و (ITAC-co-VBS) SA-g-P)و (RC) كمواد ماصة حيث توضح النتائج اعلى نسبة الإزالة (E٪)) للهلام المائي النانوي (ITA-co- VBS) / RC) SA-g-P) مقارنة بالأسطح الاخرى حيث كانت النتائج (92،451٪ ، و 82.56٪ لـ MG ، و BG بنفس الترتيب.

تم دراسة إعادة التدوير وتنشيط السطح المحضر للحصول على أداء افضل لإعادة التدوير للمركب المحضر. بناءً على النتائج ، يمكن أن تكون المركبات النانوية المحضرة مفيدة كمواد واعدة وصديقة للبيئة وفعالة من حيث التكلفة وفعالة لإزالة تلوث الأصباغ.حيث اعتمدة عمليه اعادة تنشيط السطح (ITAC-co-VBS) / RC) SA-g-P)، تم تجديده بنسبة 100٪ يمكن امتصاصه في حامض الهيدروكلوريك المخفف.

تمت دراسة النشاط البيولوجي لنوع واحد من الفطريات (Aspergillus flavus) ونوعين) من البكتيريا موجبة الجرام (Staphylococcus) والبكتيريا سالبة الجرام (Pseudo monas) باستخدام ثلاثة أسطح . أظهرت نتائج مناطق التثبيط الثلاثة مركبات حيث تم إعطاء المركب ((ITAC-co-VBS) / RC) SA-g-P نشاطًا عاليًا مضادًا للبكتيريا. في غضون يومين إلى سبعة أيام ، وفقًا للنتائج ، هناك شفاء كامل للفئران وعودة الجلد إلى لونه الطبيعي. هذا يرجع إلى حقيقة أن (ITAC-co-VBS) / RC) SA-g-P) لها كفاءة عالية في علاج الفئران وشفاءها.

بسم الله الرحمن الرحيم

(وَلَقَدْ آتَيْنَا دَاوُودَ وَسُلَيْمَانَ عِلْمًا وَقَالَا الْحَمْدُ لِلَّهِ الَّذِي فَضَّلَنَا عَلَى كَثِيرٍ مِنْ عِبَادِهِ الْمُؤْمِنِينَ).

صدق الله الْعَلِيُّ العظيم

"سورة النمل، آية: ١٥"

جمهورية العراق
وزارة التعليم العالي والبحث العلمي
جامعة بابل/ كلية العلوم للبنات
قسم الكيمياء

تحضير سطح هلام مائي (SA-g-P(ITAC-co-VBS)/RC) نانوي عالي الكفاءة لإزالة الأصباغ و دوره كمادة لاصقة للجروح

رسالة مقدمة

الى مجلس كلية العلوم للبنات- جامعة بابل

جزء من متطلبات نيل شهادة الماجستير في الكيمياء / الكيمياء التحليلية

من قبل

إشراق طالب حسن مسافر

بكالوريوس علوم كيمياء– جامعة بابل– كلية العلوم للبنات

2020-2019

بإشراف

أ.م .د. اسيل مشتاق كاظم الجبوري

1444 هـ **2023 م**